

INFORMATION TO USERS

This manuscript has been reproduced from the microfilm master. UMI films the text directly from the original or copy submitted. Thus, some thesis and dissertation copies are in typewriter face, while others may be from any type of computer printer.

The quality of this reproduction is dependent upon the quality of the copy submitted. Broken or indistinct print, colored or poor quality illustrations and photographs, print bleedthrough, substandard margins, and improper alignment can adversely affect reproduction.

In the unlikely event that the author did not send UMI a complete manuscript and there are missing pages, these will be noted. Also, if unauthorized copyright material had to be removed, a note will indicate the deletion.

Oversize materials (e.g., maps, drawings, charts) are reproduced by sectioning the original, beginning at the upper left-hand corner and continuing from left to right in equal sections with small overlaps. Each original is also photographed in one exposure and is included in reduced form at the back of the book.

Photographs included in the original manuscript have been reproduced xerographically in this copy. Higher quality 6" x 9" black and white photographic prints are available for any photographs or illustrations appearing in this copy for an additional charge. Contact UMI directly to order.

U·M·I

University Microfilms International
A Bell & Howell Information Company
300 North Zeeb Road, Ann Arbor, MI 48106-1346 USA
313/761-4700 800/521-0600

Order Number 9309744

**Determining the surface heat flux distribution over the tropical
Pacific Ocean by the adjoint method**

Yu, Lisan, Ph.D.

The Florida State University, 1992

U·M·I
300 N. Zeeb Rd.
Ann Arbor, MI 48106

THE FLORIDA STATE UNIVERSITY
COLLEGE OF ARTS AND SCIENCES

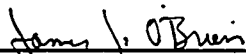
DETERMINING THE SURFACE HEAT FLUX DISTRIBUTION
OVER THE TROPICAL PACIFIC OCEAN BY THE ADJOINT METHOD

By
LISAN YU

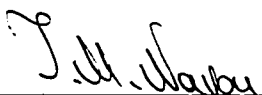
A Dissertation Submitted to the
Department of Oceanography
in partial fulfillment of the requirements for
the degree of Doctor of Philosophy

Degree Awarded:
Fall Semester, 1992


The members of the Committee approve the dissertation of Lisan Yu defended on November 6, 1992.



James J. O'Brien
Professor Directing Dissertation



I. Mike Navon
Outside Committee Member



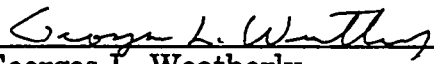
William K. Dewar
Committee Member



Richard L. Iverson
Committee Member

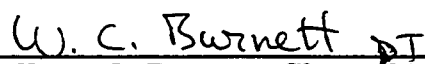


Kenneth W. Johnson
Committee Member



Georges L. Weatherly
Committee Member

Approved:



William C. Burnett, Chair, Department of Oceanography

Acknowledgments

The Supercomputer Computations Research Institute (SCRI) at the Florida State University is sincerely thanked for awarding me a graduate student assistantship and for their sponsorship during the course of my Ph.D. studies. I am grateful for the time taken by Drs. W.K. Dewar, R.L. Iverson, K.W. Johnson, I.M. Navon and G.L. Weatherly while serving on my doctoral committee. Their comments and suggestions are greatly appreciated. Thanks are extended to Drs. P. Malanotte-Rizzoli and J. Marotzke at MIT for the beneficial discussions on my dissertation research.

It is with my deepest respect that I thank Dr. J.J. O'Brien as my major professor and dissertation advisor. His guidance, motivation and support during my five-year graduate study are greatly appreciated. I always feel so fortunate for having been accepted into his group. He provides such a creative atmosphere and such unparalleled working conditions for the group -- from which I have greatly benefited. He supported my interest in doing data assimilation from the beginning. He has given me so many opportunities to let me develop my interest and style in doing research. I owe him my sincerest gratitude.

It is with my deepest appreciation that I thank Dr. I.M. Navon for his advice and much help. He has always been so supportive whenever I had problems. He has constantly helped me out in many technical difficulties

during my dissertation research. His advice to me on choosing a career has been especially influential. I wish to express my sincerest thanks to him.

I wish to thank every member of the Mesoscale Air-Sea Interaction Group for their care and support. Together they create such a wonderful environment that has made my stay at FSU so productive, enjoyable and unforgettable. Special thanks go to Brian Kelly and Ming Liu for the fruitful discussions on a wide range of topics and Alan Davis for his superior computer technical help.

It is with the deepest affection that I thank my husband Dr. Jiayan Yang for his so much love, so much patience, and so much support. Besides being a considerate husband and a best friend, he is a very cooperative colleague. My research has greatly benefited from the numerous scientific discussions with him through e-mail and telephone. Without his complete understanding and unconditional support, I could never have been able to decide to do my postdoctoral research at the Massachusetts Institute of Technology -- far away from the University of California in Los Angeles where he is. I owe him all my love.

I could never thank enough my parents for their love, guidance and many sacrifices. They have always given me the best education opportunities they could ever provide. They guided me to study the earth sciences -- which makes my life so enriching. I dedicate this dissertation to my parents with my love.

Table of Contents

1. Introduction	
1.1 Motivation	1
1.2 Oceanic Data Assimilation Techniques	3
1.3 Applications of Adjoint Method in Oceanography	6
1.4 Objectives	10
2. Parameter Estimation: Theory and Application	12
2.1 Optimal Control Theory	12
2.2 Optimal Control Applied to Parameter Estimation	13
2.2.1 <i>Mathematical Formulation of Parameter Estimation</i>	13
2.2.2 <i>Weak, Strong Constraint Formalisms and the Augmented Lagrangian</i>	15
2.3 Adjoint Method	17
2.4 Minimization Algorithms	22
2.4.1 <i>Steepest Descent Method</i>	22
2.4.2 <i>Quasi-Newton and Conjugate-Gradient Methods</i>	26
3. Estimating the Heat Flux Distribution over the Tropical Pacific Ocean by the Adjoint Technique	30
3.1 Oceanic Model	30
3.1.1 <i>Choice of Models in the Tropical Oceans</i>	30
3.1.2 <i>Description of the Physical Model</i>	32
3.2 Importance of Scaling in Variational Procedure	37
3.2.1 <i>The Role of the Hessian</i>	37
3.2.2 <i>Variable Scaling</i>	40
3.2.3 <i>Choosing the Scales of the Physical Variables</i>	41
3.3 Formulating the Cost Function Using the <i>a priori</i> Information	42

3.4 Adjoint Model and the Variational Procedure	46
3.5 Numerical Models	50
3.5.1 <i>Dynamical Model</i>	50
3.5.2 <i>Data</i>	51
3.5.3 <i>Variational Procedure</i>	53
3.5.4 <i>The Boundary conditions</i>	54
4. Seasonal Variability in the Tropical Pacific	55
4.1 Dynamics	55
4.2 Thermodynamics	64
5. Results and Discussions	70
5.1 Estimates of the Surface Heat Flux by the Adjoint Procedure	70
5.1.1 <i>The Form of the Cost Function on the Rate of the Convergence</i>	70
5.1.2 <i>Determining the Initial Condition and Its Effect on the Parameter Estimation</i>	75
5.1.3 <i>The Heat Flux Pattern Estimated from the Adjoint Procedure</i>	85
5.2 Results Analysis	89
5.2.1 <i>Comparisons with the Existing Heat Flux Patterns</i>	89
5.2.2 <i>The Physical Processes Determining the Heat Flux Distribution</i>	97
5.2.3 <i>Examining the Results from the Thermodynamic Point of View</i>	99
5.2.4 <i>Data Misfits</i>	103
6. Summary and Conclusions	107
7. Appendices	111
A. Derivation of the Continuous Adjoint Equation	111
B. Verification of the Correctness of the Gradient Calculation	118
C. Comparison with Residual Heat Flux	122

D. Why Can't the Cost Function Be Zero When Assimilating the Real Observed Data	130
E. The Effect of Choice of the Guess Field \tilde{Q} on the Estimated Net Heat Flux Field	135
8. References	153
9. Biography Sketch	164

List of Tables

Table 1. The values of the model parameters used in the model integration.	51
Table 2. Verification of the gradient of the cost function	121

List of Figures

- Figure 1. Illustration of the method of steepest descent and of obtaining the optimum stepsize for a two-dimensional problem. 24
- Figure 2. The vertical structure of the reduced-gravity model with thermodynamics. The model has two layers above the thermocline with the same constant density. The upper of the two active layers is a constant depth surface layer which is acted upon directly by the wind stress. 33
- Figure 3. The pattern of the pseudo-stress in (a) December; (b) March; (c) June; and (d) September. The seasonal variations of the wind field are characterized by the seasonal migrations of the ITCZ. 57
- Figure 4. The pattern of the surface current in (a) December; (b) March; (c) June; and (d) September. The prominent features of the circulation are the alternating bands of eastward and westward flowing currents, namely, the westward NEC and SEC and the eastward NECC. The strength of the surface currents vary seasonally in response to the variation of ITCZ. 60
- Figure 5. The pattern of the upwelling in (a) December; (b) March; (c) June; and (d) September (the contour interval is 0.25 m/day). The upwelling maximum occurs in the northern summer. 62
- Figure 6. The pattern of the observed sea surface temperature (SST) in (a) December; (b) March; (c) June; and (d) September. The most striking feature of the seasonal cycle is the strengthening of the horizontal SST gradient in the equatorial Pacific during the northern summer time. 65
- Figure 7. Experiments to test the form of the cost function on the rate of the convergence. In this case, a constant first guess field for the control parameter is used.
(a) The evolution of the cost function (initialized by the value at the first iteration) during the iterative process.

(b) The evolution of the norm of the gradient (initialized by the value at the first iteration) during the iterative process. The process is truncated once a steady state is approached. The experiment with cost function J_1 has a faster convergence rate than the experiment with J_2 .	72
Figure 8. Same as Figure 7 except that a first guess with thermodynamic meaning is used in these experiments. It shows that the value of the cost function J_1 does not change with the choice of the first guess and a good first guess speeds the convergence of the descent algorithm.	73
Figure 9. The loss of information in the estimated parameter field from September to December due to the errors in the chosen initial SST state. The SST model integration uses the observation SST field as an initial condition. The periodicity of the SST evolution is not satisfied at the end of the assimilation cycle.	78
Figure 10. The evolution of the surface heat flux is continuous from September to December by adjusting the initial SST field in addition to the estimated parameters. The periodic condition is retained.	83
Figure 11. The evolution of the cost function and the norm of the gradient during the iterative process.	86
Figure 12. The pattern of the estimated net downward surface heat flux in (a) December; (b) March; (c) June; and (d) September (the contour interval is 20 W/m ²).	87
Figure 13. The pattern of the net downward surface heat flux according to Oberhuber (1988). (a) December; (b) March; (c) June; and (d) September (the contour interval is 25 W/m ²).	91
Figure 14. The pattern of the net downward surface heat flux according to Fu et al. (1990). (a) December; (b) March; (c) June; and (d) September (the contour interval is 40 W/m ²).	93
Figure 15. The pattern of the modeled sea surface temperature (SST) in (a) December; (b) March; (c) June; and (d) September.	100
Figure 16. Data misfits between the modeled and the observed SST in (a) December; (b) March; (c) June; and (d) September (the contour interval is 0.25°C).	104

Figure 17. Verification of the gradient calculation	120
Figure 18. (a) Heat flux pattern from the residual calculation; (b) The optimal heat flux obtained from the adjoint procedure.	124
Figure 19. The data misfit between the observed SST and the modeled SST.	127
Figure 20. The heat flux pattern of the sum of the optimal heat flux and the data misfit induced heat flux. It is remarkably similar to Fig. 18a.	128
Figure 21. The pattern of the estimated net downward surface heat flux from experiment 1 in (a) December; (b) March; (c) June; and (d) September (the contour interval is 20 W/m ²).	139
Figure 22. The pattern of the estimated net downward surface heat flux from experiment 2 in (a) December; (b) March; (c) June; and (d) September (the contour interval is 20 W/m ²).	141
Figure 23. The pattern of the modeled sea surface temperature from experiment 1 in (a) December; (b) March; (c) June; and (d) September.	143
Figure 24. The pattern of the modeled sea surface temperature from experiment 2 in (a) December; (b) March; (c) June; and (d) September.	145
Figure 25. Data misfits between the modeled (experiment 1) and the observed SST in (a) December; (b) March; (c) June; and (d) September (the contour interval is 0.25°C).	147
Figure 26. Data misfits between the modeled (experiment 2) and the observed SST in (a) December; (b) March; (c) June; and (d) September (the contour interval is 0.25°C).	149
Figure 27. The evolution of the cost function and the norm of the gradient during the iterative process in (a) experiment 1; (b) experiment 2	151

Abstract

A simple oceanic model with thermodynamics is used to determine the surface thermal forcing field by the variational adjoint technique. Two data-sets are chosen, the climatological monthly-mean sea surface temperature (SST) and winds. We have been able for the first time to calculate the seasonal surface heat flux patterns which are consistent with the ocean's dynamics and thermodynamics and which agree with the observations.

The use of *a priori* information is investigated in the formulation of the cost function to obtain meaningful model parameters. Experimental evidence has verified that adding *a priori* information of the estimated parameters can increase the probability for the solution to be unique. The *a priori* information also plays the role of bogus data. It serves not only to increase the number of observations but to improve the conditioning of the Hessian matrix. Hence the practical benefit of adding the *a priori* information is to accelerate the convergence of the descent algorithm.

We learned from many test runs that surface heat flux pattern can not be fully derived without the optimal adjustment of the model initial SST state. The importance of a correct initial SST condition in our study is to ensure a periodic seasonal cycle and therefore reduces the level of the data misfit.

The result illustrates that the model, albeit simple, is capable of assimilating the sea surface temperature (SST) observations in deriving the surface heat flux. The comparison with the existing heat flux atlases of Oberhuber (1988) and Fu et al. (1990) has shown that our adjoint procedure has successfully captured the main seasonal signals of the surface heat flux distribution over the tropical Pacific ocean, though some differences exist.

The result from this research is very promising. The methodology used here can be easily extended to simultaneously derive the surface wind forcing and the surface heat flux. Thus, it can provide the information useful for the studies of climate prediction and air-sea interaction.

1. Introduction

1.1 Motivation

The process of combining data with model dynamics, known as data assimilation, has proven to be a powerful tool for extracting the maximum amount of information from the observations. Data assimilation is now used extensively in meteorology (see Thepaut and Courtier, 1991; Navon et al., 1992) and, recently, in oceanography. As reviewed by Ghil and Malanotte-Rizzoli (1991) and Anderson (1991), the fundamental difference between data assimilation in oceanography and in meteorology is the motivation. Oceanographic assimilation is not driven by the need to forecast as is the case for meteorological assimilation. It is motivated by the need to improve our understanding of ocean dynamics/thermodynamics and by the need to use the much-expanded yet still insufficient available datasets in an optimal fashion. Therefore, the emphases of oceanographic assimilation are on model parameter estimation, formal testing of the model against the data, and exploration and intercomparison of assimilation techniques.

Three elements comprise a data assimilation approach. These are an oceanic model, assimilation technique and observations. The oceanic model describes the physical mechanisms of ocean behavior. The assimilation technique provides the means for extracting and filtering the information from data. These two processes combined give the computed

atmospheric/oceanographic fields which are consistent with both model physics and observations.

The development and implementation of the data assimilation techniques in meteorology have dramatically improved the ability of theoretical models to diagnose and predict the atmospheric behavior. However, oceanic models are less realistic and sophisticated than their meteorological counterparts with respect to the parameterizations of internal physics and forcing functions. This is largely due to the inadequacy of observations in providing effective tests for verifying model formulations.

Even with new technology, oceanic datasets are still insufficient to provide complete, uniform and accurate information in space and time. A major challenge confronting oceanographers is to develop data assimilation techniques to obtain a better estimate of the ocean fields while improving the less well-known aspects of the model, especially the surface forcing fields. The process which derives the model parameters from the available observations is known as *parameter estimation*.

The ocean is forced thermally through direct insolation, through evaporation and precipitation, through sensible heat transfer from the overlying atmosphere, and through the surface wind stress. Because of limited direct measurements, the variability of the surface forcing (the surface heat fluxes in particular) has been a vexed question in the study of climate changes and air-sea interactions. For a long time, researchers have been using the aerodynamic bulk formulae to study climatological surface heat fluxes over the tropical oceans. It is commonly accepted that

such heat flux parameterization contains a large degree of uncertainty in the values of the empirical constants and some less known physical parameters such as the cloud covers and near-surface humidity (Blanc, 1987; Blumenthal et al., 1989; Harrison, 1991; Seager et al., 1988). It is not surprising to see that existing atlases (e.g. Esbensen and Kushnir, 1981; Weare et al., 1981; Oberhuber, 1988; Fu et al., 1990) have shown substantial differences in the overall patterns and magnitudes of the climatological heat fluxes over the tropical Pacific ocean. The climate prediction of upper ocean properties with these prescribed heat fluxes have been unsuccessful.

Hence deriving the heat flux fields by assimilation techniques will not only lead to better understanding of heat flux variability but aid in climate prediction studies. The motivation of this research is to estimate the annual distribution of net downward surface heat flux distribution over the tropical Pacific ocean using the data assimilation technique called the adjoint method. This research is an application of parameter estimation.

1.2 Oceanic Data Assimilation Techniques

There have been two general approaches for oceanic data assimilation, that is, the *continuous data assimilation* and the *variational method*. Continuous data assimilation inserts observations directly into the model while the model is being integrated forward over some time interval. The variational method finds a solution of model inputs by

minimizing some measure of the distance (or lack of fit) between observations and model counterparts.

(a) Continuous Data Assimilation

Continuous data assimilation has been largely technology motivated. That is, it was developed for assimilating the asynoptic data from satellite-borne systems such as sea surface height from altimetry. The technique that has been applied to continuous data assimilation with real data is dynamic relaxation (or nudging, Newtonian relaxation). Dynamical relaxation has been studied theoretically by meteorologists Anthes (1975), Hoke and Anthes (1976) and Davies and Turner (1977). It was introduced into oceanography by Verron and Holland (1988) and by Holland and Malanotte-Rizzoli (1989). This technique has been used widely in assimilating the altimetry data and found to be very successful both in quasi-geostrophic experiments (Holland and Malanotte-Rizzoli, 1989; Haines, 1991) and primitive equation tests (Malanotte-Rizzoli et al., 1989; 1990). Recently a technique allowing optimal nudging based on variational adjoint parameter estimation was developed by Zou, Navon and Le Dimet (1992).

(b) Variational Approach

The Kalman-Bucy filter, the inverse model and the adjoint equation method are the commonly used techniques of variational approach. The formulation of the KB filter (Jazwinski, 1970; Ghil et al., 1981; Dee et al., 1985; and Parrish and Cohn, 1985) is an elegant and comprehensive

mathematical description of the data assimilation problem. This method is based upon the ideas of sequential estimation theory which explicitly includes the prediction of the background error statistics. Therefore, the KB filter is capable of providing the error estimates such as the error bars or the error covariance matrix of the obtained solution. However, this technique suffers from two serious drawbacks. The first and foremost is the computational expense of updating the error covariance matrices. The computational requirements rapidly increase with model complexity and are seldom affordable. The second is the difficulty in identifying the systematic model errors from the observational errors. Because of these limitations, most applications of this technique in oceanography have been done for relatively simple dynamical models (Miller, 1986; Bennett and Budgell, 1987 and 1989; Gaspar and Wunsch, 1989; Miller and Cane, 1989; Miller and Ghil, 1990).

The inverse model and the adjoint equation method are all derived from optimal control theory of partial differential equations. The inverse model is often formulated as a set of linear equations relating data and unknown parameters. The equations are written in matrix form and solved by methods such as singular value decomposition or linear programming. This technique needs to store a matrix with the size of (number of unknowns \times number of equations) in performing the computation. As a result, it has been limited to low spatial resolution or to simple local dynamics (Wunsch, 1978; Olbers and Wenzel, 1988; Schröter and Wunsch, 1986; Wunsch, 1987, 1988 and 1989; Tziperman and Hecht, 1988; and Tziperman and Malanotte-Rizzoli, 1991).

The studies by Lewis and Derber (1985), Le Dimet and Talagrand (1986), Talagrand and Courtier (1987), Courtier and Talagrand (1987), Derber (1987), Thacker (1987), and Thacker and Long (1988) have made significant contributions to the adjoint approach and developed it as one of the important strategies in variational data assimilation. More recently the method has been applied to 3-D operational models by Thepaut and Courtier (1991) and Navon et al. (1992). The adjoint method has been used successfully in both meteorology and oceanography. For a review of its applications in meteorology, one may refer to Lorenc (1986), Navon (1986), Le Dimet and Navon (1988) and Ghil and Malanotte-Rizzoli (1990).

1.3 Application of Adjoint Method in Oceanography

The adjoint method incorporates the physics of the problem in the definition of the cost function (representing the misfits between model and observations) and constrains the dynamics. A Lagrange multiplier term is used to enforce the dynamical constraints. It is the solution of the adjoint equation of the linearized model equations called the tangent linear model. The first and most significant advantage of this technique is the introduction of the adjoint equation which allows the gradient of the cost functional with respect to the control variable vector to be efficiently and accurately evaluated. As a result, the computation of the minimum of the cost function is greatly simplified. This technique has proven to be very versatile. It can assimilate all types of data as long as data can be represented in terms of model variables or functions. It can also be used to

adjust any model parameters (initial condition, boundary condition, forcing, mixing coefficients, etc.) once there is sufficient data available.

Thacker and Long (1988) have made the first attempt to apply the adjoint method in oceanographic data assimilation by fitting the model dynamics to observations. The research work to date can be grouped into four categories, namely, initialization, parameter estimation, steady state circulation investigation, and Gulf Stream study.

(a) Application to the tropical oceans - Initialization

The motivation for initialization in oceanography is primarily driven by the crucial need of climate studies. As oceanic observations increase dramatically in quality and quantity in the near future, and oceanic and atmospheric models become more sophisticated, using the coupled ocean-atmosphere system for climate forecasting is an ever important subject. Initialization is a process that can provide diagnostic constraints used to generate approximate but model-consistent data that are not available from the observation network. The resulting balanced initial conditions will damp out the spurious high-frequency oscillations in the integration of the forecast model. This process is of vital importance for the success of the forecasting of weather as well as climate. The oceanic model must first be able to be initialized in order to find the balanced initial state of the coupled models for the climate forecast. The feasibility studies by many researchers, e.g. Thacker and Long (1988), Thacker (1988), Derber and Rosati (1989), Bennett (1990), Long and Thacker (1989a, 1989b), and Sheinbaum and Anderson (1990a, 1990b), have

shown the potential of oceanic model initialization using the adjoint technique. Similar work was done in meteorology by Courtier and Talagrand (1990), Zou et al. (1992a) and Zou et al. (1992b).

(b) Application to parameter estimation - Understanding ocean physics

The application of the adjoint method by O'Brien's group at FSU addresses the issue of parameter estimation. Although oceanic models have become quite sophisticated in recent years, they still cannot accurately represent the state of the ocean. This is largely due to many uncertainties of the model inputs, such as eddy-mixing coefficients, surface wind forcing, surface heat and fresh water fluxes, etc. Normally there is no direct information on many of these input parameters in oceanic measurements. The purpose of parameter estimation is to deduce the unknown model inputs from the existing data (wind, temperature, salinity, currents, or whatever available datasets) with the aid of the numerical model and, at the same time, to obtain an optimal estimate of the observed field. This process can provide information useful for improving the model itself. Besides the work done by O'Brien's group, e.g., Panchang and O'Brien (1989), Smedstad and O'Brien (1990), and Yu and O'Brien (1991), we have also seen other studies of the parameter estimation, e.g., Schröter (1989), Das et al. (1991), Das and Lardner (1992), and Lardner (1992).

(c) Application to the North Atlantic Ocean - Establishing a steady state oceanic circulation

Ocean dynamics are characterized by a wide range of temporal scales. The high frequencies, associated with the gravity waves, set the upper limit for the size of the time step for most numerical models; the low frequencies, associated with the slow process in the establishment of the oceanic equilibrium circulation, determine the number of time steps needed to spin up the model. The need of using the optimization method to compute the steady state arises because of the high computational expense of the conventional method in doing so. Efforts are being taken by the groups at AOML (Atmospheric and Oceanic Marine Laboratory, Miami) and MIT to determine whether a state of the North Atlantic ocean can be estimated which is consistent both with the observations and with the North Atlantic models (either a simple barotropic vorticity-equation model or a fully three-dimensional baroclinic, primitive-equation model) in a dynamical steady state (Tziperman and Thacker, 1989; Tziperman et al., 1992; Marotzke, 1992; Bergamasco et al., 1992).

(d) Application to the Gulf Stream - Characteristics study

The Harvard Oceanography Group has applied the adjoint technique to the Harvard quasi-geostrophic open-ocean model (Robinson and Walstad, 1987) to study the characteristics of the Gulf Stream. For example, Moore (1991) studied the ability of the adjoint method in correcting large errors in the speed and position of the Gulf Stream jet by assimilating GEOSAT sea surface height observations. The adjoint approach has also been used to investigate the fastest growing unstable modes of a Gulf Stream-like jet (Farrell and Moore, 1992).

Each category is not isolated. Thacker and Long (1988) and Tziperman and Thacker (1989) present examples where the sea surface forcing and coefficients of friction are also treated as unknowns and are determined by the adjoint procedure besides computing the optimal model state. Yu and O'Brien (1992) pointed out that the combination of initialization and parameter estimation can result in a better model-data fitting. One thing we should remember is that a problem is well-posed only when the initial conditions, the boundary conditions, and the model parameters can all be resolved.

1.4 Objectives

In this study an attempt is made to explore the potential of determining the surface heat flux distribution by the adjoint method. We choose the datasets of the climatological sea surface temperature (SST) (Shea et al., 1990) and the climatological wind (Stricherz et al., 1992) because of their fairly good temporal and spatial coverage in the domain of interest. The seasonal variation of the surface heat flux over the tropical Pacific ocean is investigated by assimilating the observations into a relatively simple reduced-gravity model with thermodynamics (Cane, 1979).

The objective throughout this research is *not* to provide a pattern to be rigorously adjusted for the use of climate and air-sea interaction studies. Rather we devote this research as an application of the adjoint

method in parameter estimation, with the aim of formulating a suitable procedure for determining time-dependent field parameters. The application of the adjoint technique in oceanography is in its primitive stage and so is oceanic modeling in the tropics. The extensive use of the adjoint technique is not only to perfect the technique itself but to improve the model. Our research serves this purpose.

The study is organized as follows. In section 2, we present the optimal control theory, its application in parameter estimation, and the adjoint method in solving the parameter estimation problem. The commonly used minimization algorithms, i.e., the steepest descent, quasi-Newton and conjugate gradient methods, are also compared in this section. In section 3, the oceanic model is described and the adjoint equation is derived. The variational adjoint procedure is then formulated. The important issues in data assimilation, such as the variable scaling and cost function formulation, are discussed comprehensively in this section. Section 4 presents the dynamics/thermodynamics of the seasonal variability in the tropical Pacific ocean, in which the variations of SST, wind, currents and upwelling are discussed. The seasonal surface heat flux distribution obtained using the adjoint method are given in section 5. Our results are compared with the existing atlases. The differences are examined both through the air-sea interaction viewpoint and the thermodynamic viewpoint. A summary and conclusions are included in section 6. The derivation of the continuous adjoint equation is given in Appendix A. The optimal heat flux pattern is compared with the residual calculation in Appendix B.

2. Parameter Estimation: Theory and Application

In this section, we introduce the theoretical foundation of parameter estimation, namely, optimal control theory of partial differential equations. We then demonstrate how this theory can be employed to solve parameter estimation problems in meteorology and oceanography.

2.1 Optimal Control Theory

The theory of optimal control addresses the dependence of the output parameters in a model described by a set of coupled partial differential equations on any or all of the input parameters, or more specifically, how the outputs can be controlled by the inputs.

A general class of parameter estimation problems involves finding the values of a control parameter vector (input) u that minimize a cost function (output) $J(x,u)$ which is a scalar function of u and state vector $x(u)$. The state vector x of the system to be controlled is given by the solution of equations $E(x,u) = 0$.

For a given parameter estimation problem, the choice of which parameters to be designated as the control vector is not unique. However, the choice must be such that u determines x through the model of the system $E(x,u) = 0$.

The objectives of the optimal control theory are to obtain necessary and sufficient conditions for $J(x,u)$ to be a unique minimum, and to study the structure and properties of the equations which express these conditions (where the model $E(x,u) = 0$ naturally intervenes). The ultimate goal is to construct algorithms amenable to numerical computations for the approximation of a control u which minimizes $J(x,u)$ (such a control is termed an "optimal control").

Optimal control theory has been generalized for systems governed by partial differential equations (Lions, 1971; Bryson and Ho, 1975). This suggests a method to solve the data assimilation problem in meteorology and oceanography. The application of optimal control theory with the variational method for data assimilation has developed the adjoint technique for solving a large variety of problems.

2.2 Optimal Control Applied to Parameter Estimation

2.2.1 Mathematical Formulation of Parameter Estimation

Parameter estimation is one aspect of data assimilation. It assimilates the observations into an atmospheric or oceanic model in order to obtain an estimate for a designated model control parameter and at the same time to give an optimal state of the atmosphere or the ocean. This process is able to provide an exact consistency between the analysis and dynamics using various kinds of available datasets.

When applying optimal control theory to parameter estimation, the cost function, that measures the lack-of-fit between the observation and

the model counterpart, is the output. Inputs can be any or all of the parameters, for example, initial conditions, boundary conditions and any physical or numerical parameters that enter the model formulation. The input parameters are called the control variables. Once they are determined, they define a model trajectory in space and time. The purpose of parameter estimation is not only to know the sensitivity of the cost function to the control variables (sensitivity test), but to know how to adjust each of the control variables in order to make the cost function as small as possible (in a weighted least-squares sense).

There are two basic rules required for parameter estimation. The fields produced by an assimilation must obey some constraints. These are provided by the dynamical model and/or statistical relationships known to be satisfied by the real atmospheric or oceanographic fields. In addition, the fields produced by the assimilation must be as close as possible to the observations within the accuracy of the observations themselves, at the required spatial and temporal scales. These two requirements define the optimal control procedure in solving the parameter estimation. In its most condensed way, the procedure searches for a solution for the control parameter which makes the corresponding state of the atmosphere/ocean closest to the given observational field in a given norm.

Therefore, the mathematical formulation for finding the optimal solution can be described as follows:

$$\begin{aligned} & \text{minimize the cost function } J(x,u) \\ & \text{subject to the equality constraint } E(x,u) = 0 \end{aligned} \tag{2.1}$$

2.2.2 Weak, Strong Constraint Formalisms and the Augmented Lagrangian

Sasaki (1970) in his historical paper has introduced two formalisms, namely the *weak* and *strong* constraint methods, to enforce the constraint (2.1) in order to numerically solve the problem. The weak constraint formalism is related to the penalty method (e.g. Daley, 1991; Le Dimet and Navon, 1988), in which the constraints are imposed with a prespecified weight μ :

$$J_l(x,u) = J(x,u) + \mu \| E(x,u) \|^2 \quad (2.2)$$

where $\|E(x,u)\|$ is a suitable norm of $E(x,u)$. In this approach, the cost function is minimized while penalizing the constraint violations. If one wants to satisfy the constraint very precisely, one should specify μ to be very large. Otherwise, the constraint is only approximately satisfied if μ is chosen to be small. In other words, the value of μ controls how accurate the model E is as a representator of the observed state of atmosphere/ocean.

Taking the first variation of (2.2) to be zero with respect to the variables u and x yields the Euler-Lagrange equation:

$$\frac{\partial J_l}{\partial x}(x^*, u^*) = 0 \quad (2.3a)$$

$$\frac{\partial J_l}{\partial u}(x^*, u^*) = 0 \quad (2.3b)$$

where u^* and x^* are the optimal values of u and x .

The strong constraint formalism requires the optimal solution to satisfy the constraint $E(x,u) = 0$ exactly. A Lagrange function $L(x,u,\Lambda)$ is defined to impose this condition. This is written as

$$L(\Lambda,x,u) = J(x,u) + \{ \Lambda, E(x,u) \} \quad (2.4)$$

where $\{ , \}$ is an inner product of two vectors and Λ is a vector of as yet unknown Lagrange multipliers with the same number of components as E has equations. The Euler-Lagrange optimality conditions, which require the first variation of $L(\Lambda,x,u)$ with respect to Λ , x , and u to vanish, are given by

$$\frac{\partial L}{\partial \Lambda}(\Lambda^*, x^*, u^*) = 0 \quad (2.5a)$$

$$\frac{\partial L}{\partial x}(\Lambda^*, x^*, u^*) = 0 \quad (2.5b)$$

$$\frac{\partial L}{\partial u}(\Lambda^*, x^*, u^*) = 0 \quad (2.5c)$$

The optimal estimates x^* , u^* , and Λ^* are obtained by solving (2.5a) through (2.5c).

A combination of weak and strong constraint formalisms is the *augmented Lagrangian* (Navon and De Villiers, 1983). It has the form:

$$L_A(x,u) = J(x,u) + \mu \| E(x,u) \|^2 + \{ \Lambda, E(x,u) \} \quad (2.6)$$

In Sasaki's terminology, $E(x,u)$ is considered both as a weak constraint and as a strong one. A major advantage of this method is its ability to prevent the numerical instability associated with the ill-conditioning of the weak constraint problem (2.2) (Bertsekas, 1982; Fletcher, 1987; Bryson and Ho, 1975). Numerical instability is induced when a variable is

approaching the optimum. In this case, the procedure involves the product of a large value of the penalty parameter μ by a small vector $E(x,u)$ and is subject to considerable round-off errors. This is expressed mathematically by the condition number of the Hessian matrix approaching infinity (the role of the condition number of the Hessian matrix is discussed in section 3.2).

Another advantage of the augmented Lagrangian (2.6) is that it tends to converge faster than the strong constraint formalism (2.4) (Gill et al., 1981; Navon and De Villiers, 1983; Fletcher, 1987). It has been mathematically proved (Gill, 1981) that the weak constraint (penalty term) has the convexification property and can thus improve the global convergence properties of the strong constraint formalism. This is illustrated in section 3.3 when formulating a cost function for our parameter estimation problem.

2.3 Adjoint Method

The constrained minimization problem (2.1) can in principle be solved through its Euler-Lagrange equations either (2.3) or (2.5). But except in particular cases, no standard method exists for directly solving the system (2.3) and (2.5). For most cases, an iterative procedure has to be implemented in order to compute the optimal solution of the system numerically.

The number of control variables in meteorological/oceanographic applications is usually very large, typically upwards of 10^7 . Efficient

variational techniques are needed in order to practically and economically perform the iterative procedure. There do exist efficient minimization routines, e.g., conjugate gradient, quasi-Newton and truncated-Newton methods, all of which require at least gradient information. Therefore the optimal control procedure needs to establish the connection between the variations of the control variables and the corresponding variations of the cost function.

Among the various tools of optimal control, the adjoint equations prove to be an elegant and efficient method for computing the local gradient of a complicated function numerically for time-dependent problems. The nomenclature *adjoint* arises because one uses an operator that bears a precise relationship to the adjoint operator in a dynamical constraint. This operator arises in a natural fashion when the gradient of the functional is found.

Adjoint equations are, in essence, a tool to solve the variational data assimilation problem. The derivation of the adjoint equations can be achieved by three methods: the classical variational method, namely the derivation of the Euler-Lagrange equations (Morse and Feshbach, 1953); the control theory approach (Le Dimet and Talagrand, 1986; Lions, 1971); and the Lagrange multiplier approach (Thacker and Long, 1988; Lanczos, 1968). The approach through control theory, though mathematically elegant, has difficulties in dealing with complicated boundary conditions. The Lagrange multiplier method gives a simple and direct way to derive the equations of the adjoint formulation without recourse to the mathematics of adjoint operators. However it is inefficient to verify the

accuracy of the adjoint model using the Lagrange multiplier method when one uses a 3-D model. The illustration of the strong constraint formalism of (2.4) is an example of how the Lagrange multiplier approach works.

Let's go back to relation (2.4). Under simple regularity conditions (differentiability to a sufficient order) it can be shown (Bertsekas, 1982) that the problem of determining the minimum of $J(x,u)$ subject to the constraint $E(x,u) = 0$ is equivalent to the problem of determining the stationary point of $L(\Lambda,x,u)$. This leads to requiring the first derivatives of $L(\Lambda,x,u)$ with respect to the variables Λ , x and u to vanish, which results in a set of the Euler-Lagrange equations of (2.5).

Condition (2.5a) recovers the model itself: $E(x,u) = 0$. If the state of the atmosphere/ocean, namely x , evolves according to the model dynamics, (2.5a) is satisfied by definition. Condition (2.5b) yields the so-called adjoint equation. It is the equation governing the evolution of the Lagrange multiplier. The practical procedure to derive the adjoint equations uses partial integration of the assimilation model E . This is demonstrated in the appendix A to derive the adjoint equation for our heat flux parameter estimation problem. In general, the adjoint equations are always linear in Λ , and do not depend on the nonlinearity of the dynamical constraints. However, for nonlinear time-dependent or forward models the adjoint model depends on the state of the forward model (such as the velocity and/or temperature fields) as a function of time. In this case the time history of the forward model has to be stored in memory in order to be used for the integration of the adjoint model.

Condition (2.5c) provides the gradient information for the cost function J . Consider a simple calculation to demonstrate why this is true.

The contribution of the second term in (2.4) to the value of the Lagrange function is zero because condition (2.1) holds. So the value of $L(x,u)$ is always equal to the value of the cost function $J(x,u)$, i.e.,

$$J(x,u) = L(x,u) \quad \text{for } E(x,u) = 0$$

Then the gradient of the cost function with respect to the control variable u can be calculated as

$$\begin{aligned} \nabla_u J &= \frac{dJ}{du} \\ &= \frac{dL}{du} \\ &= \frac{\partial L}{\partial u} + \frac{\partial L}{\partial x} \frac{dx}{du} \end{aligned} \quad (2.7)$$

Condition (2.5b) gives $\partial L/\partial x = 0$ and therefore the second term vanishes. Inserting (2.4) into condition (2.7) yields:

$$\nabla_u J = \frac{\partial J}{\partial u} + \left\{ \Lambda, \frac{\partial E}{\partial u} \right\} \quad (2.8)$$

This is the gradient information of the cost function J with respect to the control variable u . It implies that it is easy to compute $\nabla_u J$ once the trajectory of Λ of the adjoint model has been determined. The gradient information (2.8) is actually a sensitivity estimator. Any of the model parameters can be designated as the control variable. Even though we may not like to change some of the control variables during the optimization process, (2.8) can provide useful information on whether these likely candidates need to be improved (if $\|\nabla_u J\|$ is large). This analysis has been used in uncertainty analysis. For example, Hall and

Cacuci (1983) and Hall (1986) applied it to assess the sensitivity of the model forecasts to changes in the model parameters and boundary conditions.

To sum up, the variational approach for solving problem (2.1) by the strong constraint formalism (2.4) involves the computation of the time evolution of the model state x by (2.5a) and the adjoint model by (2.5b). With the information of the Lagrange multiplier Λ , one can calculate the gradient of the cost function with respect to the control variables u (equation (2.5c)). This gradient is then used to provide a "descent direction" in the space of the control variables. The process is iterated until a convergence criterion has been satisfied at which the cost function has achieved its local minimum. The issue of the uniqueness of the local minimum is not addressed here.

Our approach assumes that the model is perfect. To take into account forecast model error one can use continuous variational assimilation (Derber 1989).

Many different algorithms are available for performing the minimization process (Gill et al., 1981; Tarantola, 1987; and Luenberger, 1984). However, only three types of minimization algorithms, namely conjugate-gradient, quasi-Newton and truncated-Newton (Zou et al., 1992) methods, are practical for meteorological and oceanographic applications due to the large number of control variables. In the next section, we discuss the efficiency associated with these algorithm methods (we consider only the case in which the cost function J is at least a twice-continuously differentiable function).

2.4 Minimization Algorithms

The essence of an iterative method is in how to decide whether a updated point is better than the previous point. In the case of variational data assimilation, the natural measure of this progress is provided by the value of the cost function J . It is reasonable to require a decrease in J at every iteration, and to impose the *descent condition* that $J_{k+1} < J_k$ for all $k \geq 0$, where k is the iteration number. A method that imposes this requirement is termed a *descent method*. The algorithms implementing the descent method can be described as follows.

Let u_k be the current estimate of u^* .

Step 1. [Test for convergence.] If the conditions for convergence are satisfied, the algorithm terminates with u_k as the solution.

Step 2. [Compute a search direction.] Compute a non-zero n -vector p_k , the *direction of search*.

Step 3. [Compute a step-size.] Compute a positive scalar α_k , the *step-size*, for which it holds that $J(u_k + \alpha_k p_k) < J(u_k)$.

Step 4. [Update the estimate of the minimum.] Set $u_{k+1} \leftarrow u_k + \alpha_k p_k$, $k \leftarrow k+1$, and go back to Step 1.

2.4.1 Steepest Descent Method

If the search direction is always taken as the negative of g (where $g = \nabla_u J$), i.e., $p_k = -g_k$, the algorithm becomes the *steepest-descent method*.

The steepest-descent method is the oldest and most widely known descent method. It is also one of the simplest methods for which a satisfactory analysis exists. The steepest descent process is illustrated in Figure 1 in which the cost function has two variables u_1 and u_2 . From Step 4, the update of the control variable can be written as

$$u_{k+1} = u_k - \alpha_k g_k$$

The descent condition requires that $J(u_{k+1}) < J(u_k)$, which as shown in Figure 1 is that u_{k+1} should be closer to the minimum than u_k . If we descend along the direction $-g_k$, eventually we reach a point at which $J(u)$ is a minimum along that line (denoted $J(u_{k+1})$ in Figure 1). At that point, $-g_k$ is parallel to the contours of constant J . Therefore,

$$\{g_{k+1}, g_k\} = 0 \quad (2.9)$$

where $\{ , \}$ is the inner product in the n -dimensional space. Condition (2.9) is used to find the optimum step-size α_k ; a procedure called a *line search*.

Unfortunately, a proof of global convergence for the steepest descent algorithm does not ensure that it is an efficient method. This can be seen by considering the rate of convergence of the steepest-descent method through examining the behavior of the method on a quadratic function. The reason we choose to analyze a quadratic function is that the special properties of a quadratic give a simplified analysis; furthermore, some general properties of a method can usually be deduced from its performance on a quadratic, since every smooth function behaves like a quadratic in a sufficiently small region.

Consider $J(x) = \frac{1}{2} x^T G x + c^T x$, where c is a constant vector and G is a symmetric positive-definite matrix. If the steepest-descent method is

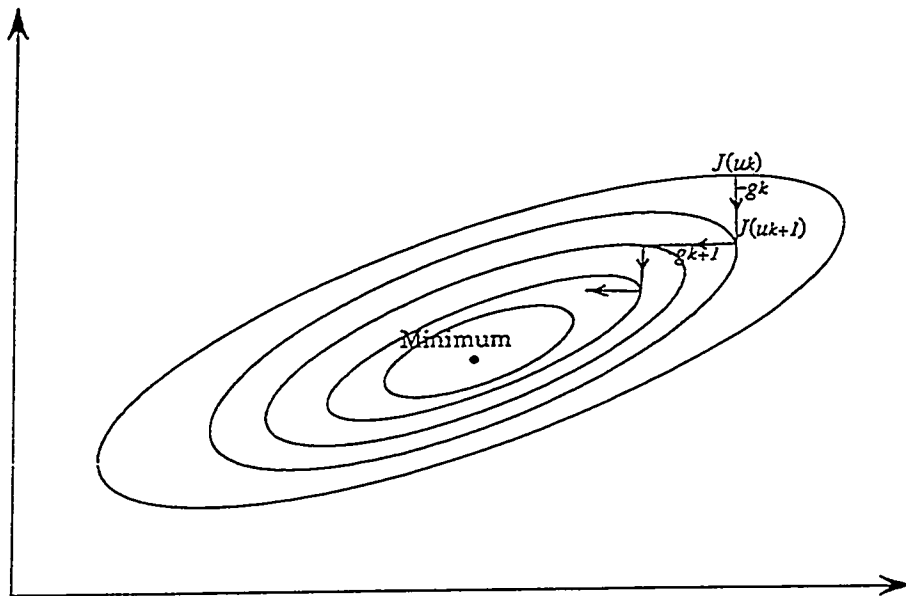


Figure 1. Illustration of the method of steepest descent and of obtaining the optimum stepsize for a two dimensional problem.

applied to J , using an exact line search to determine the step length, its rate of convergence is linear. Suppose that λ_{\max} and λ_{\min} are the largest and smallest eigenvalues of G , then it can be shown that (Luenberger, 1984)

$$\begin{aligned} J(x_{k+1}) - J(x^*) &= \frac{(\lambda_{\max} - \lambda_{\min})^2}{(\lambda_{\max} + \lambda_{\min})^2} (J(x_k) - J(x^*)) \\ &= \frac{(\kappa - 1)^2}{(\kappa + 1)^2} (J(x_k) - J(x^*)) \end{aligned} \quad (2.10)$$

where x^* is the model true solution and κ denotes $\text{cond}(G)$, the spectral condition number of G . The striking feature of this result is that the asymptotic error constant, which gives the factor of reduction in the error at each step, can be arbitrarily close to unity. For example, if κ is given to be 50 (so that G is mildly ill-conditioned), the error constant is $(49/51)^2 \approx 0.92$. As a result there is only a very small gain in accuracy at each iteration. In practice, the steepest-descent method usually needs hundreds of iterations to make very little progress towards the solution. This conclusion holds for the rate of convergence of the steepest-descent method on a general function.

It is often true, unfortunately, that a method with a linear rate of convergence is slow in convergence (Gill et al., 1981). Other methods, such as the Newton-type with second-derivatives, have a quadratic convergence to the local minimum if the Hessian matrix (the second derivative matrix of the cost function) is positive definite. We therefore expect a fast convergence rate with a Newton method.

2.4.2 Quasi-Newton and Conjugate-gradient Methods

The key for the fast convergence of the Newton method is that the Hessian matrix provides the curvature information which allows a local quadratic model of J to be developed (Gill et al., 1981). But the large computation requirements associated with the Newton method make it impossible for use in data assimilation. Hence quasi-Newton and conjugate-gradient methods have been developed (Hestenes, 1980; Gill et al., 1981; Fletcher, 1982; Luenberger, 1984).

The theory of the quasi-Newton method is based on the fact that an approximation to the curvature information can be computed without explicitly forming the Hessian matrix and therefore, only the first derivatives are required. The quasi-Newton method has, however, only a superlinear rate of convergence (Gill et al., 1981). Each Hessian approximation produces a specified curvature along the particular search direction. At a given iteration, the matrix of the Hessian approximation is a low-rank modification of the matrix from the previous iteration (Luenberger, 1984). The quasi-Newton method still requires the same storage size as the Hessian matrix and therefore is an option which is not feasible for large-scale problems because of memory limitations.

In contrast to the quasi-Newton method, the conjugate-gradient method generates search directions without storing a matrix (Hestenes, 1980). Each search direction p_k is computed by using the current and previous gradients g_k and g_{k-1} and the previous conjugate direction p_{k-1} , i.e.,

$$p_k = -g_k + \beta_k p_{k-1}$$

where $\beta_k = \frac{g_k^T(g_k - g_{k-1})}{p_{k-1}^T(g_k - g_{k-1})}$. The search directions $\{p_j\}$, $j = 0, \dots, k$, are mutually conjugate, in the sense that for $i = 0, \dots, k$ and $j = 0, \dots, k$

$$p_i^T G p_j = 0, \quad i \neq j$$

where G is a positive definite symmetric matrix. The conjugate-gradient method with an exact linear search is n -step superlinearly convergent (Luenberger, 1984), i.e.,

$$\lim_{j \rightarrow \infty} \frac{\|u_{n+j+n} - u^*\|}{\|u_{n+j} - u^*\|} = 0$$

However, in practice rounding errors may destroy the superlinear convergence property, so that the conjugate-gradient method is nearly always linearly convergent (Gill et al., 1981). Although this type of algorithm is far from ideal, regarding to its restarting strategy and convergent property (Beale, 1972; Liu and Nocedal, 1988), it is currently the *only* reasonable method available for data assimilation in meteorology and oceanography, where the number of the control variables is extremely large.

Navon and Legler (1987) have tested several conjugate-gradient algorithms for large-scale minimization problems in meteorology. They concluded that for most applications the Shanno-Phua (1980) limited-memory quasi-Newton conjugate-gradient algorithm is the most efficient algorithm from the viewpoints of both computational complexity and storage requirements. Limited-memory quasi-Newton conjugate-gradient methods can be viewed as extensions of the conjugate-gradient method, in

which additional storage is used to accelerate convergence. They also can be viewed as implementations of quasi-Newton methods, in which storage is restricted. These methods are based upon the idea of computing the direction of search p_k as $-Mg_k$, where M is a positive-definite matrix obtained by updating the identity matrix with a limited number of quasi-Newton corrections (Nazareth, 1979). Although the direction of search is equivalent to the product of a matrix and a vector, the matrix is never stored explicitly; rather, only the vectors that define the updates are retained (Shanno, 1978). Different methods can be developed by varying the number of updating vectors stored and choosing different quasi-Newton updating formula. Shanno and Phua's CONMIN algorithm (Shanno and Phua, 1980) was implemented with the "two-step" limited-memory BFGS (Broyden-Fletcher-Goldfarb-Shanno) quasi-Newton update (e.g. Gill et al., 1981; Luenberger, 1984). A detailed description of the CONMIN algorithm was given in Legler et al. (1989) and Legler and Navon (1991).

The conjugate-gradient type algorithms provide fast functional reduction within the first few iterations when dealing with a well-conditioned problem, in which case the eigenvalues of the Hessian are clustered into groups of approximately equal value (Gill et al., 1981). In particular, for linear dynamics the convergence will occur in m ($m \leq n$) iterations, where m is the number of distinct eigenvalues of the Hessian and n is the number of control variables. In fact the rate of the convergence depends to a large extent on several factors. If in an application the algorithm converges too slowly, it can either be due to the

adverse effects of rounding errors which cause the computed directions to lose conjugacy; or due to the ill-conditioned Hessian which has a very broad eigenvalue structure; or due to noisy data which can not reflect the model dynamics well (Gill et al., 1981; Thacker, 1988).

In summary, one requires adequate preconditioning (or scaling) techniques to speed up convergence. For experience with various algorithms, see a recent paper by Navon et al. (1992).

3. Estimating the Heat Flux Distribution over the Tropical Pacific Ocean by the Adjoint Technique

As discussed in the previous section, when the variational adjoint method is applied to parameter estimation, a solution is sought by best fitting the model state to the observations within the observational space-time domain. In this section, we apply this technique to determine the heat flux distribution over the tropical Pacific ocean by assimilating the SST observations. A variational adjoint procedure has four parts: an oceanic model (including the representation of dynamics and thermodynamics in the physical model), an adjoint model whose solution yields Lagrange multiplier vector fields, a formula for calculating the gradient of the cost function with respect to the control parameters, and an efficient large-scale unconstrained minimization algorithm which iteratively performs the procedure to locate the local minimum, which is assumed to be unique.

3.1 Oceanic Model

3.1.1 Choice of Models in the Tropical Oceans

Different numerical models are available to study the ocean dynamics/thermodynamics in the tropical regions. On the one hand, we have simple models such as the reduced-gravity models (Busalacchi and

O'Brien, 1980; Schopf and Cane, 1983; Zebiak and Cane, 1987; Seager et al. 1988), which have demonstrated the relevance of the linear dynamics to the observed seasonal and interannual variability of the tropical Pacific. While on the other hand, we might select a general circulation model (GCM) (Philander and Sieglar, 1985; Philander and Hurlin, 1988; Harrison et al. 1989). Although a GCM is the most complex model existing, it always presents difficulties in the interpretation of its behavior due to the number and complexity of the processes involved.

Surface heat flux itself is a complicated process in which radiative, latent and sensible heat fluxes all contribute to the changes of the resulting flux pattern. No one has systematically studied the variability of the heat flux by assimilating observed data into an oceanic model. As an initial work in doing this, we hope that the estimated heat flux pattern can be explained both from the air-sea interaction viewpoint and from the thermodynamical viewpoint inherent in the model. Therefore, a reduced-gravity model with thermodynamics is chosen which is capable of representing the main mechanisms of the dynamics/thermodynamics processes. A suitable model is Zebiak and Cane's reduced-gravity model with a constant-depth surface-layer (Zebiak and Cane, 1987).

The model consists of two layers above the thermocline with the same constant density. The ocean below the thermocline, with a higher density, is assumed to be sufficiently deep so that its velocity vanishes. The upper of the two active layers is a fixed-depth surface layer. These two layers are coupled through entrainment/detrainment at their interface and through frictional horizontal shearing. The adoption of the linear,

frictional, surface layer is based on the following considerations (Cane, 1979; Zebiak, 1985). The model should not be expected to give a good estimate for the near-surface current field if the entire upper layer is taken to be homogeneous. We expect that, in reality, a turbulent well-mixed layer exists near the surface and accordingly, nearly all of the frictionally induced vertical transport in the upper ocean should occur in this region alone. Additionally, the air-sea interaction process sufficiently changes the ocean thermodynamics near the surface. In attempting to simulate changes in sea surface temperature it is important to include the physics of the near-surface region. By this reasoning it follows that the wind stress is applied only to this surface layer; in this sense, *this layer plays the role of the ocean mixed layer*.

3.1.2 Description of the Physical Model

As discussed above, the oceanic model describes the linear dynamics of a homogeneous upper layer, overlying a motionless deep layer, on an equatorial β -plane. A constant-depth, frictional, linear surface layer is added to this layer (Figure 2). Thermodynamics are included only in this surface layer. We assume that there is no density difference across the base of the surface layer, i.e., the surface layer is treated as a part of the upper layer. Following Seager et al. (1988), the equations for the depth-averaged currents are :

$$\frac{\partial u_1}{\partial t} - \beta y v_1 = -g \frac{\partial h}{\partial x} + \frac{\tau^x}{\rho_0 H} + A \nabla^2 u_1 \quad (3.1a)$$

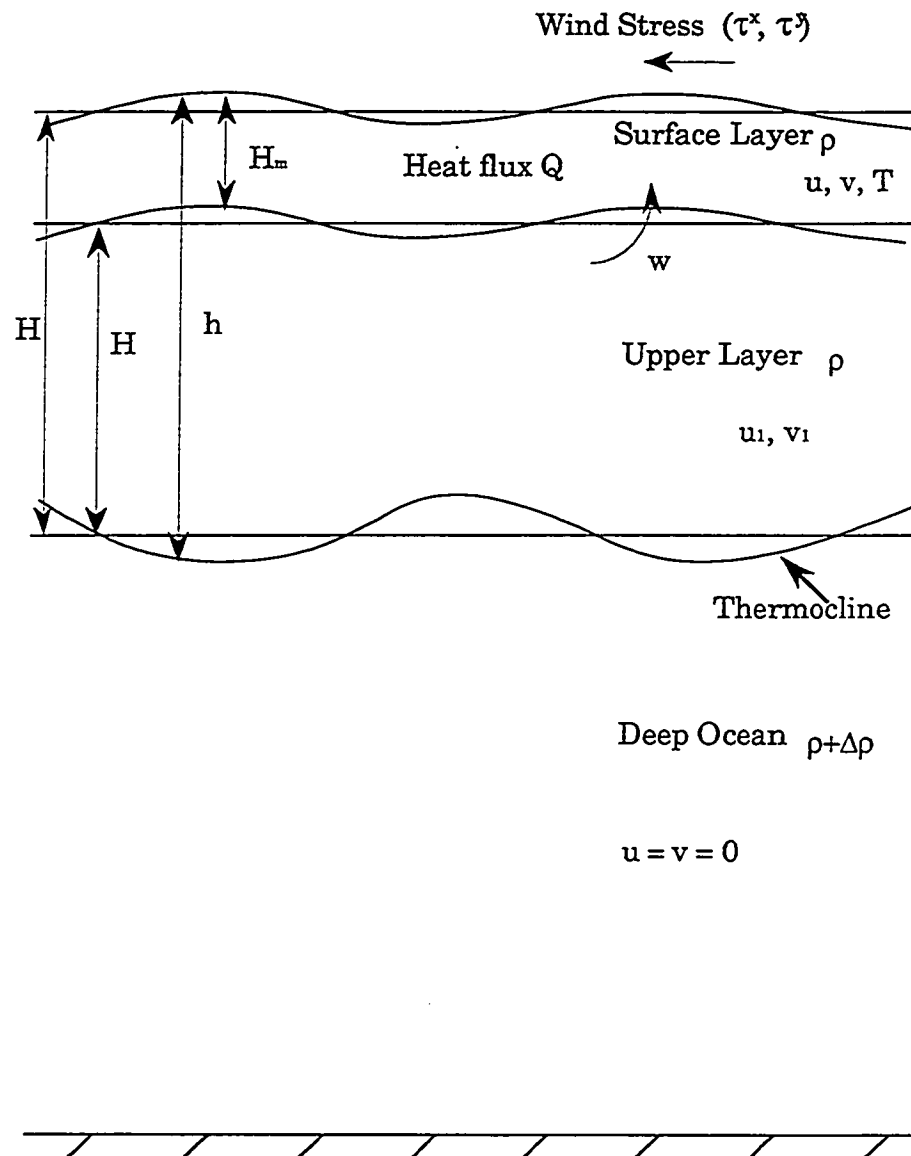


Figure 2. The vertical structure of the reduced-gravity model with thermodynamics. The model has two layers above the thermocline with the same constant density. The upper of the two active layers is a constant depth surface layer which is acted upon directly by the wind stress.

$$\frac{\partial v_1}{\partial t} + \beta y u_1 = -g \frac{\partial h}{\partial y} + \frac{\tau^y}{\rho_0 H} + A \nabla^2 v_1 \quad (3.1b)$$

$$\frac{\partial h}{\partial t} + H \left(\frac{\partial u_1}{\partial x} + \frac{\partial v_1}{\partial y} \right) = 0 \quad (3.1c)$$

where (u_1, v_1) are the horizontal velocity components of the depth-averaged currents; h is the total layer thickness; H is the mean depth of the layer; ρ_0 is the density of water; and A is the horizontal viscosity coefficient. The wind stress is calculated by the aerodynamic bulk formula:

$$(\tau^x, \tau^y) = \rho_a c_D |U| (U, V)$$

where ρ_a is the density of air; c_D is the wind stress drag coefficient; U is the wind speed vector; and (U, V) are the components of the wind velocity.

The equations governing the shear between the surface layer and the lower upper-layer are represented by the Ekman dynamics:

$$r_s u_s - \beta y v_s = \frac{\tau^x}{\rho_0 H_m} \quad (3.2a)$$

$$r_s v_s + \beta y u_s = \frac{\tau^y}{\rho_0 H_m} \quad (3.2b)$$

where (u_s, v_s) are the frictional velocity components; r_s is the friction coefficient; and H_m is the depth of the surface layer over which the stress is applied and is taken to be a constant by assumption.

The solution of equations (3.1a-c) is the sum of the Ekman transport (u_E, v_E) and the pressure-gradient-driven current (u_p, v_p) , i.e.,

$$(u_1, v_1) = (u_E, v_E) + (u_p, v_p) \quad (3.3a)$$

The total surface-layer velocity (u, v) consists of the shear flow (u_s, v_s) and the pressure-gradient-driven current (u_p, v_p) , i.e.

$$(u, v) = (u_s, v_s) + (u_p, v_p) \quad (3.3b)$$

The total Ekman transport calculated from (3.1) and (3.2) should be the same. This gives the relation

$$(u_E, v_E) = (u_s, v_s) \frac{H_m}{H} \quad (3.3c)$$

The surface-layer current (u, v) can then be derived from relations (3.3a-c), which is

$$(u, v) = (u_s, v_s) + (u_1, v_1) - (u_s, v_s) \frac{H_m}{H} \quad (3.4)$$

From this, the entrainment velocity can be calculated from the divergence of the surface-layer current field,

$$w_e = H_m \left(\frac{\partial u}{\partial x} + \frac{\partial v}{\partial y} \right) \quad (3.5)$$

The thermodynamics describe the evolution of temperature in the surface layer. The evolution of SST is governed by horizontal advection, vertical entrainment, surface heating and horizontal diffusion (Seager et al. 1988) and is given by:

$$\frac{\partial T}{\partial t} + u \frac{\partial T}{\partial x} + v \frac{\partial T}{\partial y} = \frac{Q}{\rho_0 c_p H_m} + \frac{M(w_e)(T_d - T)}{H_m} + A_T \nabla^2 T \quad (3.6)$$

where T is the sea surface temperature; c_p is the specific heat; A_T is the horizontal diffusion coefficient. The net surface heat flux Q , which is a function of time and space, involves a field of parameters to be determined by the variational adjoint process. The second term on the right hand side is the bulk representation of the turbulent heat flux which occurs when the surface layer entrains fluid from the layer below. The quantity, T_d , is the subsurface water temperature. Entrainment brings the cooler

subsurface water to the surface and cools the surface mixed layer. Detrainment, however, warms up the subsurface water but does not change the temperature in the surface directly. So the Heaviside step function $M(w_e)$ is introduced, which is defined to be zero for w_e less than zero and equal to w_e for w_e greater than or equal to zero.

As is common in a reduced-gravity model, the surface layer pressure gradient is assumed to vary with the thermocline depth alone. This excludes the effect of the temperature change on the surface pressure gradient. It cannot be justified rigorously since the assumption that the influence of the SST changes on the pressure gradient is usually negligible may not hold universally. Fortunately by assuming this, the model physics are greatly simplified since dynamics and thermodynamics become decoupled.

Equations (3.1), (3.2) and (3.6) describe the evolution of the current fields and the upper-layer thickness. These dynamic fields will not be affected by any change of the SST at all, although they have a significant influence on the SST evolution through the advection process. In other word, the changes of the SST do not have a feedback into the dynamical field. Since we are going to assimilate the SST observations only, the optimal distribution of the surface heat flux will not affect the dynamical model. This further simplifies the parameter estimation problem since the constraints of the system reduce to the SST equation only and the SST evolution equation can be viewed as a linear equation with non-constant coefficients. The surface current structure (3.4) can be determined by the equations (3.1) and (3.2). These currents along with the thermocline depth

are available for one year after the model has been fully spun up. They are used to compute the advective components in the temperature evolution equation.

3.2 Importance of the Scaling in Variational Procedure

Before we proceed further, we would like to present an important issue in variational procedure: *scaling*. We discuss the role of scaling in determining the condition number of the Hessian and therefore in determining the convergent rate of the minimization algorithms. Many opinions on the inefficiency of the variational adjoint method for data assimilation exist. These can be attributed to no or poor scaling of the model problem (Luenberger, 1981; Gill et al. 1981; Navon and De Villiers, 1983; Thacker, 1989; and Zou et al. 1992).

3.2.1 The Role of the Hessian

The conjugate-gradient method implemented as a memoryless quasi-Newton method is a modified Newton method (approximating Newton's method without evaluating the inverse of the Hessian). According to the general theory of modified Newton methods, it is the condition number of the Hessian that influences the convergence properties of these algorithms (Gill et al., 1981). The condition number of a matrix, which is the ratio of its largest to its smallest eigenvalues, represents the singularity of the matrix. If the condition number is large,

the matrix is ill conditioned (almost singular); and if it is close to unity, the matrix is well conditioned. As discussed by Thacker (1989), an ill-conditioned Hessian indicates that some model variables are poorly determined by the data. This can occur because of inappropriately scaled variables in the model. This can be corrected and is discussed in this section. In addition, the ill-condition may be due to inadequate observations. This second possibility was studied by Thacker (1988) in which bogus data are introduced to bias the fit toward some preferred solution. It is also examined in our study.

Experimental evidence has verified that at least an initial well-scaled functional can lead to a significant improvement in the performance of the memoryless quasi-Newton conjugate-gradient algorithms (Gill et al, 1981; Yu and O'Brien, 1992). The memoryless BFGS (Broyden-Fletcher-Goldfarb-Shanno) update procedure does, in general, give a more favorable condition number if the cost function is well scaled and thus the eigenvalues of the Hessian are near unity. Therefore, the condition number of the Hessian matrix has a substantial influence on the convergence of the descent algorithm.

Let's consider the shape of the cost function and ask how it relates to the condition number of the Hessian. The shape of the cost surface is determined by the eigenvalues and eigenvectors of the Hessian: the eigenvectors are in the directions of the principal axes of the ellipse of constant cost and the eigenvalues determine the lengths of the radii along these axes. For a well-conditioned problem (eigenvalues equal to unity), all radii of the constant-cost contour are equal, in which case the

algorithm converges in one iteration and all model variables are equally well determined. As the condition number increases, the contours become more elongated.

Suppose the condition number is large so that the cost contours are highly elliptical. The relative change in the cost function due to a perturbation of variables will vary radically depending on the direction of the perturbation. The directions that produce the largest and smallest changes in the cost function value are the eigenvectors associated with the largest and smallest eigenvalues. When the Hessian is ill-conditioned, the cost function may change very slowly along an eigenvector (or direction) associated with a near-zero eigenvalue. In this case, the cost function is very flat in this particular direction. The algorithm becomes inefficient since the changes in the cost function that "should" be significant may be lost amongst the rounding error. An ill-conditioned Hessian of the solution is thus a form of bad scaling, in the sense that similar changes in the variable do not lead to similar changes in the cost function.

The conditioning of the Hessian matrix can be improved by the technique of scaling. All the methods of scaling can be divided into three groups: scaling the variable, scaling the cost function, scaling the constraints (Gill et al., 1981). Here we use the technique of variable scaling. For an in-depth analysis of the adjoint of the Hessian model (second order adjoint) and its impact on scaling, see Wang et al. (1992).

3.2.2 Variable scaling

Variable scaling transforms the variables from units that typically reflect the physical nature of the problem to units that display certain desirable properties for the minimization process (Gill et al., 1981; Navon and De Villiers, 1983). The basic rule of variable scaling is to make all the variables in the scaled problem to be of order unity, so that each variable has a similar weight during the optimization. If typical values of all the variables are known, a problem can be transformed so that the variables are all the same order of magnitude.

Normally, only linear transformations of the variables should be used for scaling. The most commonly used transformation has the form

$$z = Dy$$

where $\{z_j\}$ are the original variables, $\{y_j\}$ are the transformed variables, and D is a constant diagonal matrix. By doing this, the derivatives of the cost function are also scaled. If g_y and H_y represent the gradient vector and Hessian matrix of the transformed problem respectively, the relationships of the derivatives of the original to the transformed problem are given by

$$g_y = Dg; \quad H_y = DHD$$

It is obvious that there is a substantial effect on the Hessian when variable scaling is applied. This will in turn significantly change the condition number of the Hessian and hence improve the convergence rate of optimization algorithms.

3.2.3 Choosing the Scales of the Physical Variables

All physical variables in the SST evolution equation should be scaled because the SST equation is the physical constraint in the minimization process. By scaling the variables, the constraints are scaled implicitly.

The data-sets used in this research are the climatological SST and climatological winds. We therefore concentrate on studying the seasonal variability of the surface heat flux in the tropical Pacific ocean. It follows that the suitable time scale for the SST evolution should be

$$[t] = 12 \text{ months} \quad (3.7)$$

The seasonal variations of the SST over the tropical Pacific are mainly due to the advection and surface thermal forcing, which both occur in a wide spatial domain. The spatial scales for the temperature are then chosen as

$$[x] = \text{longitude extension of model domain}$$

$$(\text{Pacific zonal basin scale}) \quad (3.8)$$

$$[y] = \text{latitude extension of model domain} \quad (3.9)$$

As for the SST scale, we choose

$$[T] = T_0 \quad (3.10)$$

where $T_0 = 29^\circ\text{C}$, representing the climatological SST value in the equatorial warm pool region.

The maximum strength of climatological zonal surface current computed from our dynamical model is less than 70 cm/sec. We scale the zonal current component by

$$[u] = 60 \text{ cm/sec} \quad (3.11)$$

in order to have them all be the same order of magnitude. The corresponding scale for the meridional surface current is

$$[v] = [u] \times \frac{[y]}{[x]} \quad (3.12)$$

which can be deduced from the continuity equation (3.5). Equation (3.5) also gives the upper bound of the upwelling, which is

$$[w_e] = [H] \times \frac{[u]}{[x]} \quad (3.13)$$

where $[H]$ represents the value of H_m .

Using the scales of (3.7) - (3.13), the SST equation (3.6) can be non-dimensionalized as (all primes have been dropped for convenience)

$$\frac{\partial T}{\partial t} + \delta_A \left(u \frac{\partial T}{\partial x} + v \frac{\partial T}{\partial y} \right) = \delta_Q Q + \delta_A M(w_e) (T_d - T) + \delta_{vx} \frac{\partial^2 T}{\partial x^2} + \delta_{vy} \frac{\partial^2 T}{\partial y^2} \quad (3.14)$$

where the δ 's are the scaling parameters whose values are given by

$$\begin{aligned} \delta_A &= \frac{[u][t]}{[x]} \\ \delta_Q &= \frac{[Q][t]}{\rho_0 c_p H_m [T_0]} \\ \delta_{vx} &= \frac{A_T [t]}{[x]^2} \\ \delta_{vy} &= \frac{A_T [t]}{[y]^2} \end{aligned}$$

3.3 Formulating the Cost Function Using the *a priori* Information

In variational analysis, the solution of a problem is sought by minimizing the cost function, which measures the distance between the

observations and the corresponding model outputs. The model equations serve as the constraints. Considering the linear dynamics of our model, we choose a least-squares fitting for the cost function corresponding to a L_2 Euclidean norm. The cost function is then defined as the misfit of the model and the observed SST, which can be written as

$$J_T = \frac{1}{2} \int_{\Sigma} (T - \hat{T})^T \mathbf{K}_T (T - \hat{T}) d\sigma \quad (3.15)$$

where the superscript T denotes transpose; the carrot ($\hat{\cdot}$) denotes observed data. The integral is summed over the observational space-time domain Σ . \mathbf{K}_T is a weighting matrix and theoretically should be taken to be the inverse of the observation error covariance matrix. By assuming that the errors in the data are uncorrelated and equally weighted, \mathbf{K}_T is reduced to a unit matrix multiplied by a constant K_T . The data used in this study are the climatological SST which provide a total of twelve monthly-mean SST patterns.

A unique minimum of (3.15) exists when two conditions are satisfied. First, it is required that the problem be well-determined (Menke, 1984). Theoretically this can occur if the number of unknowns is exactly equal to the number of observations. However this is not always true in the applications of data assimilation in meteorology/oceanography. Even if there is exactly the information to determine the model parameters, a noisy model-data fit can result when there are insufficient independent estimates to reduce the uncertainties introduced by observational errors (Thacker, 1988). The second condition is that the cost function (3.15) should be convex within the domain of definition of the parameters

(Carrera and Neuman, 1986a and 1986b). This requirement is satisfied only if the Hessian matrix is positive definite. The Hessian of the cost function (3.15) is

$$\frac{\partial^2 J_T}{\partial Q^2} = \int_{\Sigma} K_T \left[\left(\frac{\partial T}{\partial Q} \right)^T \left(\frac{\partial T}{\partial Q} \right) + (T - \hat{T})^T \frac{\partial^2 T}{\partial Q^2} \right] d\sigma \quad (3.16)$$

The first term on the right-hand side is positive semi-definite and the second term could be negative. Therefore, one can not guarantee the positive definiteness of the Hessian in (3.16) and so it is possible to find more than one solution of the minimization problem (3.15). In this case, although the data provide information about the unknown parameters, they do not provide enough to determine them uniquely. See a study of the second order adjoint method by Wang et al. (1992).

A strategy is proposed here to circumvent the difficulties associated with (3.15), that is, adding *a priori* information (Menke, 1984; Thacker, 1988). The *a priori* knowledge is not the information based on the observations but some conditions one expect to have in general. It plays the role of bogus data, which are used to supplement the insufficient real data that are available. Its usefulness is in the great reduction of the range of possible solutions - or even causing the solution to be unique (Carrera and Neuman, 1986b).

Defining a new term J_Q for our problem, which is

$$J_Q = \frac{1}{2} K_Q \int_{\Sigma} (Q - \bar{Q})^T (Q - \bar{Q}) d\sigma \quad (3.17)$$

where the tilde ($\tilde{\cdot}$) denotes the guess field and K_Q is the computational weight. Adding (3.17) to (3.15), we then have a new cost function, J , which is

$$J = J_T + J_Q \quad (3.18)$$

From the mathematical point of view, the term J_Q functions as the penalty term in which \tilde{Q} corresponds to shifts of the origin and K_Q controls the size of the penalty (Fletcher, 1987).

A priori information can take many forms and in each case it quantifies expectations about the character of the solution that are not based on the actual data (Menke, 1984). We define the parameter \tilde{Q} in (3.17) taken to be the value of the parameter Q at previous iteration. By doing so, the term J_Q measures the closeness of the estimated parameters within two consecutive iterations of the minimization process. It then penalizes the departures from the previous estimate when searching the optimal solution, which is the *a priori* prejudice towards the smoothness. With this *a priori* information, the Hessian of (3.18) becomes

$$\frac{\partial^2 J}{\partial Q^2} = \frac{\partial^2 J_T}{\partial Q^2} + K_Q \mathbf{I} \quad (3.19)$$

where \mathbf{I} is a unit matrix. Clearly, the second term on the right-hand side is positive definite. Although one can not guarantee the positive definiteness of (3.18), the inclusion of the *a priori* information increases the probability that this will be the case and therefore enhances the convexity of the cost function J in (3.18). Carrera and Neuman (1986b) have studied several examples which clearly show the *a priori* information on the formation of the unique solution. This problem is also

addressed by Bennett and Miller (1991) in which an explicit contribution from the initial condition was included in the formation of the cost function in order to ensure a unique, low-noise forecast.

Actually, the term J_Q not only provides the *a priori* information for the estimated parameter but accelerates the convergence of the minimization algorithm (Bertsekas, 1982; Fletcher, 1987; Thacker, 1988). An ill-conditioned Hessian, which may be due to inadequate observations, has a severe impact on the algorithm efficiency (Thacker, 1988). The *a priori* information serves as bogus data and hence increases the number of observations. Thus adding the term J_Q can improve the conditioning of the Hessian with the practical benefit of speeding up the convergence of the minimization algorithm.

The minimization problem will not be altered if (3.18) is scaled by K_T . It follows that the cost function has the form

$$J(T, Q) = \frac{1}{2} \int_{\Sigma} (T - \hat{T})^T (T - \hat{T}) d\sigma + \frac{1}{2} K_Q' \int_{\Sigma} (Q - \tilde{Q})^T (Q - \tilde{Q}) d\sigma \quad (3.20)$$

where $J = \frac{J'}{K_T}$ and $K_Q' = \frac{K_Q}{K_T}$. The latter represents the relative weight. A similar cost functional was used by Zou et al. (1992) to estimate optimal nudging parameters.

3.4 Adjoint Model and the Variational Procedure

The natural way to enforce the SST equation (3.14), which serves as a strong constraint, is by introducing a set of Lagrange multipliers λ_T . The inclusion of the *a priori* information, as the penalty in the cost

function (3.20), allows the variational approach to incorporate both strong and weak constraints into a common least squares framework. As mentioned in section 2.2, this leads to the formation of the augmented Lagrange function (Navon and De Villiers, 1983), which is

$$\begin{aligned}
L(T, Q, \lambda_T) = & \frac{1}{2} \int_{\Sigma} (T - \hat{T})^T (T - \hat{T}) \, d\sigma + \frac{1}{2} K_Q' \int_{\Sigma} (Q - \bar{Q})^T (Q - \bar{Q}) \, d\sigma \\
+ \int_{\Sigma} \lambda_T \left\{ \frac{\partial T}{\partial t} + \delta_A \left(u \frac{\partial T}{\partial x} + v \frac{\partial T}{\partial y} \right) + \delta_A M(w_e) (T - T_d) - \delta_Q Q - \delta_{vx} \frac{\partial^2 T}{\partial x^2} - \delta_{vy} \frac{\partial^2 T}{\partial y^2} \right\} d\sigma
\end{aligned} \tag{3.21}$$

The constrained optimization problem is now replaced by a series of unconstrained problems with respect to T , Q , and λ_T . But not all the parameters are independent. The variations of the control variable Q will be determined by the optimization process and the subsequent variations of the dependent variable T will be given by the SST equation. As discussed in section 2.2, the condition of the stationary point of the Lagrange function $L(T, Q, \lambda_T)$ requires that the first variation of $L(T, Q, \lambda_T)$ with respect to all the variables vanishes. We have shown that the condition

$$\frac{\partial L(T, Q, \lambda_T)}{\partial \lambda_T} = 0$$

recovers the original SST equation. Combining the scaled continuity equation with equation (3.14), one can write the SST equation as

$$\frac{\partial T}{\partial t} + \delta_A \left\{ \frac{\partial(Tu)}{\partial x} + \frac{\partial(Tv)}{\partial y} \right\} - \delta_{vx} \frac{\partial^2 T}{\partial x^2} - \delta_{vy} \frac{\partial^2 T}{\partial y^2} - \left\{ \begin{array}{l} \delta_A T_d w_e \text{ for } w_e \geq 0 \\ \delta_A T w_e \text{ for } w_e < 0 \end{array} \right\} = \delta_Q Q \tag{3.22}$$

The condition that

$$\frac{\partial L(T, Q, \lambda_T)}{\partial T} = 0$$

results in the adjoint equation, which is given by

$$\begin{aligned} \frac{\partial \lambda_T}{\partial t} + \delta_A \left\{ \frac{\partial(u\lambda_T)}{\partial x} + \frac{\partial(v\lambda_T)}{\partial y} \right\} + \delta_{vx} \frac{\partial^2 \lambda_T}{\partial x^2} + \delta_{vy} \frac{\partial^2 \lambda_T}{\partial y^2} \\ - \begin{cases} \delta_A \lambda_T w_e & \text{for } w_e > 0 \\ 0 & \text{for } w_e \leq 0 \end{cases} = T - \hat{T} \end{aligned} \quad (3.23)$$

The derivation of the adjoint equation and the associated boundary conditions can be found in appendix A. Comparing equations (3.22) with (3.23), one can find that the adjoint equation has a similar form to the SST equation except for two prominent features. The driving factor in the adjoint equation is the square root of the data misfit, in contrast to the surface heat flux in the SST equation. In addition, the diffusion term in the adjoint equation has an opposite sign to that in the SST equation. This requires that the integration of the adjoint equation should be backward in time in order to satisfy the stability condition of a well-posed problem. Therefore the Lagrange multiplier provides the information about how different the observations and the model counterparts are. This information is transmitted back to the initial time of the assimilation cycle to influence the reconstruction of the model state.

The condition that

$$\frac{\partial L(T, Q, \lambda_T)}{\partial Q} = 0$$

gives the equation which is:

$$\dot{K}_Q(Q - \tilde{Q}) - \lambda_T = 0 \quad (3.24)$$

As is proved in (2.7) - (2.8), the left hand side of (3.24) is actually the gradient of the cost function J with respect to the control variables Q , which is:

$$\nabla_Q J = K'_Q(Q - \tilde{Q}) - \delta_Q \lambda_T \quad (3.25)$$

Equations (3.22) and (3.23) can be performed iteratively with a descent algorithm which uses the gradient information (3.25) to search an optimal control field Q . The value of \tilde{Q} is chosen in a way that it equals to the most recently computed Q .

With the equations (3.22) and (3.23) and the gradient information (3.25), an iterative procedure can then be formed as follows: (i) Start with a first-guess for the control variable Q . (ii) Integrate the SST equation (3.22) forward in time and store the values of the field variables at each time step. (iii) Compute the data misfits. (iv) Integrate the adjoint equation (3.23) backward in time to solve for the Lagrange multiplier vector fields. (v) Use (3.25) to compute the gradient of the cost function and then perform the CONMIN large-scale unconstrained minimization routine to adjust the value of the control variable Q . (vi) Repeat steps (ii) (with the new estimate of the control Q), (ii) and (iv) until some convergence criteria are satisfied.

Note that in the integration of both the SST equation and the adjoint equation, one needs to know the dynamical fields such as the currents and thermocline depth. So the trajectory of the dynamical model (3.1), (3.2) and (3.5) must be computed in advance in order to perform the

minimization process. In the next section, we discuss the numerical techniques used in the model integration.

3.5 Numerical Models

In section 3.1, we have shown that the decoupling between dynamics and thermodynamics greatly simplifies the problem of estimating of the surface heat flux distribution over the tropical Pacific ocean. It allows the dynamical model integration and the variational procedure to be handled separately. The physical processes involved in the dynamical and thermodynamical models are so different that the associated temporal and spatial scales are different.

3.5.1 Dynamical Model

The dynamical model is governed by the wave dynamics. For the chosen model domain which extends from 25°S to 25°N in latitude and from 120°E to 70°W in longitude, all possible equatorially trapped waves, e.g., Kelvin, Rossby, Yanai and gravity waves, can be excited by the applied wind forcing (Moore and Philander, 1978). The temporal and spatial resolutions of the numerical model must be chosen appropriately in order to resolve all the possible waves and also to make the model integration numerically stable.

We choose the spatial interval for the dynamical model to be: $\Delta x = \Delta y = 0.5$ degree and the time step to be: $\Delta t = 15$ minutes. The model (3.1),

(3.2) and (3.5) are driven by the FSU climatological monthly-mean winds (Stricherz et al, 1992), which are projected into each time step by a linear interpolation and into $0.5^{\circ} \times 0.5^{\circ}$ spatial grids by cubic-spline interpolation. The values of the numerical parameters used in the model integration are listed in Table 1. It takes about 12 years for the model to reach a periodic constant seasonal cycle. The main seasonal variability of the dynamical fields in the tropical Pacific ocean has been successfully captured when the periodic state is established. The currents and the upper layer thickness of the 16th year are saved every two days to be used in the minimization process.

3.5.2 Data

The data used in this study are the climatological SST and winds. The Shea-Trenberth-Reynolds (STR) monthly SST climatology (Shea et al., 1990) was derived from a 30-year CAC (Climate Analysis Center) SST climatology. It provides a fairly smoothed coverage over the global ocean. The spatial resolution is 2° latitude by 2° longitude.

The wind monthly climatology is from the *Atlas of Florida State University Tropical Pacific Winds for TOGA 1966-1985* (Stricherz et al., 1992). This atlas was constructed from all the available ship observations over 20 years (includes merchant ships, buoys, and other marine observing stations). It gives the monthly-mean pseudo-stress (defined as the wind components multiplied by the wind magnitude) with $2^{\circ} \times 2^{\circ}$ spatial resolution in the tropical Pacific region, 30°S to 30°N and 120°E to 70°W .

Table 1. The values of the model parameter used in the model integration

Parameter	Value	Remarks
H	150 m	mean depth of upper-layer
H_m	50 m	depth of the constant surface layer
g'	3.7×10^{-2}	reduced gravity
c_D	1.5×10^{-3}	wind stress drag coefficient
ρ_a	1.2 kg m^{-3}	density of air
ρ_0	1025 kg m^{-3}	density of seawater
R	$6.3784 \times 10^6 \text{ m}$	radius of earth
Ω	$0.729 \times 10^{-4} \text{ sec}^{-1}$	angular rotation rate of earth
c_p	$3.994 \times 10^3 \text{ J (kg } ^\circ\text{C)}^{-1}$	specific heat
A	$750 \text{ m}^2 \text{ sec}^{-1}$	coefficient of horizontal viscosity
A_T	$2000 \text{ m}^2 \text{ sec}^{-1}$	coefficient of horizontal thermal diffusion
r_s	0.5 (day)^{-1}	dissipation coefficient

3.5.3 Variational Procedure

Advection and surface heating are the dominant components responsible for the thermodynamical variability in the oceanic upper layer. They can effectively occur over the whole basin. The large spatial scale associated with the advection and the thermal forcing permits us to choose a relatively low resolution while still be able to resolve the main features of the SST seasonal variability. Based on this reasoning, the spatial intervals for the SST and the adjoint model are chosen to be: $\Delta x = \Delta y = 2$ degrees. Correspondingly, one can choose a longer time-step which is: $\Delta t = 6$ hours. In the variational adjoint procedure, we need to perform one forward SST model integration and one backward adjoint integration in order to compute the gradient of the cost function. Several such iterations are required to obtain the minimum value of the cost function. By choosing a coarse resolution, the computation time is greatly reduced.

The estimated parameters Q are a function of time and space since the physical emphasis is to study the seasonal variability of heat flux. In order to perform the minimization process, the evolution of the model computed currents and thermocline depth are stored in advance because they enter the SST and adjoint integration through the advection terms. We also need to save the time history of the SST and the Lagrange multiplier in addition to the storage required by the CONMIN routine. The CONMIN algorithm requires the storage of at least seven vectors of length M , where M is the number of the control variables in the discretized model (Navon and Legler, 1987).

The climatological monthly-mean SST data (Shea et al, 1990) are linearly interpolated into each time level. This linearly interpolated dataset is used to compute the value of the cost functional and to calculate the data misfits for the backward integrating of the adjoint model.

3.5.4 The Boundary Conditions

The model northern and southern boundaries are open. The open boundary condition described by Camerlengo and O'Brien (1980) is imposed to compute model variables along these boundaries. The effect of the coast at the eastern and western sides of the basin is simulated in the model. The no-normal flow and no-slip conditions are applied at these solid boundaries. The model is discretized on an Arakawa C-grid. The time integration uses a leapfrog scheme, with a forward scheme every 99th time step to eliminate the computational mode. A Dufort-Frankel scheme is applied for the diffusive term (O'Brien, 1986).

4. Seasonal Variability in the Tropical Pacific

The oceanic upper layer interacts with the lower atmosphere through the complicated processes of momentum and heat interchange. Understanding the physics of the upper ocean as well as the atmosphere system will help us to interpret the heat interchange pattern determined from the variational adjoint procedure. In this section, we study the variability of the surface winds, currents, upwelling, and SST on the seasonal time scales. The patterns of the surface pseudo-stress field (Figures 3a-d) and the SST (Figures 6a-d) are from the climatology by Stricherz et al. (1992) and Shea et al. (1990), respectively. The figures of currents (Figures 4a-d) and upwelling (Figures 5a-d) are the results from the model equations (3.1), (3.2) and (3.5) for the model year 16. The model takes about 12 years to achieve a periodic steady state.

4.1 Dynamics

The variability of the tropical ocean circulation is closely related to the surface wind field. In the tropics, the characteristic response times for baroclinic oceanic processes are much faster than they are at mid-latitude and are much closer to the time scales characterizing the wind variations (Moore and Philander, 1978). Therefore, an accurate knowledge of the temporal and spatial structure of the atmospheric

forcing is essential to understand the oceanic features.

(a) The Wind Field

The surface wind field over the tropical Pacific ocean is dominated by the trade wind system. The Intertropical Convergence Zone (ITCZ), which is the narrow zone of light variable winds (which is located at 8°N in December (see Figure 3a)), separates the stronger and steadier Northeast and Southeast Trades (Figures 3a-d). The seasonal variation of the surface wind field is characterized by the seasonal migration of the ITCZ. The ITCZ tends to be oriented NNE to SSW and follows the sun toward the summer hemisphere. In boreal fall it reaches its most northerly position at about 10°N and the Southeast Trades are most intensified (Figure 3d). The equator remains in the easterly Southeast Trades until boreal winter and early spring, when the ITCZ crosses the equator and the winds there are weak (Figure 3a). The Northeast Trades are strongest in this time. In late spring the ITCZ again moves northward and the equatorial easterly intensifies abruptly with the strengthening of the Southeast Trades (Figure 3c).

(b) Surface Currents

The prominent features of the ocean surface circulation in the tropical Pacific are the alternating bands of eastward and westward flowing currents. The eastward flows, in the direction counter to the easterly trade winds, are referred to as the North Equatorial Counter-Currents (NECC). The westward flows are referred to as the North

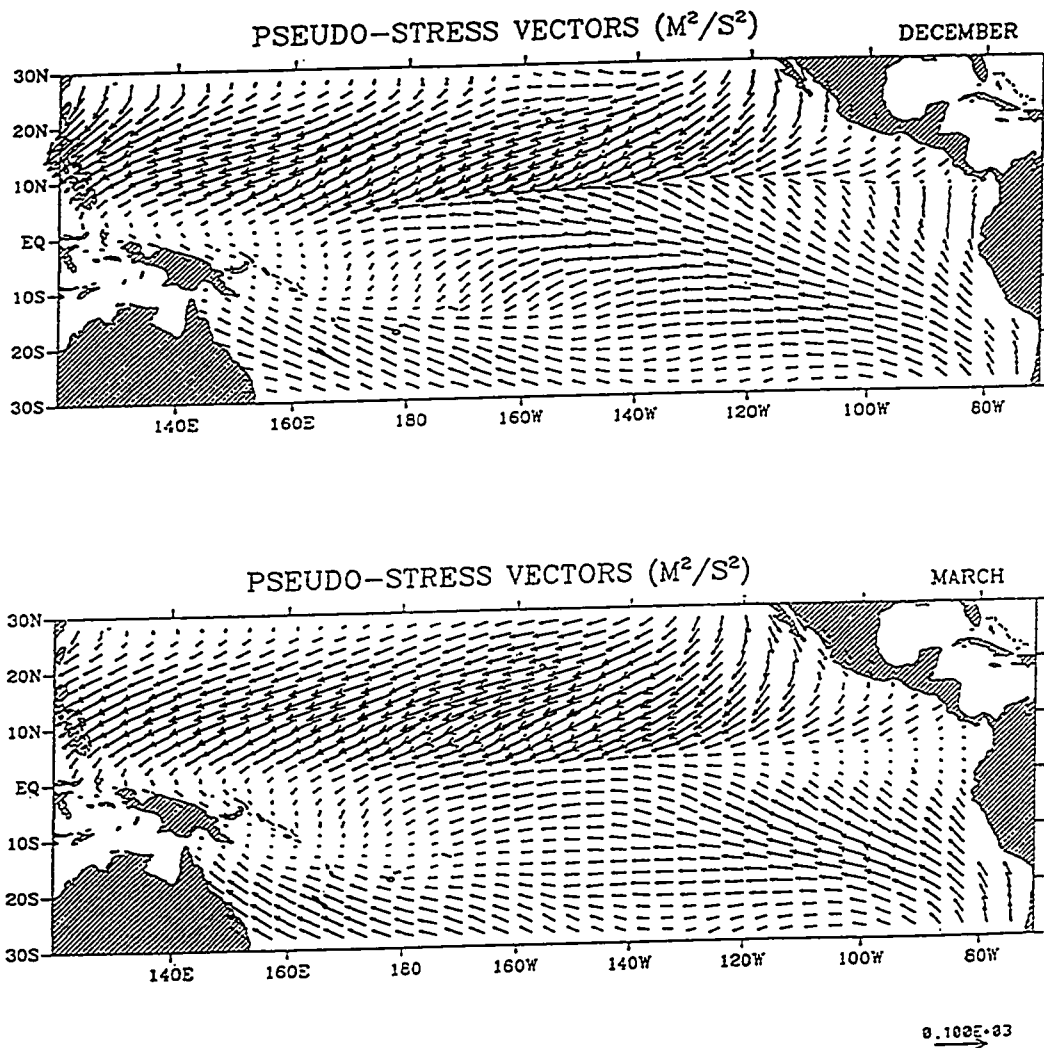
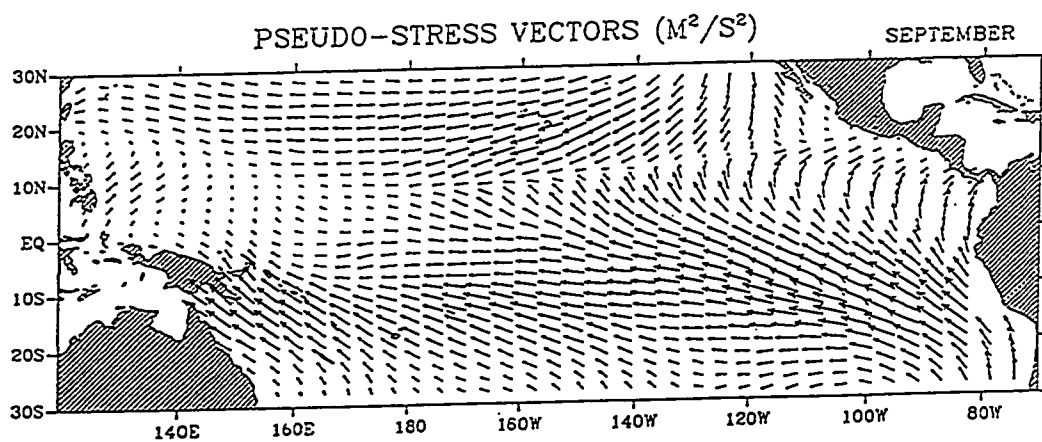
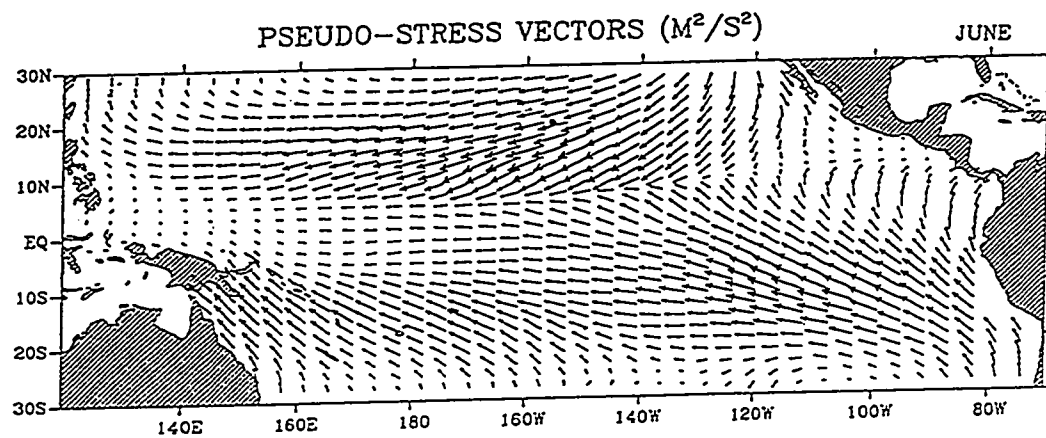


Figure 3. The pattern of the pseudo-stress in (a) December; (b) March; (c) June; and (d) September. The seasonal variations of the wind field are characterized by the seasonal migrations of the ITCZ.



$0.100E-03$

Figure 3. continued

Equatorial Currents (NEC) and the South Equatorial Currents (SEC). The dynamics of these equatorial currents have been studied by many researchers and reviewed by Leetmaa et al. (1981) and are not discussed here. The three major surface currents are evident in our model (Figures 4a-d). The NEC is located between 8°N and 20°N , the SEC is from about 17°S to 3°N , and the narrower NECC flows to the east between them.

Both the intensity and location of the surface currents vary seasonally with the variations of the trade winds. The surface currents are weak when the equatorial winds relax in boreal winter and spring (Figures 4a-b). In boreal fall the intensification of the southeast trades strengthens the westward SEC, as is evident in Figure 4d. The NECC is also intensified at this time of the year. In general, the NEC is strong during the northern winter and weak during the summer, while the SEC and the NECC are strong in the late summer and weak in the spring. The NECC assumes its northernmost position in boreal summer, whereas it lies closest to the equator in the boreal winter (Figures 4a-d). The modeled surface current system is in agreement with the observations of Meehl (1982).

(c) Upwelling

The computed upwelling fields, which are proportional to the divergence of the surface layer currents, are given in figures 5a-d. Upwelling mainly occurs in the Southern Hemisphere area of the east Pacific and in a narrow band near the equator. Equatorial upwelling is the result of divergence of the wind-driven currents. The westward

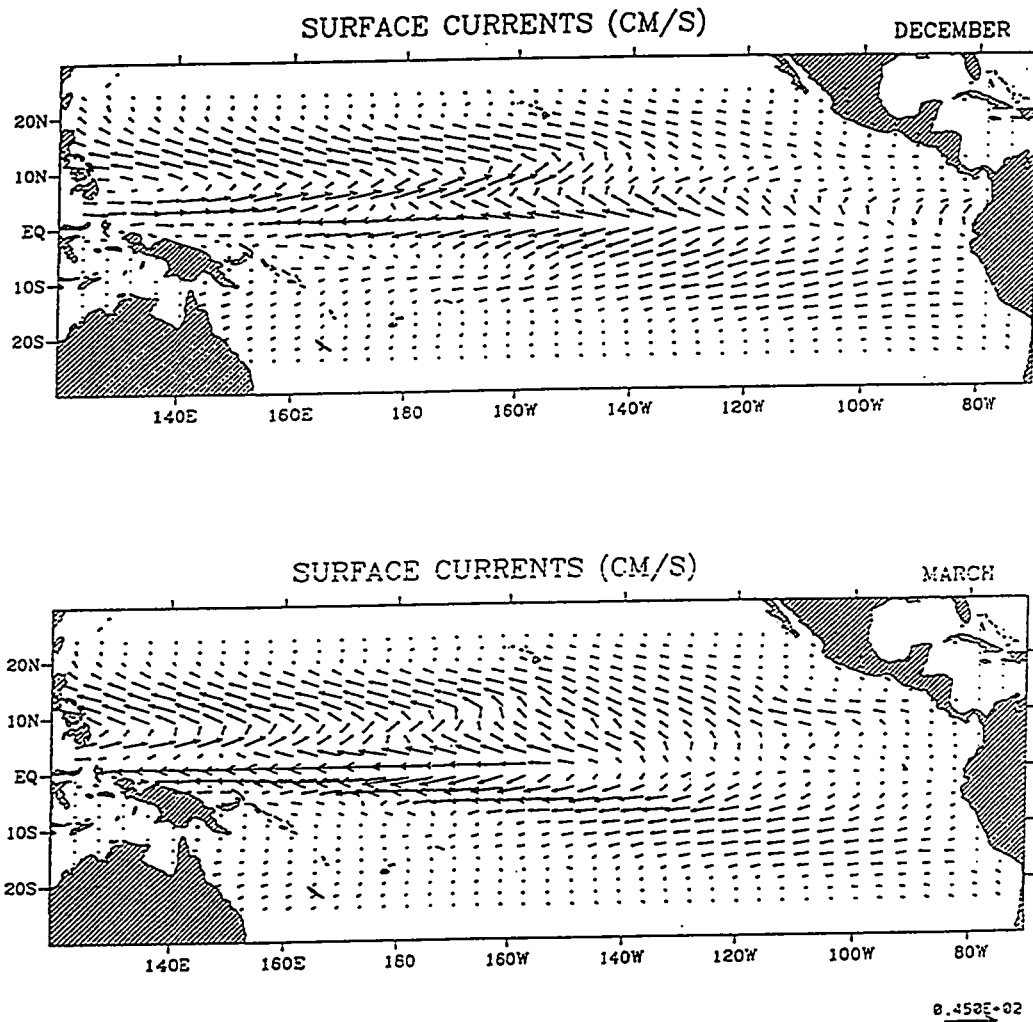
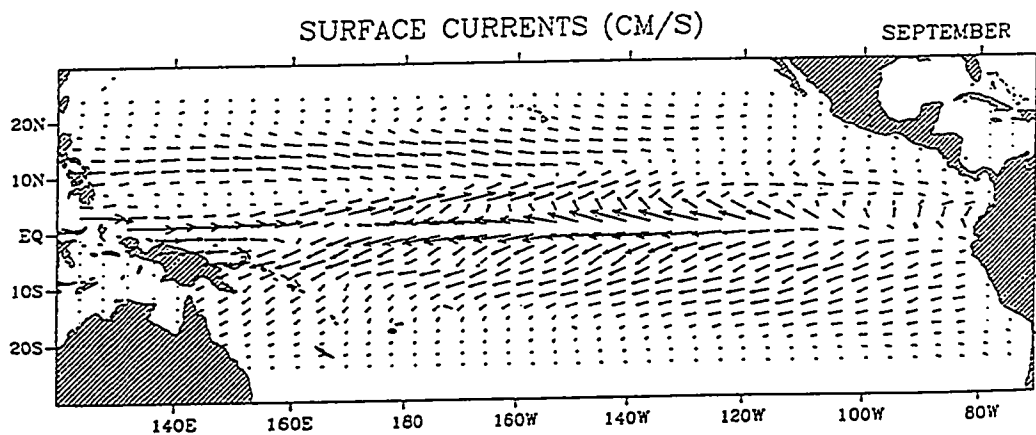
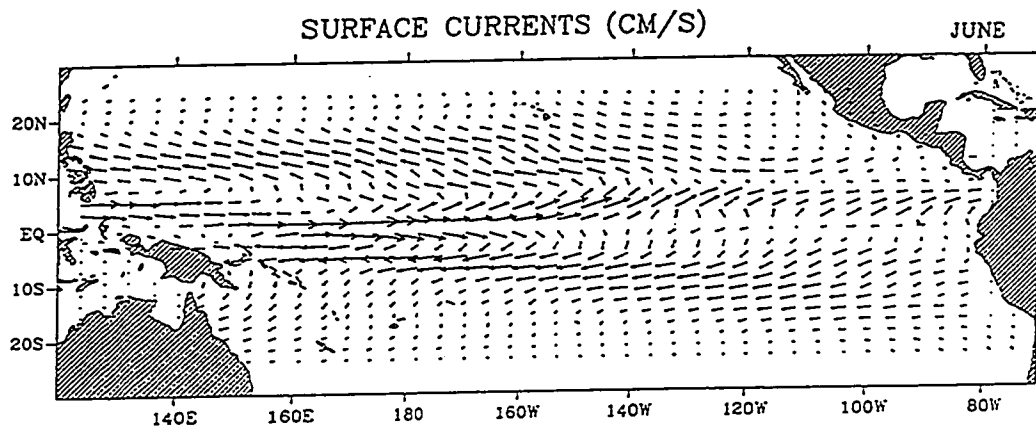


Figure 4. The pattern of the surface current in (a) December; (b) March; (c) June; and (d) September. The prominent features of the circulation are the alternating bands of eastward and westward flowing currents, namely, the westward NEC and SEC and the eastward NECC. The strength of the surface currents vary seasonally in response to the variation of ITCZ.



$0.453E-02$

Figure 4. continued

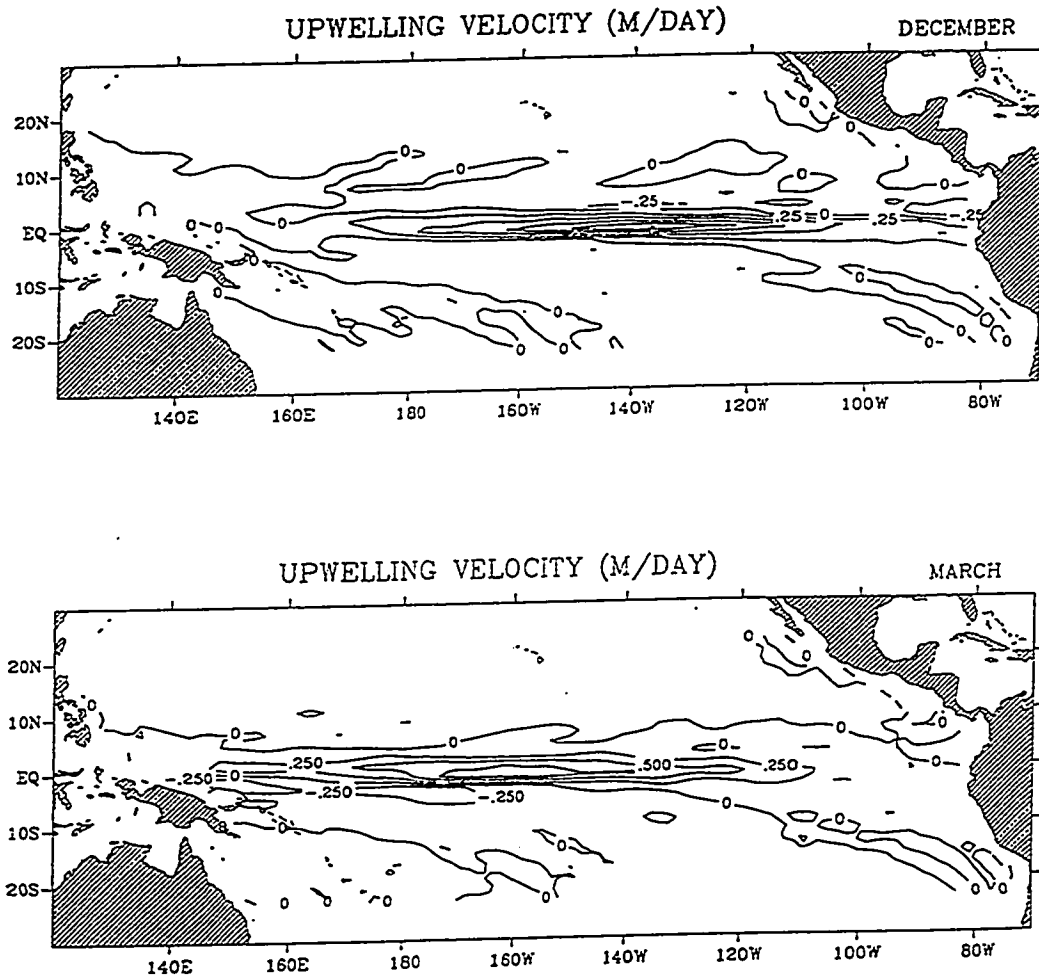


Figure 5. The pattern of the upwelling in (a) December; (b) March; (c) June; and (d) September (the contour interval is 0.25 m/day). The upwelling maximum occurs in the northern summer.

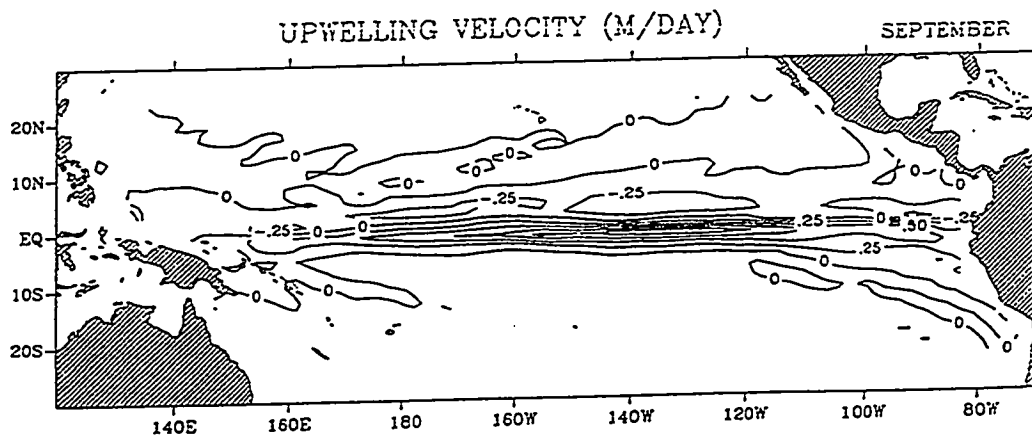
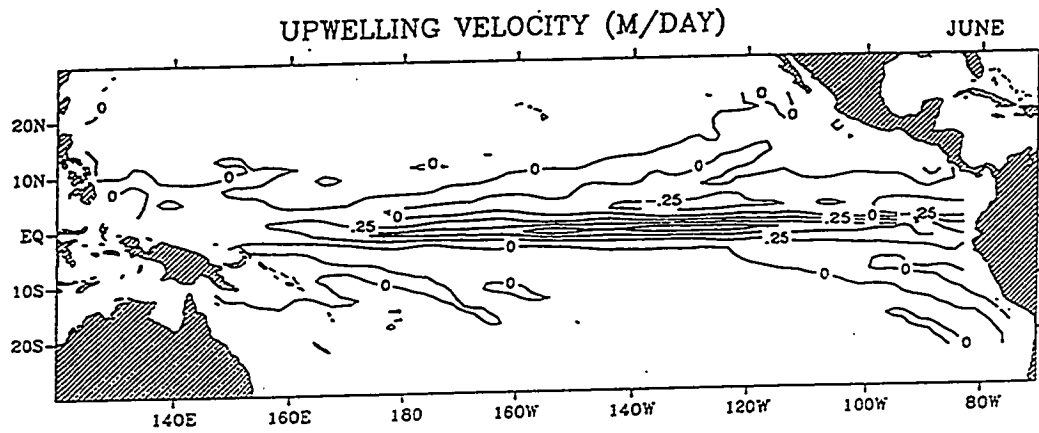


Figure 5. continued

component of the southeast trades causes poleward Ekman transport of surface water on either side of equator. In the central and eastern Pacific, upwelling is strongest in boreal summer and fall due to the increased divergence of the surface water in response to the seasonal increase in the strength of the southeast trade wind. Coastal upwelling is generally greatest a few degrees south of the equator, and is most pronounced in boreal summer. In the western Pacific, upwelling is weaker and more variable in location. In boreal summer and fall, upwelling is found to the south of the equator and downwelling to the north. In boreal winter and spring the situation is just the opposite, with upwelling to the north of the equator and downwelling to the south.

4.2 Thermodynamics

The SST seasonal variability in the tropical Pacific ocean has been well documented from many historical data analyses (e.g., Hickey, 1975; Hastenrath and Lamb, 1977; Esbensen and Kushnir, 1981; Horel, 1982; Levitus, 1987; Shea et al., 1990; Fiedler, 1992). There are three prominent SST centers in the tropical Pacific: the warm SST center in the west-central Pacific (termed the "warm pool"); the cold SST center in the southeast Pacific (known as the "cold tongue"); and a warm SST center in the eastern Pacific to the north of the equator (Figures 6a-d). The strong contrast between the warm pool in the west and the cold tongue in the east produce a remarkable SST horizontal gradient in the equatorial region. The SST isotherms are zonally oriented outside of the equatorial region (8°

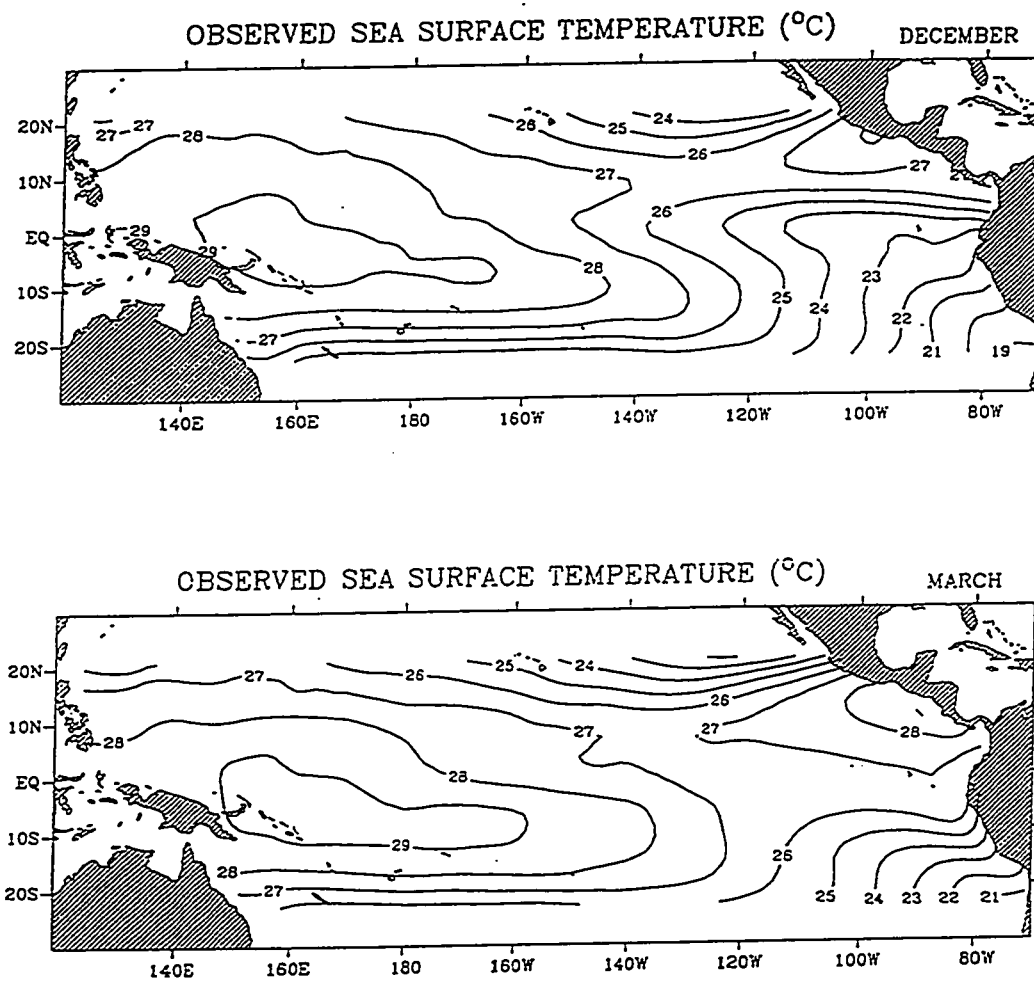


Figure 6. The pattern of the observed sea surface temperature (SST) in (a) December; (b) March; (c) June; and (d) September. The most striking feature of the seasonal cycle is the strengthening of the horizontal SST gradient in the equatorial Pacific during the northern summer time.

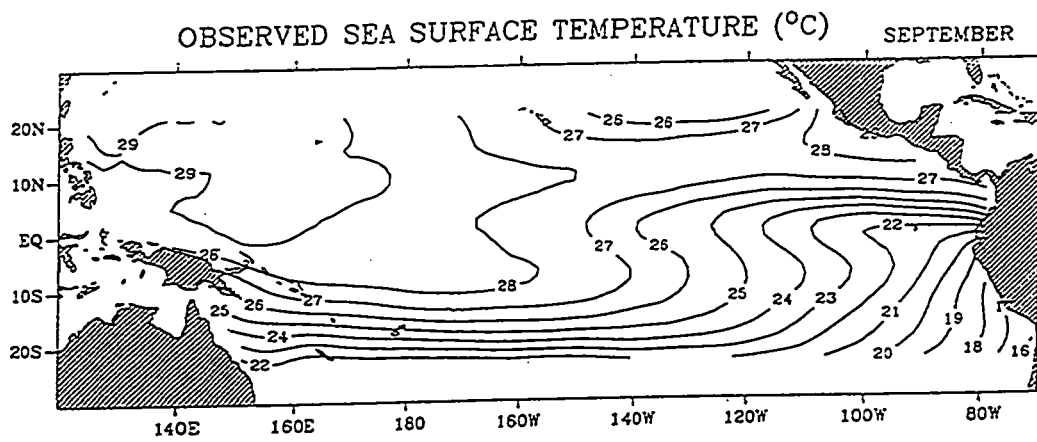
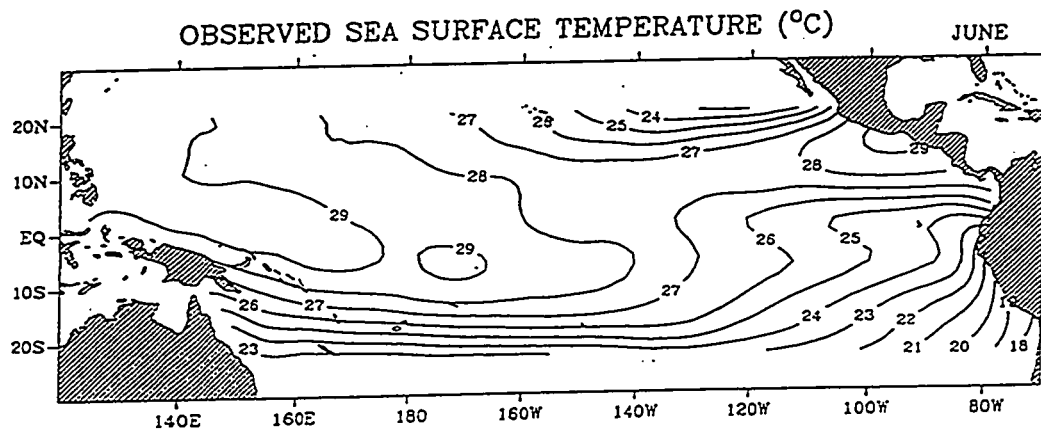


Figure 6. continued

poleward).

The changes of the warm pool and the cold tongue in their location and intensity determine the main features of the SST distribution in the Pacific in different seasons. In boreal winter (Figure 6a), the warm pool is located near the equator and west of 160°W. The other warm center is in the eastern Pacific near the coast of central America. The cold tongue is weak with a relatively high SST ($>17^{\circ}\text{C}$). There is less westward extension of the cold water. As Spring comes (Figure 6b), the warm pool is intensified and expands eastward. At the same time, the warm water in the east of the basin expands south-westward. Hence a large area of water warmer than 27°C appears in the equatorial region. The cold tongue is in its weakest. As a result the horizontal SST gradient decreases.

In boreal summer (Figure 6c), there is a warm strip which connects the warm pool in the west with the warm water in the east off the coast of Mexico. The cold tongue begins to develop and intrudes north-westward. The axis of this temperature minimum is between 1°S - 3°S and becomes symmetric about the equator at its westernmost limit. The southern ocean is cooler than in spring. By September (Figure 6d), the warm strip ($\text{SST}>27^{\circ}\text{C}$) in the central and eastern Pacific has migrated northward and is centered near 10°N in the vicinity of the ITCZ. To the south, the SST gradually decreases into the Southern Hemisphere where it is in the southern winter time. The cold tongue is most intensified at this time with a broad northwestward extension of the cold water. The strong contrast between the warm pool in the west and the cold tongue in the east leads to the sharp horizontal SST gradient in the equator.

The seasonal variations of the tropical SST are affected by several physical processes over a wide range of space and time scales. Among these processes, solar insolation, latent heat release, upwelling and advection play the dominant role. Sensible heat exchange and long wave radiation from the sea surface are also important but their effects are one order smaller than that of the latent heat flux.

The net downward radiative flux is the main heat source for the ocean. One may refer to the atlases by Esbensen and Kushnir (1981), Oberhuber (1988) and Fu et al. (1990) for the distribution of the radiative flux in the tropical Pacific. The seasonal variation of the SST away from the equator is attributed to the changes of the solar heating. In the northern hemisphere spring and summer times, the SST in the north Pacific warms up as the solar heating increases. The warm pool (e.g. the 29°C isotherm) moves northward as the center of insolation maximum shifts poleward. Meantime, the south Pacific cools because it is winter.

The existence of the equatorial SST minimum, however, cannot be explained by either the solar heating or the latent heat flux. A cold sea surface releases less heat to the atmosphere and the effect of the anomalous latent heat flux is to diminish the cooling in the cold tongue rather than to create it. In fact, the seasonal variability of equatorial SST is related to the wind-driven upwelling and its effects on the thermocline depth (Wyrtki, 1981; McPhaden, 1983; Halpern et al., 1989).

The equatorial upwelling is a coupled dynamic/thermodynamic process. The easterly-wind driven Ekman divergence at the equator is balanced by an upward mass flux from the thermocline and thus cold

water is brought to the surface. The prevailing easterly trade winds over the tropical Pacific cause the sea-surface to slope up towards the west. This results in a deeper thermocline in the west than in the east and produces the east-west variations in upwelling intensity. Because of the shallower thermocline in the east, more rapid cooling is produced by the turbulent mixing.

One can conclude that the variability of the SST in the tropical Pacific is determined by both the surface heat flux and the advection process. The implication is that the SST dataset contains useful information about heat exchanges at the air-sea interface and therefore is a valuable source to be used for studying the heat flux variations.

5. Results and Discussions

5.1 Estimates of the Surface Heat Flux by the Adjoint Procedure

In general, equations (3.22) through (3.24) constitute of the variational adjoint procedure in searching an optimal surface heat flux pattern over the tropical Pacific ocean. However, the experience we have gained from a series of experiments shows that the process of obtaining the optimal heat flux pattern is affected by a number of factors. Consistent with the theory we presented in section 3.3, it is clear that the form of the cost function indeed impacts upon the uniqueness of the solution and the performance of the descent algorithm. We also discovered that the model initial SST field has a substantial influence on determining the time-dependent parameters. A meaningful optimal surface heat flux pattern can be obtained only when the initial SST field is optimally determined.

5.1.1 The Form of the Cost Function on the Rate of the Convergence

In section 3.3 we have argued that the inclusion of the *a priori* information, J_Q , in the cost function (3.20) has the effect of both formulating a well-determined problem and increasing the probability for having a unique solution. The practical usefulness of adding J_Q is to improve the conditioning of the Hessian matrix with the benefit of speeding up the convergence of the descent algorithm.

Several experiments are therefore conducted to test the effect of the term J_Q on the rate of the convergence of the minimization algorithm. We denote the cost function

$$\begin{aligned} J_1 &= J_T + J_Q \\ &= \frac{1}{2} \int_{\Sigma} (T - \hat{T})^2 d\sigma + \frac{1}{2} K_Q' \int_{\Sigma} (Q - \tilde{Q})^2 d\sigma \end{aligned}$$

and

$$\begin{aligned} J_2 &= J_T \\ &= \frac{1}{2} \int_{\Sigma} (T - \hat{T})^2 d\sigma \end{aligned}$$

in these experiments. The evolution of the cost functions and the norm of their gradients during the iterative process is displayed in Figures 7a-b and Figures 8a-b. The same first guess of the surface heat flux field, which is set to be a constant field, is applied to the experiments in Figures 7a-b. A first guess with thermodynamic meaning is used in the experiments of Figures 8a-b. Such a first guess is obtained by letting the surface heat flux term be equal to the upwelling term in equation (3.22).

If a unique solution of a linear problem does exist, the optimal solution obtained from the variational procedure will not depend on the choices of the first guess of the control parameters. Hence the existence of a unique solution can be examined by performing the variational procedure with arbitrary choice of first guess.

The slower convergence rate associated with the cost function J_2 (excluding of the term J_Q) is clearly shown in Figures 7-8. The norm of the gradient of J_2 (represented by $|\nabla J_2|$) decreases slowly during the iterative

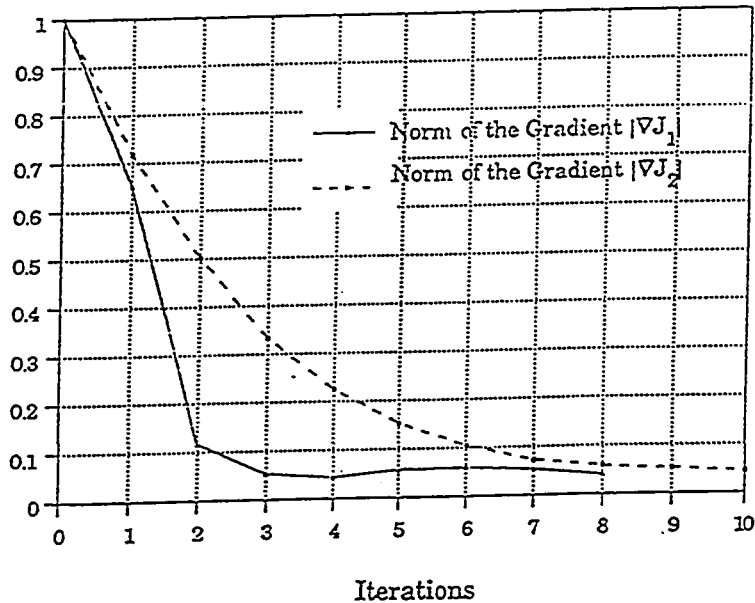
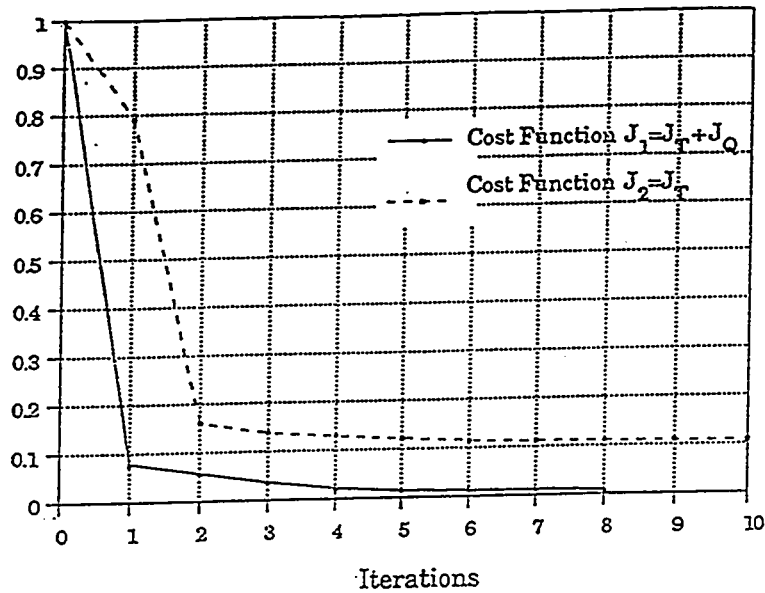


Figure 7. Experiments to test the form of the cost function on the rate of the convergence. In this case, a constant first guess field for the control parameter is used. (a) The evolution of the cost function (initialized by the value at the first iteration) during the iterative process. (b) The evolution of the norm of the gradient (initialized by the value at the first iteration) during the iterative process. The process is truncated once a steady state is approached. The experiment with cost function J_1 has a faster convergence rate than the experiment with J_2 .

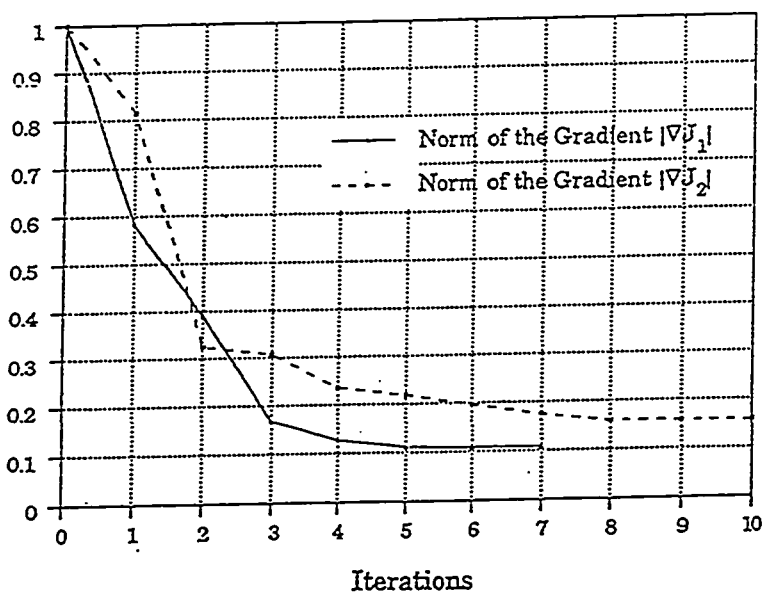
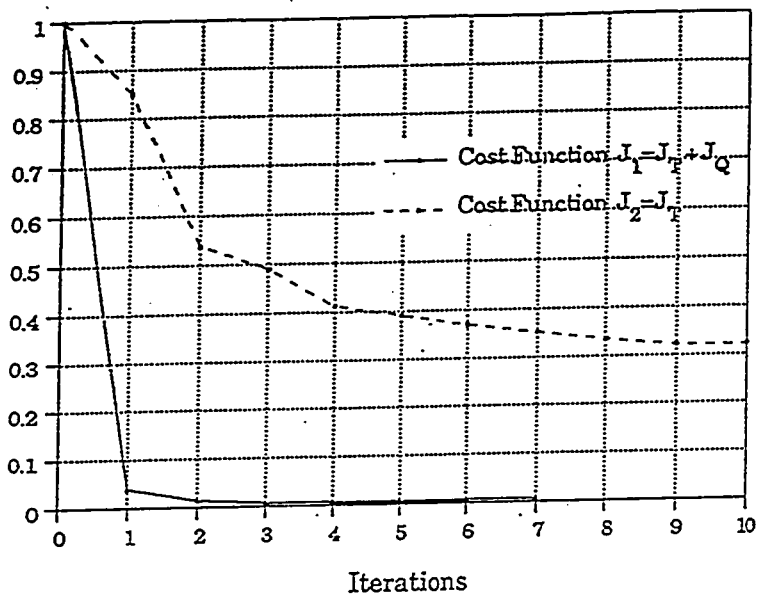


Figure 8. Same as Figure 7 except that a first guess with thermodynamic meaning is used in these experiments. It shows that the value of the cost function J_1 does not change with the choice of the first guess and a good first guess speeds the convergence of the descent algorithm.

process (Figures 7b and 8b) and so is the value of the cost function J_2 (Figures 7a and 8a). While $|\nabla J_1|$, the norm of the gradient of J_1 , decreases rapidly in the first couple of iterations. The functional value J_1 has also a fast reduction at these two iterations. Therefore it is expected to see that the procedure associated with the formulation of J_2 takes several more iterations than that of J_1 to achieve a similar computational steady state of the minimization process. In all experiments, the iterative process is truncated once a steady state is approached (i.e., when the changes in the values of the cost function and the norm of the gradient are no longer significant) since further iterations do not improve the results.

Comparing with these experiments, one can find that the minimization process associated with the cost function J_1 reaches the steady state faster in the experiment of Figure 8 than in Figure 7. This is due to the use of a more realistic first guess field, which uses a field with some thermodynamic meaning, in the experiment of Figure 8. This first guess gives a representation of what the field may be like at the beginning of the assimilation and provides a good background field for the parameter to be corrected from. So a well-chosen first guess field of the control parameter can impact the descent algorithm by reducing the number of iterations required for convergence.

Another interesting feature is that the optimal values of the cost function J_2 in Figures 7-8 are different. This means the solution of the problem associated with the cost function J_2 is not unique. The different choice of the first guess of control parameter leads to a different cost function minimum and a global minimum is not achieved in this case.

Several experiments with different first guesses have been performed. The results show that the optimal values of the cost function J_1 in Figures 7-8 are not sensitive to the choices of the first guess. It can be concluded that the uniqueness of the problem with the cost function J_1 exists.

Examining the performance of the variational procedure in these experiments, it is clear that the form of J_Q does have the convexification effect on the cost function and causes the solution to be unique. This in turn improves the global convergence property of the descent algorithm and speeds up the rate of convergence.

The convergence criterion of the algorithm, i.e., $\frac{|\nabla J|}{|\nabla J_0|} < 10^{-2}$, where $|\nabla J_0|$ is the value of $|\nabla J|$ at the first iteration, is not satisfied in these experiments. This problem is related to the topic in the next section.

5.1.2 Determining the Initial Condition and Its Effect on the Parameter Estimation

This study is concerned with the optimal parameter estimation. The unknown model field parameters, i.e., the surface heat flux distribution, are determined by minimizing the cost function which measures the distance between the modeled SST and the observed SST. In the variational adjoint procedure, the SST model (3.22) is integrated forward in time from an initial SST state; the adjoint model (3.23) is integrated backward in time using the periodic initial condition for the Lagrange multiplier. The initial condition for the adjoint model is no longer zero but periodic since we assimilate the climatological data.

The initial condition of the dynamic model has significant influence on determining the model unknown parameters in using the adjoint method. In the study by Yu and O'Brien (1992), they found that the data misfit can be significantly reduced if the initial current state is optimally determined in addition to the parameter estimation (wind stress drag coefficient and the oceanic eddy viscosity profile in their case). Similar results were obtained by Zou et al. (1992) for determining optimal nudging parameters using the variational adjoint method. In fact, by adding the initial condition to the set of the adjustable parameters, the data are equally weighted at all time steps in obtaining the optimal model solution. Since the recovery of the initial SST field at zero time is influenced by the data of the whole assimilation period, data noise will tend to average out and a better model-data fitting will result.

If we study time-independent parameter estimation, such as the wind stress drag coefficient and the oceanic eddy viscosity profile in Yu and O'Brien (1991), the optimally determined initial condition improves the accuracy of the estimated parameters. In this case, the values of the estimated parameters represent the time-averaged values corresponding to the assimilating period. These values will not be significantly distorted if the initial model state is not included in the optimization. However, for time-dependent parameter estimation, such as the problem in this study, the errors in the chosen initial model state may contaminate the estimated parameter field in such a way that the information contained in the parameter field is gradually degraded in time.

It is known that the adjoint procedure extracts only the information

from the observations which is dynamically consistent with the physical model which is assumed to be perfect. The initial condition contains part of the model's dynamic information because it represents the ocean's memory of its previously existing dynamic processes. If we take the initial model state for granted (either using the observational data or taking the fully spun-up model climatological state) in the model forward integration, the level of the accuracy of the parameter estimation depends on the distance of the chosen initial condition from the "true" model initial state (the "true" model initial state represents a *balanced* initial state with respect to the model's own dynamics). The initial inconsistency contributes to the model errors and therefore is filtered out by the adjoint assimilation. The accuracy of the estimated parameters is therefore affected since a certain level of useful information is neglected and the parameters are under-estimated. In the case of estimating the time-dependent parameters, the initial inconsistency propagates in time and influences the model evolution. Its effect on the estimated parameter is that the parameter field information is slowly degenerated in time, which is clearly shown in Figure 9.

Figure 9 shows the result of the estimated surface heat flux pattern without the optimization of the model initial condition. The SST model integration uses the observed SST field as an initial condition. The surface heat flux pattern obtained has seasonal variations for the first 9 months. However, the information is gradually lost and is much evident starting from October. By the time of December, the heat flux pattern has only a very few contours in the whole basin. The adjoint procedure fails in

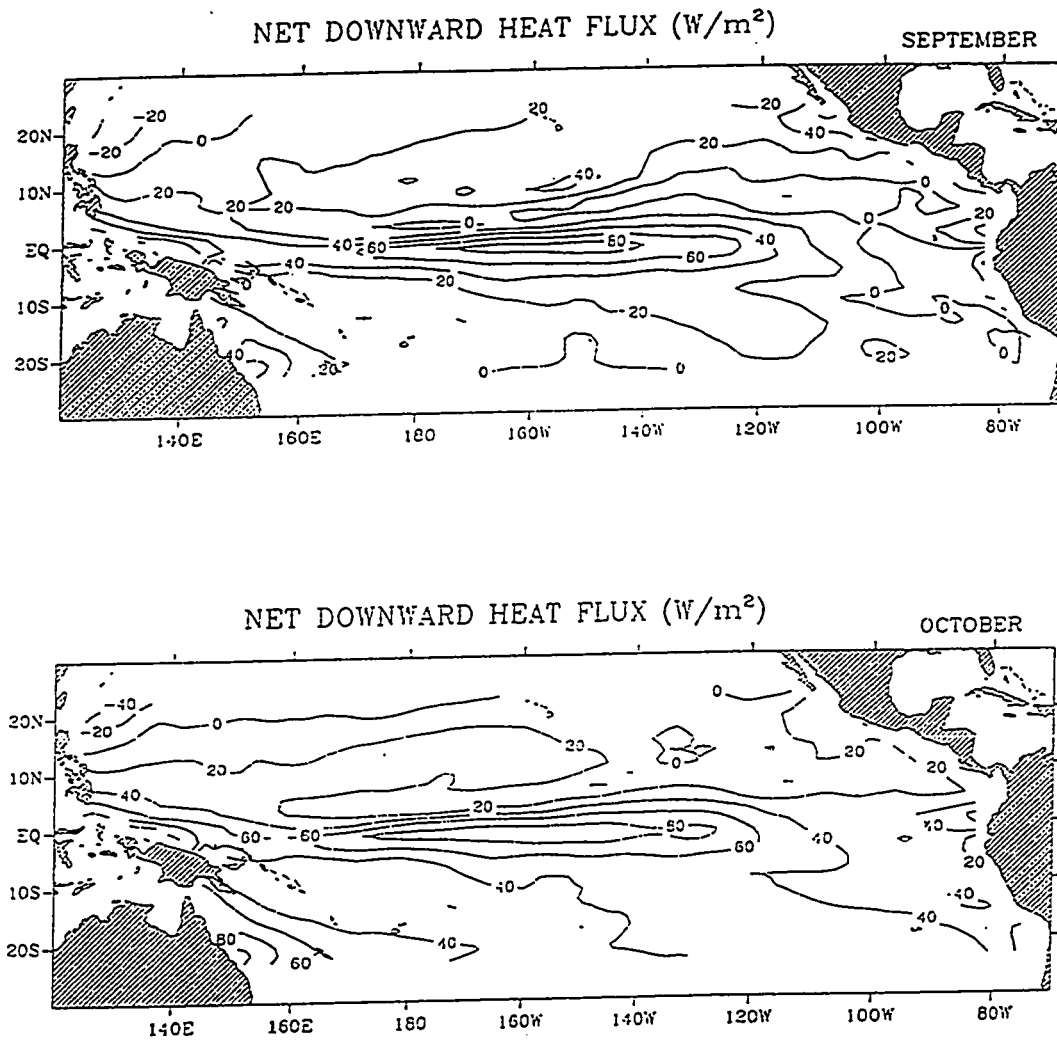


Figure 9. The loss of information in the estimated parameter field from September to December due to the errors in the chosen initial SST state. The SST model integration uses the observation SST field as an initial condition. The periodicity of the SST evolution is not satisfied at the end of the assimilation cycle.

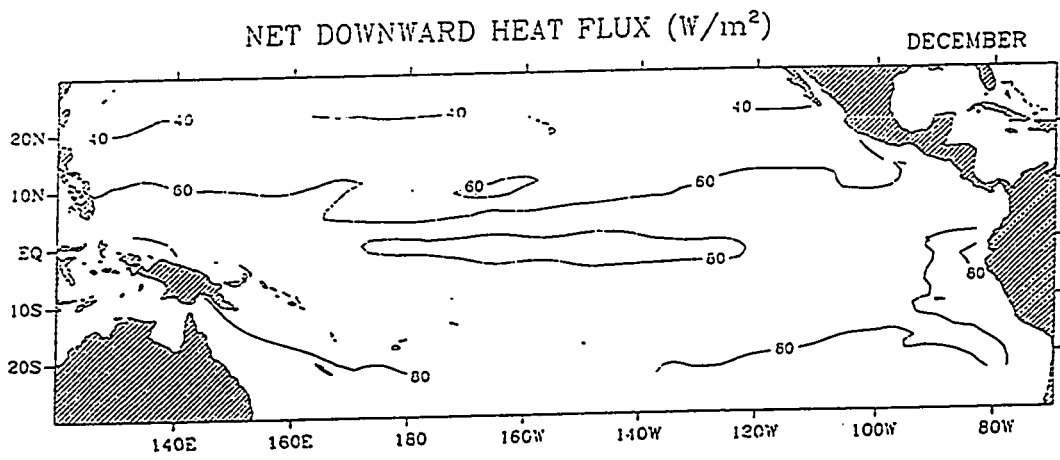
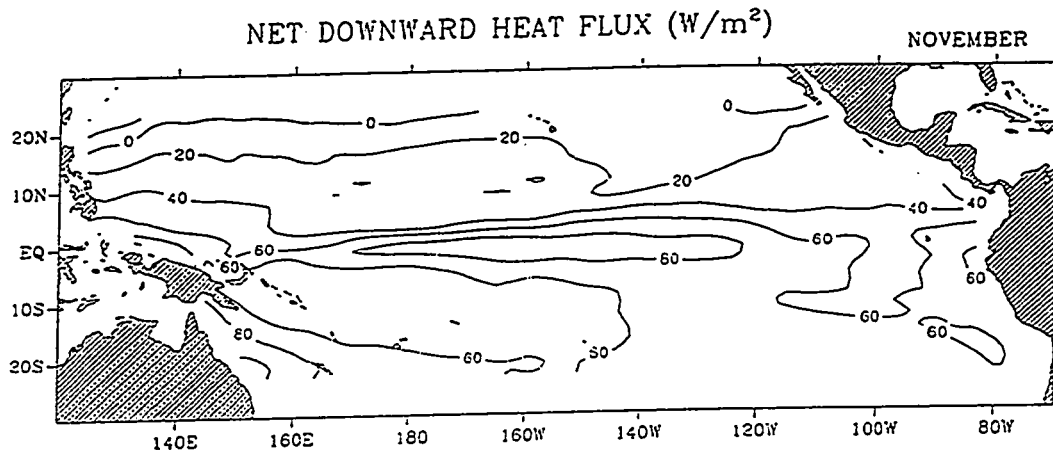


Figure 9. continued

recovering the seasonal cycle for the last 3 months due to the missing information.

This can be explained by examining the behavior of the SST and the adjoint model. The chosen initial condition is not consistent with the model's intrinsic dynamics due to either the observation error or the discrepancy between the model and the real world. The propagation of the model error at the initial time causes the model to deviate from the observations at a later time. Hence the periodicity of the SST evolution, which is the natural required condition for assimilating the climatological data, is not satisfied at the end of the assimilation period. The adjoint model, though, uses a periodic initial condition for the Lagrange multiplier and is driven by the square root of the SST data misfit. The noise-contaminated SST field at the end of the assimilation cycle affects the computations of the adjoint model at its initial time and then influences the heat flux fields, whose values are closely related to the values of the Lagrange multiplier (equation 3.24). In fact, the degree of the discontinuity in the surface heat flux pattern in December and January reflects the noisy level of the chosen SST initial condition.

The failure in the recovery of the time-dependent parameters actually reflects the characteristics of the partial differential equation. The SST equation (3.22) is a linear equation with non-constant coefficients. The heat flux plays a role of external forcing. The solution of the partial differential equation is determined by the initial condition, the boundary condition and the forcing. Regardless of the boundary condition which is proved to have negligible effect on the solution in this study, the behavior

of the SST evolution of equation (3.22) is governed by the initial SST state and the heat flux forcing field. Therefore in addition to an optimal heat flux field, a model-balanced initial condition is an important factor in determining the solution of equation (3.22).

Using the same strategy proposed by Yu and O'Brien (1992), we seek the optimal solution by estimating both the SST initial state and the heat flux field parameters. A new term, which is

$$J_{T_0} = \frac{1}{2} K_0' \int_{x,y} (T_0 - \bar{T}_0)^2 dx dy \quad (5.1)$$

is added to the cost function (3.20). The cost function now has the form:

$$\begin{aligned} J(T, Q, T_0) = & \frac{1}{2} \int_{\Sigma} (T - \hat{T})^2 d\sigma + \frac{1}{2} K_Q' \int_{\Sigma} (Q - \bar{Q})^2 d\sigma \\ & + \frac{1}{2} K_0' \int_{x,y} (T_0 - \bar{T}_0)^2 dx dy \end{aligned} \quad (5.2)$$

where T_0 denotes the initial SST, \bar{T}_0 the values of the initial SST at the previous iteration and K_0' the computational weight.

The gradient of the cost function with respect to the initial condition of the SST is given by:

$$\begin{aligned} \nabla_{T_0} J = & K_0' (T_0 - \bar{T}_0) - \\ & \left\{ \frac{\partial \lambda_T}{\partial t} + \delta_A \left(\frac{\partial(u\lambda_T)}{\partial x} + \frac{\partial(v\lambda_T)}{\partial y} \right) + \delta_{vx} \frac{\partial^2 \lambda_T}{\partial x^2} + \delta_{vy} \frac{\partial^2 \lambda_T}{\partial y^2} - \delta_A \lambda_T M(w_e) \right\}_{t=0} \end{aligned} \quad (5.3)$$

The equations (3.22), (3.23) and (3.25) remain the same. The variational adjoint procedure updates the SST initial condition and the flux field

parameters at every iteration.

Actually, it is not more costly to control the initial condition in addition to the model parameters because the correction of the initial state uses the same information from the adjoint model. The SST model integration begins from a balanced initial condition and thus eliminates the initial noise in biasing the model evolution. Figure 10 shows the evolution of surface heat flux from September to December by using (5.3) to correct the initial SST in the minimization process. It can be seen that the changes in these maps are continuous.

Another problem arises when adding the initial condition for adjustable parameters, i.e., the number of the observations is less than the model degrees of freedom. This means that we need to explore a good first guess state for all the control parameters (heat flux field and the initial SST). This is not just to reduce the number of iterations required for convergence but to give a meaningful background for the estimated parameters, i.e. to bias the solution towards the inputted *a priori* information. This technique is commonly used in determining a meaningful optimal solution for an under-determined problem in meteorology/oceanography data assimilation (e.g., Sheinbaum and Anderson, 1990).

The computational results shown in the following sections are from the variational procedure using the cost function (5.2) and including the adjustment of the initial condition (5.3).

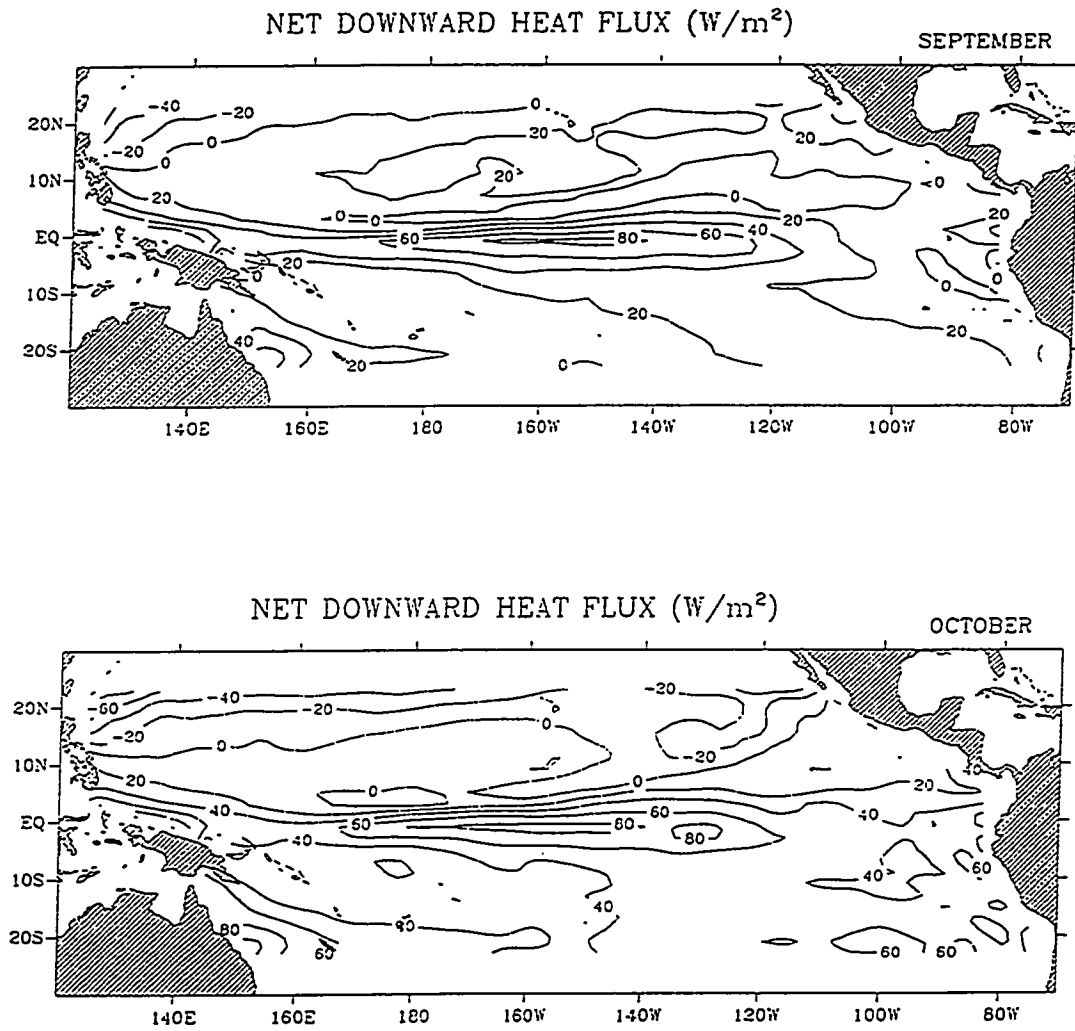


Figure 10. The evolution of the surface heat flux is continuous from September to December by adjusting the initial SST field in addition to the estimated parameters. The periodic condition is retained.

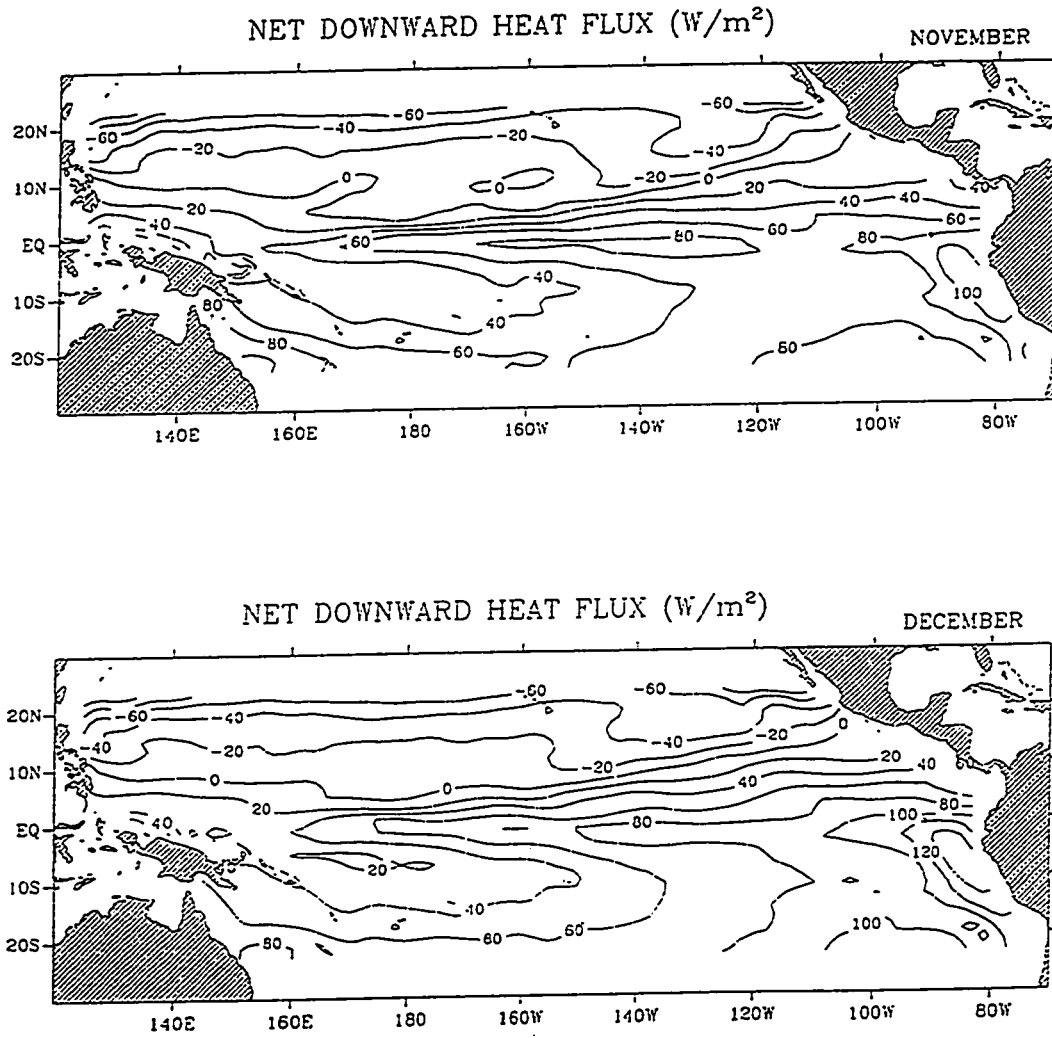


Figure 10. continued

5.1.3 The Heat Flux Pattern Estimated from the Adjoint Procedure

The control field parameters Q in the equation (3.22) are computed by the variational procedure through minimizing the cost function (5.2). Figure 11 is a plot of the evolution of the normalized cost function and the norm of its gradient during the minimization. The norm of the gradient displays a fast reduction during the first six iterations. Correspondingly, the cost function drops to about 98% of its initial value during these six iterations. One can observe that the norm of the gradient does not exhibit any significant decrease during the further iterations. The cost function could not be improved any further. We concluded that the computational steady-state solution is achieved.

The resulting optimal net downward surface heat flux distribution is shown in Figures 12a-d. The estimated surface heat flux pattern has a strong seasonal cycle. During the northern winter time (Figure 12a), the zero net heat flux line is located at about 8°N across the whole basin. Heat loss appears to the north of the zero line, with the most significant heat loss, over $100\text{W}/\text{m}^2$, in the northwestern part of the Pacific over the Kuroshio region. The ocean gains heat to the south of the zero line. The large net heat gain area is off the coast of Peru which is the area associated with the cold tongue. As the spring comes (Figure 12b), the pattern begins to change. The heat loss in the northern ocean decreases. In the meantime, heat loss occurs in the southern ocean. The maximum heat gain in the equatorial region expands and moves offshore to about 135°W .

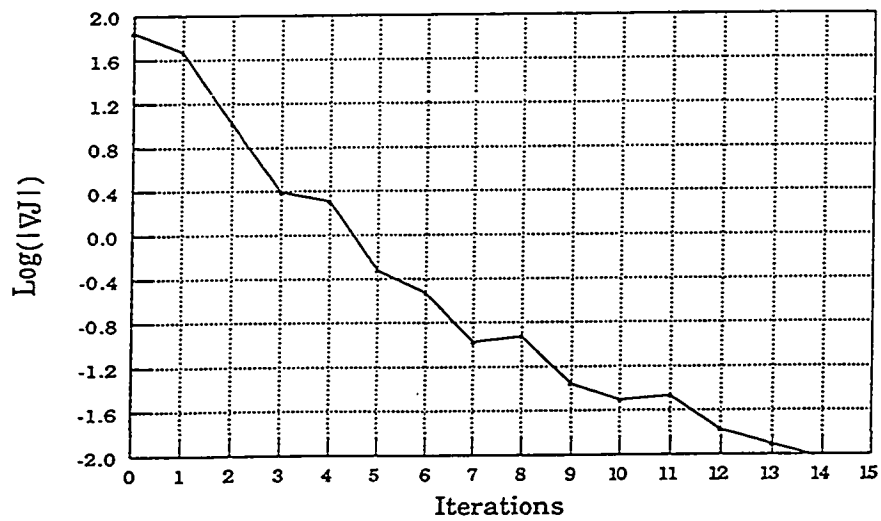
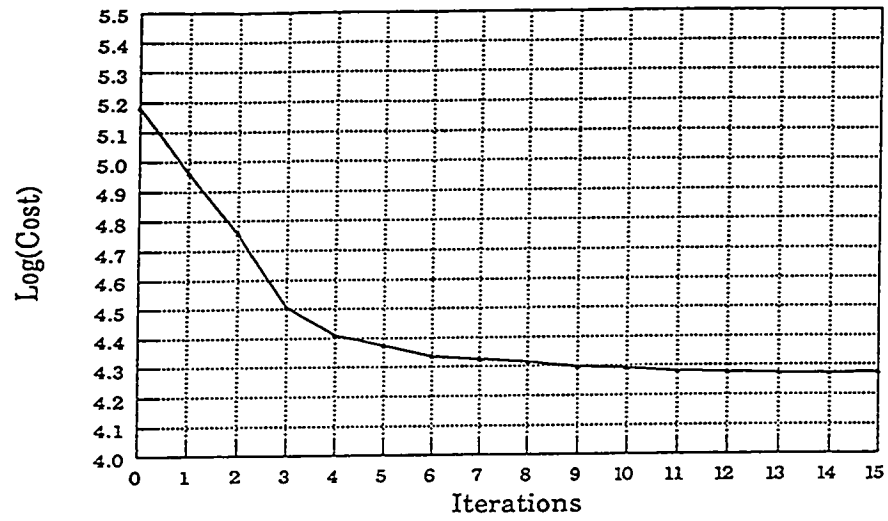


Figure 11. The evolution of the cost function and the norm of the gradient during the iterative process

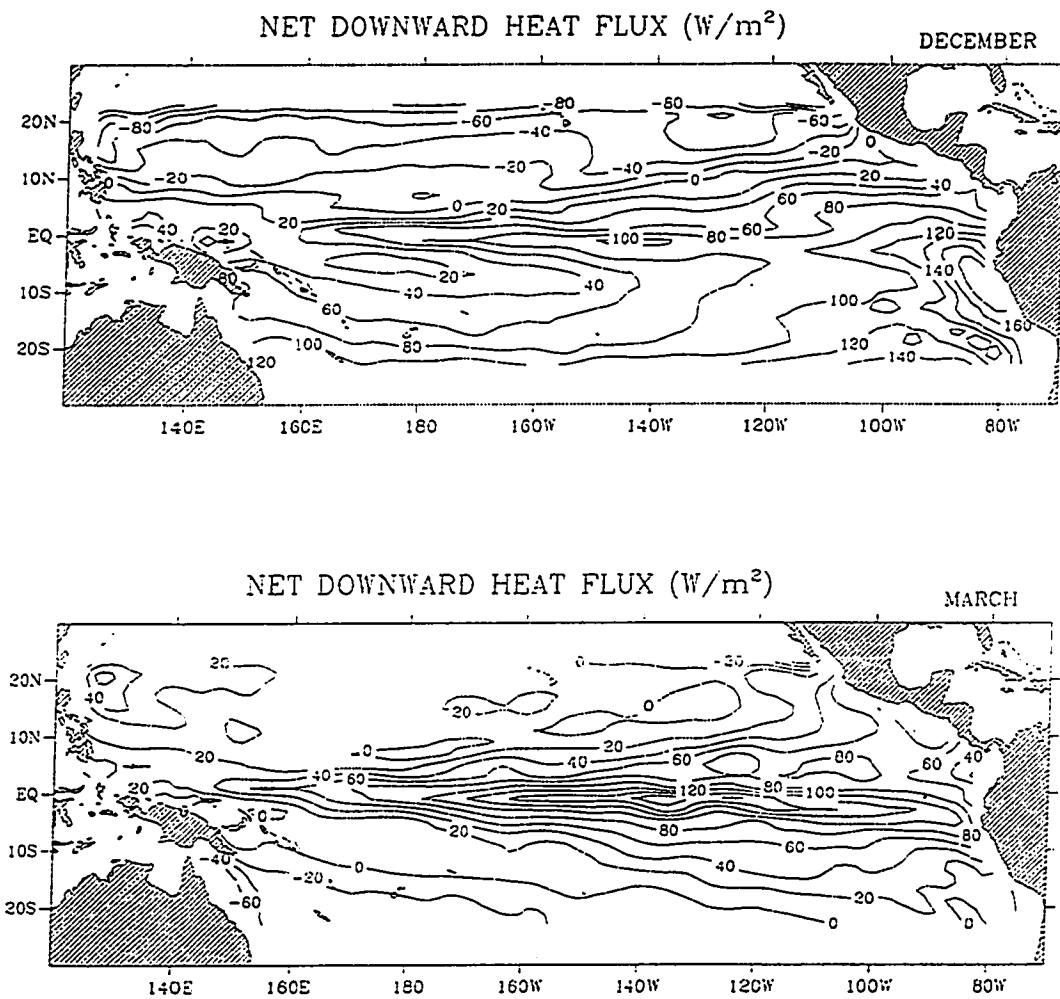


Figure 12. The pattern of the estimated net downward surface heat flux in (a) December; (b) March; (c) June; and (d) September (the contour interval is $20 \text{ W}/\text{m}^2$).

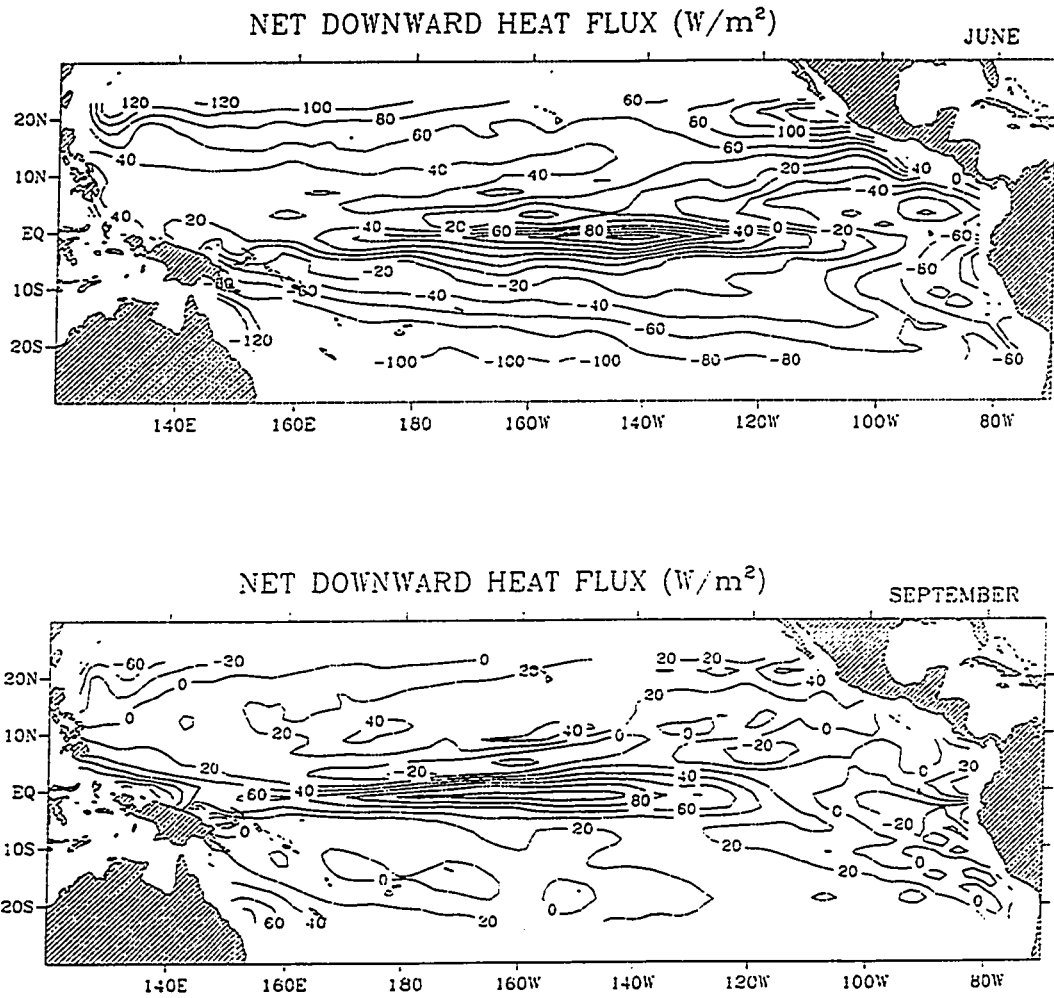


Figure 12. continued

The net downward heat flux in the northern earlier summer (Figure 12c) has the opposite pattern to that in the winter time. The obvious change is the appearance of the positive heat flux in the broad area of the northern hemisphere and the negative heat flux in the south and along the coast of the South America. The strength of the heat gain in the central equator decreases and the maximum heat gain occurs in the northeast (off the coast of Mexico). In September when the northern fall comes (Figure 12d), the area where the ocean gains heat is confined to the equatorial zone (between 8°S to 8°N). The heat loss/gain is small outside of the equator except in the Kuroshio region where the heat loss to the atmosphere is more than 60W/m².

5.2 Results Analysis

5.2.1 Comparison with the Existing Heat Flux Atlases

We compare our estimated heat flux pattern with those existing atlases in order to verify the results. However, we find ourselves in a difficult situation when searching for a good atlas. Although many versions of climatological fluxes are available, a considerable uncertainty exists among these atlases due to the different heat flux parameterizations adopted. Each of these climatologies qualitatively agrees on the seasonal variations of the heat flux distribution over the tropical Pacific, but differs (sometimes significantly) on the quantitative values. There is no standard version in existence allowing us to make a good judgment about our calculations. Hence the chosen two atlases

(Oberhuber (1988) and Fu et al. (1990)) serve only to illustrate the general features of the heat flux seasonality.

The data used to produce the heat flux maps of Oberhuber (hereafter O88) (Figures 13a-d) and Fu et al. (hereafter FU90) (Figures 14a-d) are the same COADS (Comprehensive Ocean-Atmosphere DataSet) described by Woodruff et al. (1987). The 30-year data for the period of 1950-1979 are projected on to $2^\circ \times 2^\circ$ grids in O88's atlas and to $4^\circ \times 4^\circ$ grids in the atlas of FU90. Even though the data source are exactly the same, the net heat flux they computed are quite different in some places. Nevertheless, they can be used as a reference for our comparison.

Comparing Figures 12-14, one can find that the main seasonal features in all of the three heat flux maps, i.e., seasonal alternating of heat loss/gain outside of the equatorial zone and seasonal changes in the location and the strength of the heat flux maximum center in the eastern Pacific along the equator. The obvious failure in our map is the inadequacy in simulating the strength of the heat flux variations in the northwestern Pacific over the Kuroshio region during the northern winter time.

The major differences between these maps is in the actual values. Sometimes they are very significant. In December, O88 (Figure 13a) gives a stronger heat loss in the Northern Pacific than the map of FU90 (Figure 14a) and much more stronger than our map (Figure 12a). Meanwhile, the ocean gains more heat in the Southern Pacific in FU90 than the other two maps. The great difference occurs in the Eastern Pacific to the north of the equator (about 10°N) where one finds a very strong surface heating,

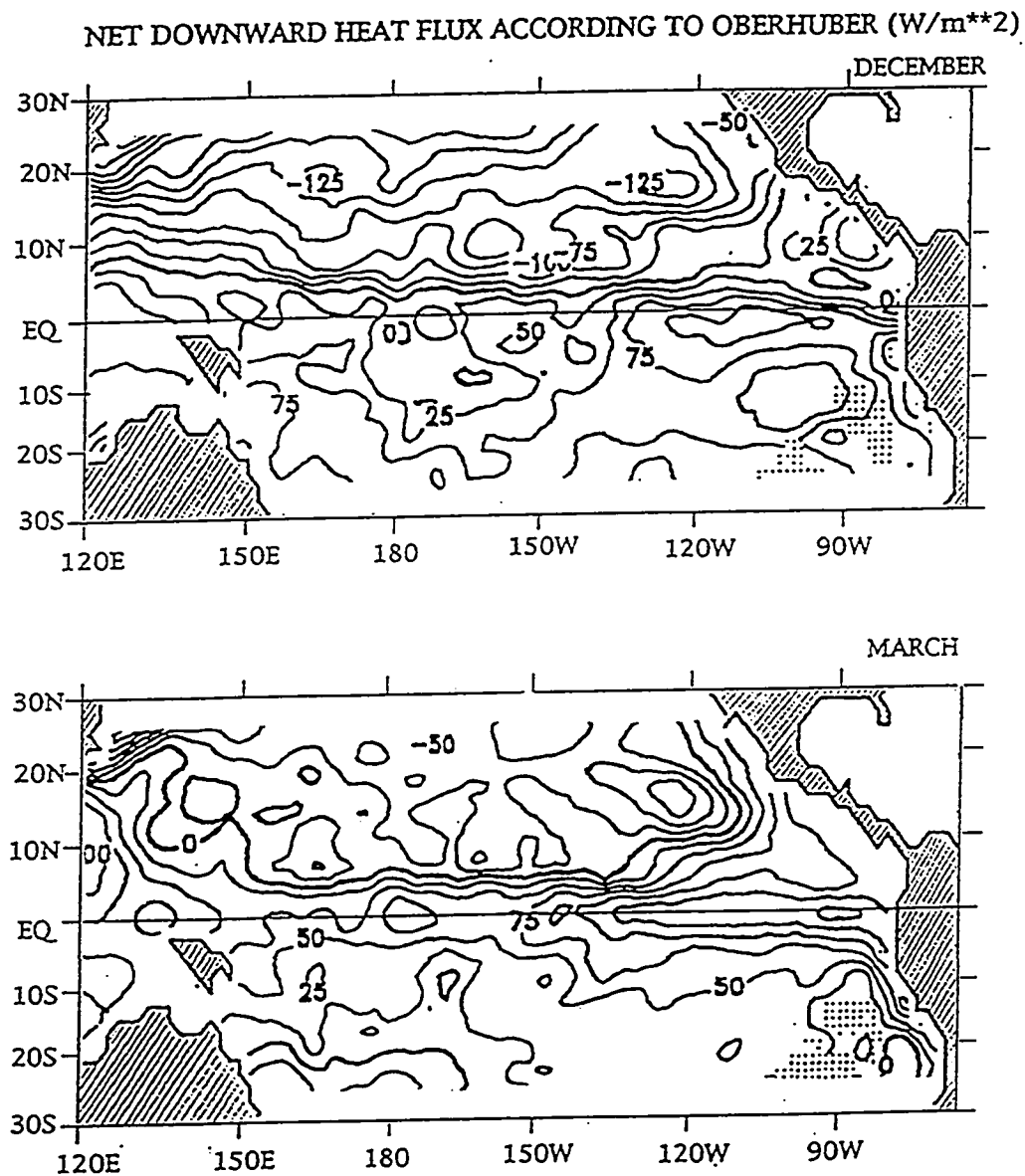


Figure 13. The pattern of the net downward surface heat flux according to Oberhuber (1988). (a) December; (b) March; (c) June; and (d) September (the contour interval is 25 W/m^2).

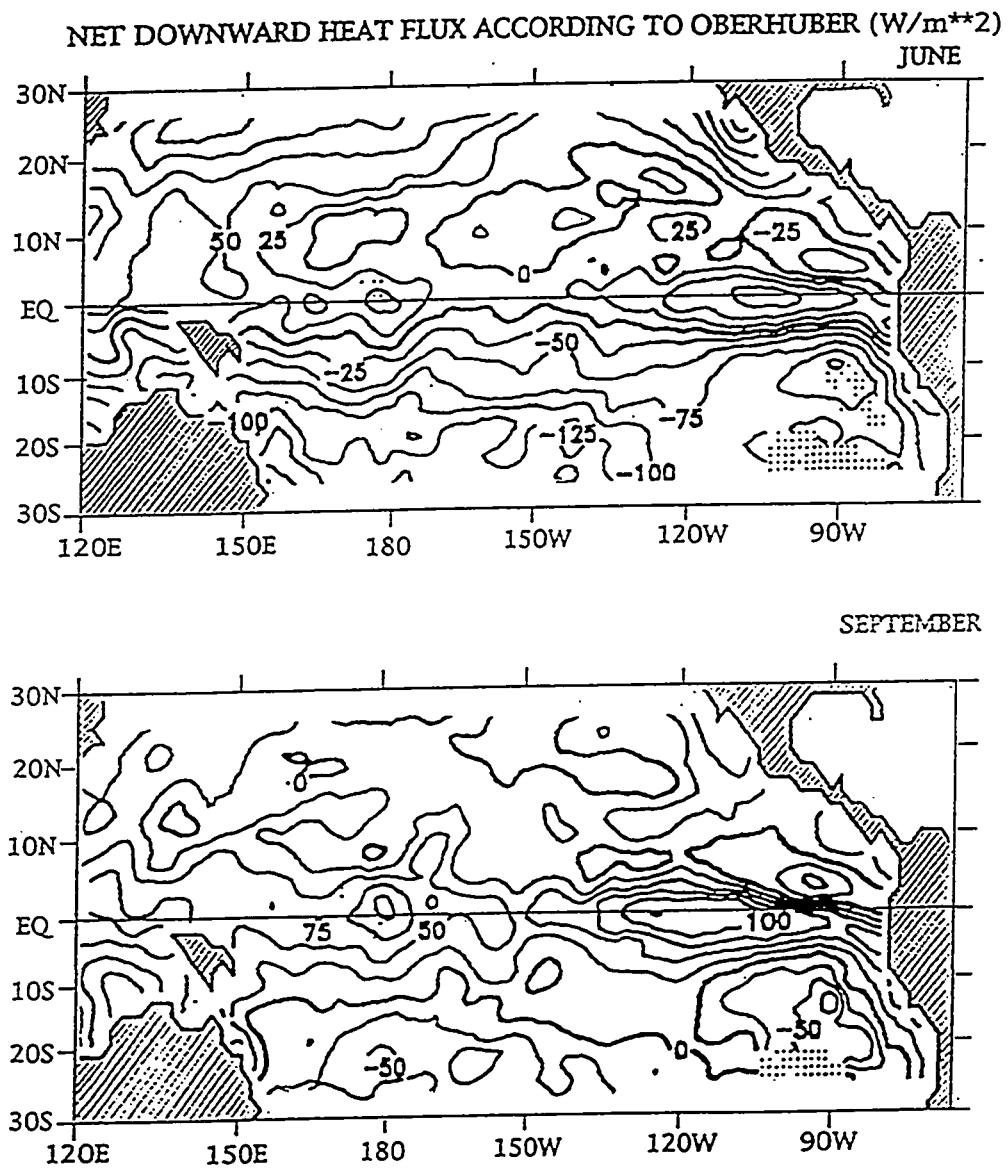


Figure 13. continued

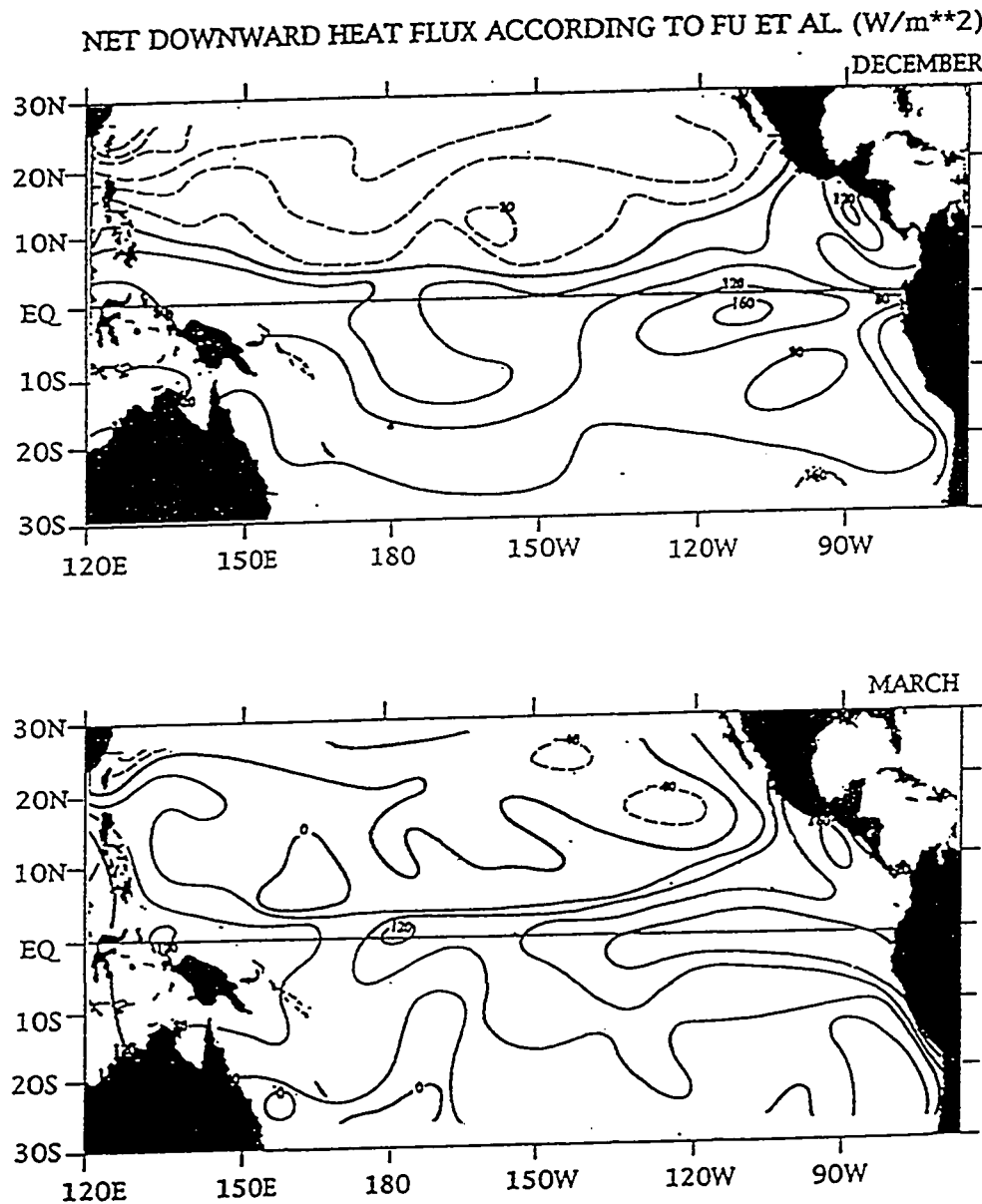


Figure 14. The pattern of the net downward surface heat flux according to Fu et al. (1990). (a) December; (b) March; (c) June; and (d) September (the contour interval is $40 W/m^2$).

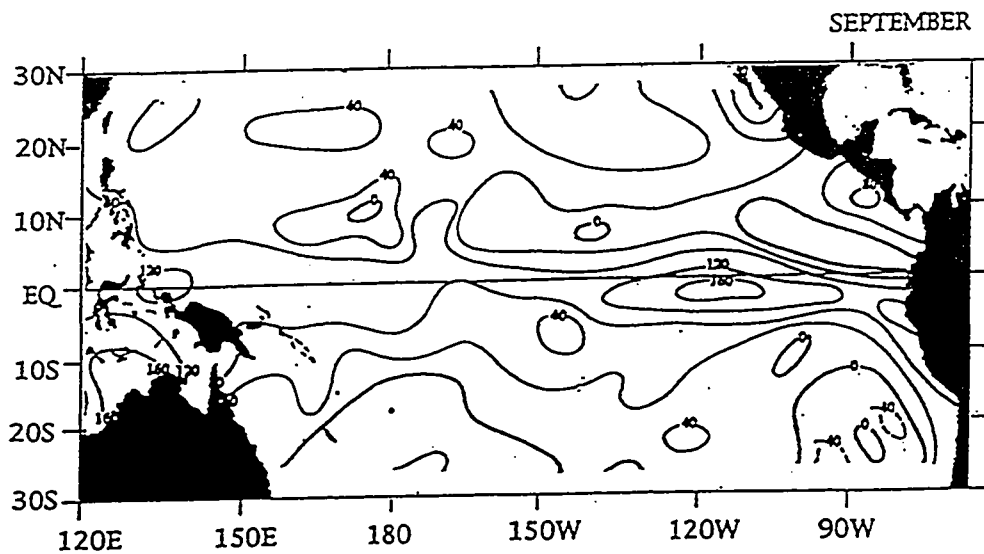
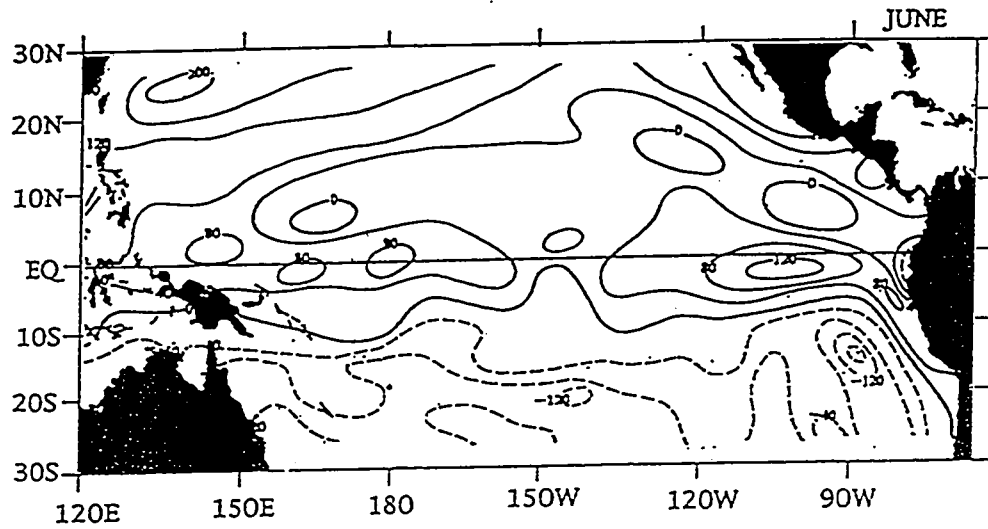
NET DOWNWARD HEAT FLUX ACCORDING TO FU ET AL. (W/m^{**2})

Figure 14. continued

over 120 W/m^2 , in FU90; while the heating in the other two maps is compatible, about 50 W/m^2 .

As northern spring approaches, the surface heat loss is greatly reduced. The heat budget is near zero over a broad area of the northern Pacific in both FU90 (Figure 14b) and our map (Figure 12b). But the surface heat loss is still visible in O88 (Figure 13b) and is most noticeable in the northeastern Pacific where the value is over 75 W/m^2 . The intense heating of 160 W/m^2 along the coast of Mexico and central America exists only in FU90. The warm pool gains more heat in FU90 than O88 and our map. The heating in the southern Pacific decreases and negative values appear in O88 and our map. The largest difference between our pattern and either O88 or FU90 is the strength and the location of the maximum heat gain in the eastern Pacific. The heat surplus center, stretching westward from the coast of south America, forms a belt along the equator with the maximum value about 160 W/m^2 in O88 and FU90. Compared with their own patterns in December, the strength of the center increases in O88 and, oppositely, it decreases in FU90. The equatorial maximum heating center in our map moves offshore to about 135°W and its strength has a slight decrease. Therefore, whether this equatorial belt should be enhanced or reduced during spring time can not be judged by comparing with these two chosen atlases.

Our heat flux pattern in the northern early summer (Figure 12c) differs from those of O88 (Figure 13c) and FU90 (Figure 14c) at the location of the maximum center of the equatorial belt. In our map, the maximum center is located at 140°W and the value decreases to about 80° W/m^2 . Heat

loss occurs along the coast of South America and its value significantly increases compared with March. Although the heating in this area is reduced from March to June to about 75 W/m^2 in O88 and 120 W/m^2 in FU90, the center is located at 100°W in both maps. There indeed exists a small heat loss area in the Eastern Pacific at the equator in FU90, but its strength is only half of ours. The FU90 has a stronger heating in the Western Pacific warm pool area than both O88 and ours. The common features of all the maps are the increasing heating in the north but with greater strength in O88 and FU90 than our map; the strong heat loss in the southern ocean; and the intense heating in the northeast along the cold California current.

The belt of our heat surplus in the equator is centered at 150°W in September (Figure 12d). It slightly moves westward and spreads wider along the equator. The heat loss off the coast of south America is greatly reduced. The center in both O88 (Figure 13d) and FU90 (Figure 14d) has a westward movement and increases its heating strength. Again the heat gain in the warm pool in FU90 is much stronger than our map and O88. All these maps show the reverse heating pattern to that in the spring time for the region outside of the equator.

To summarize, outside of the equatorial zone ($8^\circ\text{S} - 8^\circ\text{N}$), the seasonal variations of the heat flux pattern from our calculation agrees with those of O88 and FU90 but the strength is weaker. FU90 gives the maximum strength throughout the climatology year. Our map fails in simulating the strong seasonal variations of the heat flux over the Kuroshio region in the northern winter time. In the equatorial zone, our

center of the maximum heat gain in the east Pacific, especially along the coast of the south America, has a different evolution in location and strength from O88 and FU90. The variation of heat flux in the Western Pacific warm pool area is small all year around in both O88 and our map but is very large in FU90.

The net heat flux is determined by the heat exchange process between the sea surface and the lower atmosphere. In the next section we present the air-sea interaction mechanisms controlling the distribution of the heat fluxes. We then study the thermodynamic relation between the SST and the surface heat flux from the SST equation. The divergence of our result from those atlases (O88 and FU90) which used the bulk aerodynamic formulae is discussed.

5.2.2 The Physical Processes Determining the Heat Flux Distribution

Of all the components in the downward heat budget balance, the solar radiation and latent heat flux are the major contributors for the seasonal variations of the surface heat flux. The loss of heat by sensible heat flux over the ocean surface is much less than the latent heat flux (about one-tenth).

The seasonal cycle of the solar radiative flux is mainly defined by the change in albedo and modified by seasonal variations of the cloud cover (See the atlases by Esbensen and Kushnir (1981), Oberhuber (1988), Fu et al. (1990)). The solar heating varies primarily with latitude which decreases from the equator to the polar regions. The northern ocean

receives maximum solar incoming radiation from spring to summer while the southern ocean has minimum solar heating in this period.

The latent and sensible heat fluxes are controlled by the wind speed and the vertical gradient of humidity or temperature at the ocean surface (e.g. Cayan, 1990; Large and Pond, 1982). Outside of the equatorial region (latitudes poleward of 8°), the latent and sensible fluxes are strongly seasonal. For the northern hemisphere, they reach their maxima from fall to winter because of the seasonal enhancement of the northeast trade winds and the large thermal or vapor difference near the ocean surface. The pattern reverses for the southern hemisphere. Within the equatorial region, there is a low latent heat belt stretching along the equator from 6°S to 2°N with the minimum located near the coast of Peru (e.g., Oberhuber (1988), Fu et al. (1990)).

The resulting net surface heat flux has a corresponding variation in the seasonal time scales. During the northern fall and winter time, the latent and sensible heat loss to the atmosphere over the northern ocean (the southern ocean) is much larger (less) than the net solar radiation accumulated at the surface, and therefore, the ocean releases (gains) heat to (from) the atmosphere. During the rest of the year, the northern (southern) ocean gains (loses) heat mainly due to the seasonal increasing (decreasing) of the solar incoming flux. The existence of the maximum net heat flux in the Eastern Pacific cold tongue region is the result of the minimum latent heat loss in this area.

The comparisons in section 5.2.1 show that the variational adjoint procedure has successfully simulated the main seasonal signals of the

heat flux distribution from assimilating the SST observation. But the strength of the seasonal variation is weaker and the evolution of the equatorial heat gain belt is different from the atlases of O88 and FU90.

5.2.3 Examining the Results from the Thermodynamic Point of View

Our net surface heat flux pattern is derived from the SST observations. The evolution of SST is governed by the ocean advection process as well as the surface incoming heat flux. As is discussed in section 4.2, the changes of SST in the extra-equatorial region is mainly determined by the seasonal variations of the surface heat flux, in which the solar radiation plays a dominant role, while the seasonal variability of the equatorial SST is related to the coupled dynamic/thermodynamic upwelling process occurring in the upper ocean.

The modeled SST field is displayed in Figures 15a-d. Outside of the equatorial region, the modeled SST field well resembles the observational SST field (Figures 6a-d). In the equatorial region, the seasonal variations of the cold tongue in both model and observations follow the cycle: the cold tongue is weakest in northern hemisphere spring and strongest in fall. However, the shape of the modeled cold tongue is slightly different from the observation. In what follows we attempt to explain why there is a difference of our heat flux pattern from the other maps over the region of the cold tongue.

The SST in the equatorial cold tongue is warmest in the northern winter and spring. The warmer SST at this time is due to both the weaker

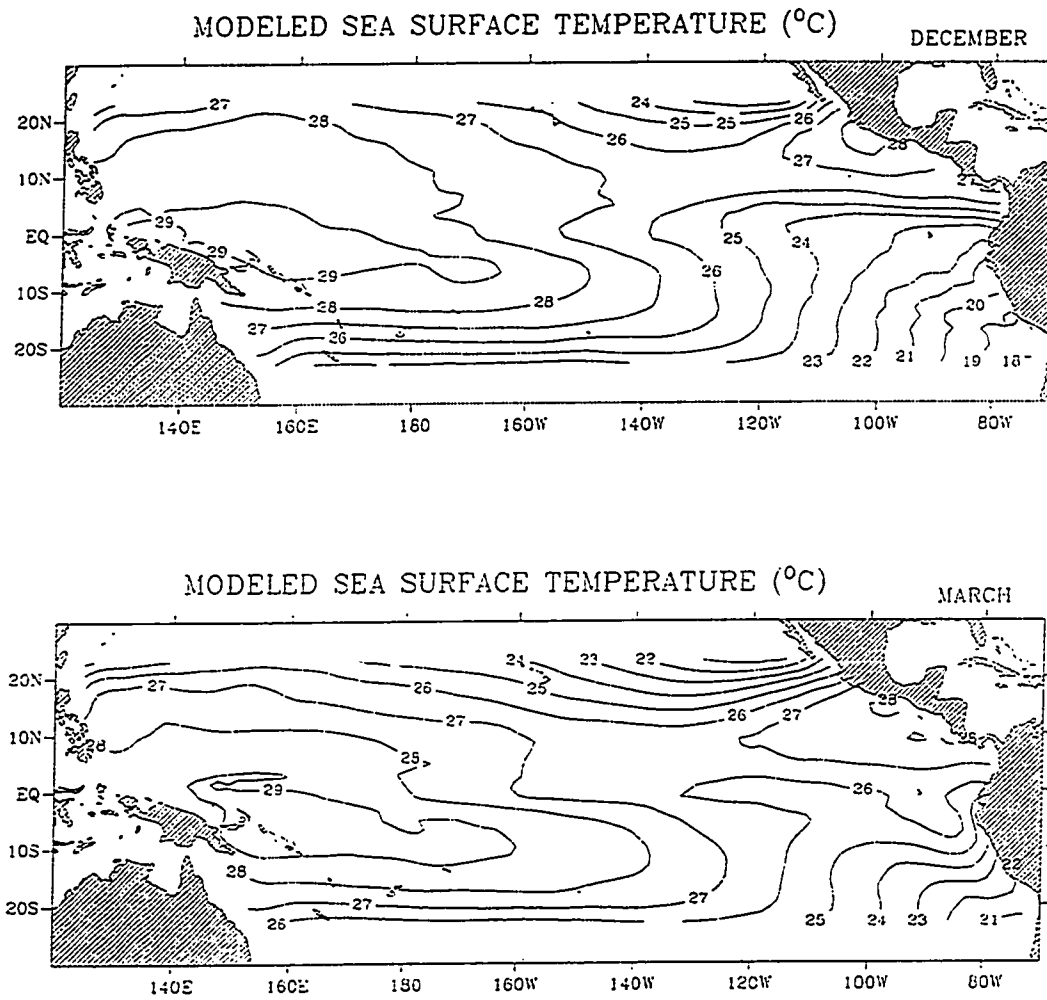


Figure 15. The pattern of the modeled sea surface temperature (SST) in (a) December; (b) March; (c) June; and (d) September.

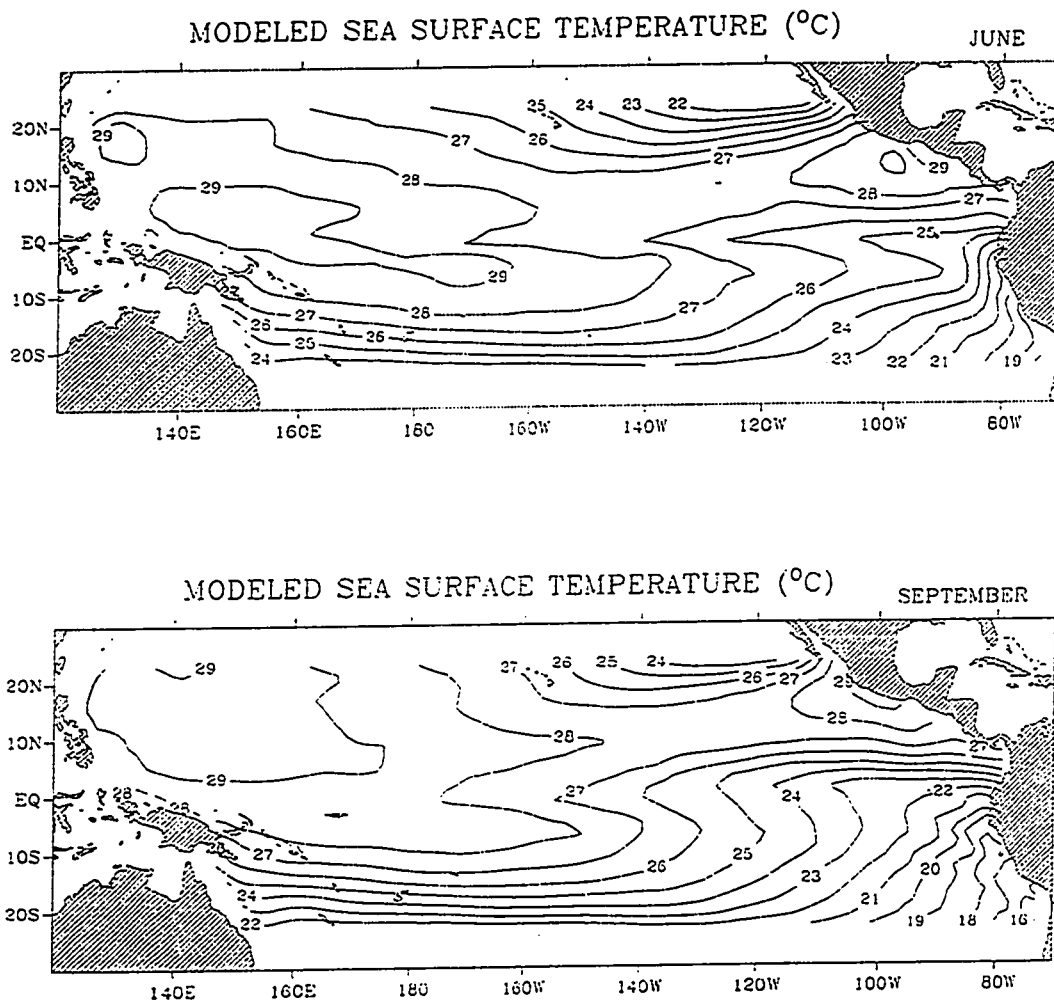


Figure 15. continued

cooling associated with the weaker upwelling (Figures 5a-b) and the stronger surface heating (Figures 12a-b). The changes of our heat flux pattern during this period is consistent with O88 and FU90.

A cold SST occurs in September along the coast of south America. There are two mechanisms responsible for the appearance of this cooler SST. One is the most intensive cooling by the strongest upwelling during this period; and the other one is the strong surface cooling starting in the earlier summer (Figure 12c). The existence of a strong heat loss area along the coast of south America in the summer time is a unique feature in our map. It does appear in FU90 (Figure 14c) but with much weaker strength and O88 does not have this cooling at all.

In the southeast Pacific along the south American coast, the SST decreases about 4 - 5°C during northern spring-summer. The upwelling pattern shows that the coastal upwelling is much weaker than the equatorial upwelling (Figures 5b-c). The SST decreases along the coast of the south America and must be caused by some other cooling mechanisms. The strong surface heat release is therefore the main contributor for reducing the temperature so significantly and rapidly.

From the analysis of the air-sea interactions during this period, we see that these large heat releases in this region are reasonable. Off the coast of south America, northern summer is the time of the year when the value of the cloud cover is maximum (relative to areas to the north and west) and therefore the incoming solar heating is a minimum (e.g. FU90). This is also the time when the southeast trade is strongest and thus the latent heating release increases (e.g. FU90). Both mechanisms have the

effect of reducing the heat received from the atmosphere. The appearance of the negative heat flux can be explained as being due to the latent heat release which overpowers the solar incoming.

Therefore it is mainly the surface cooling that causes the SST to decrease along the coast of south America in the northern summer and fall in our calculation.

5.2.4 Data Misfit

The cost function is minimized when the optimal heat flux pattern is obtained. The pattern of the data misfit between the model SST and the observed SST is shown in Figures 16a-d. The data misfits in the northern summer and fall are larger than those in the winter and spring. The largest discrepancies between the model and the observations are in the regions associated with the cold tongue and the Kuroshio, where the misfit of 0.75°C appears.

We suspect that the larger data misfits in the cold tongue and the warm Kuroshio are partly attributable to the model's own shortcomings. The model uses a constant surface layer in resolving the physics of the near-surface region. However, the assumption that the surface layer is a constant may not be practical in representing the intensity of the upwelling.

By choosing the surface layer depth to be 50 meters, the temperature of the entrained water (T_d) is represented by the temperature at 50-m depth (T_{50}) and parameterized in terms of the vertical

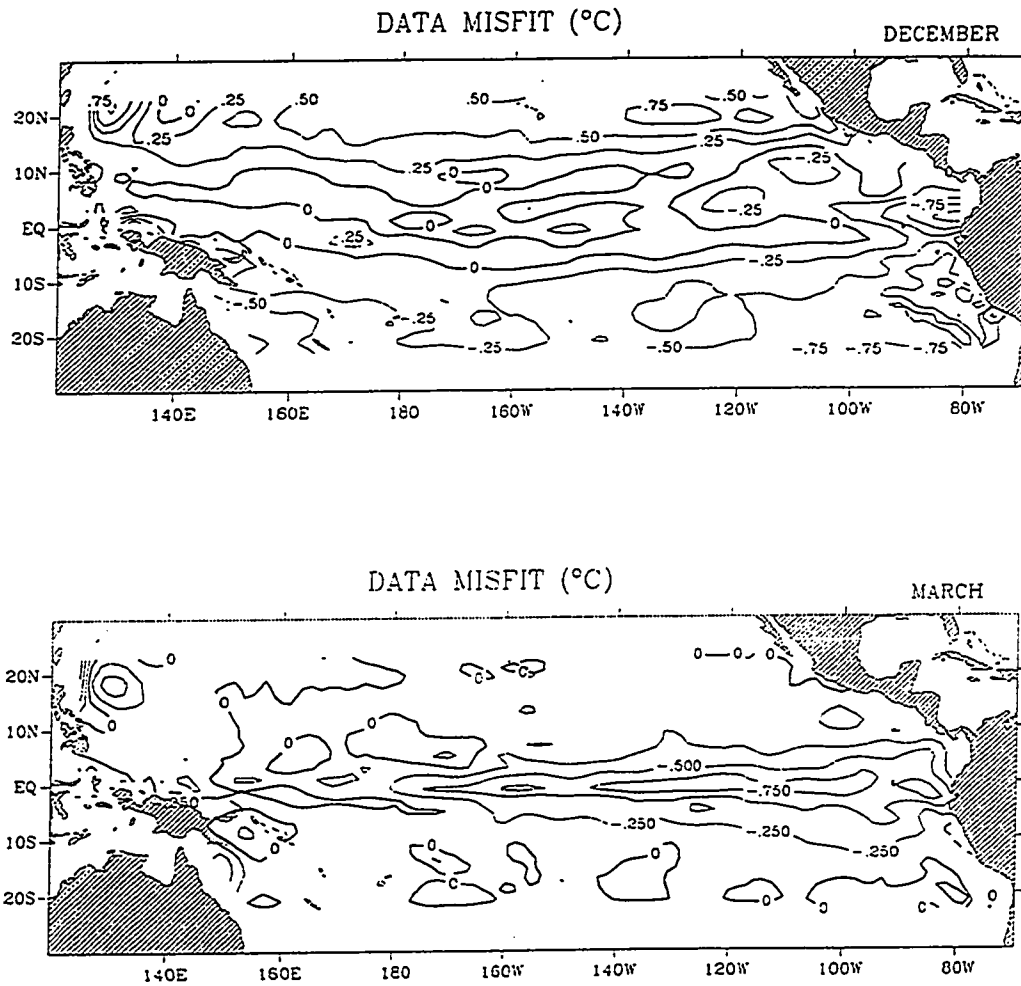


Figure 16. Data misfits between the modelled and the observed SST in (a) December; (b) March; (c) June; and (d) September (the contour interval is 0.25°C).

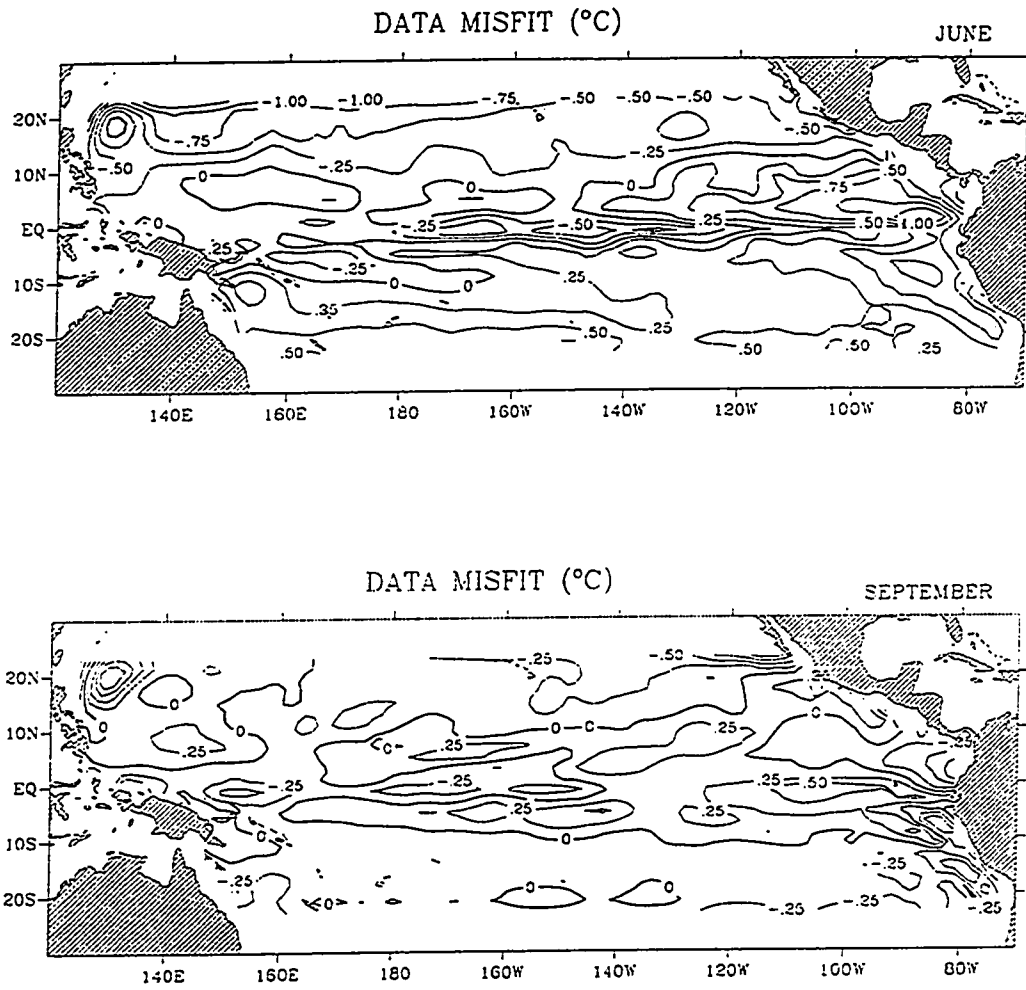


Figure 16. continued

displacements of the model thermocline, in the same way as Seager et al. did (1988). By doing so, the intensity of the upwelling is strongly dependent on the temperature at 50m. For a deep thermocline (e.g., the western equatorial Pacific), the upwelled water from above the thermocline is warm. For a shallow thermocline (e.g., the eastern equatorial Pacific), the upwelled water from the thermocline region is cold.

In reality, choosing 50-m to simulate the surface layer may not be appropriate in the eastern Pacific where one expects a shallower surface layer to exist. Hence the model may give a stronger upwelling in this region and the surface water might be cooler than it should be. This can explain the existence of the large negative data misfit associated with the equatorial upwelling region.

The model is formulated in such a way to simulate the major features of the equatorial ocean. The parameterization of the entrainment is too simple so that it may not be applied to the regions outside of the equatorial zone. The larger data misfit in the northwestern Pacific - the Kuroshio region - may be partly due to the lack of mid-latitude dynamics in the model formulation; and/or due to the open boundary condition associated with the western boundary current.

The large departure of the model SST from observed SST in the regions of the equatorial cold tongue and the western boundary current indicates that the model physics in these regions are inconsistent with the data. The modeled SST tends to be cooler than the observed SST here. However, the heat flux pattern obtained is best consistent with the model dynamics as well as the observations.

6. Summary and Conclusions

A simple oceanic model with thermodynamics is used to determine the surface thermal forcing field by the variational adjoint technique. Two data-sets are chosen, the climatological monthly-mean sea surface temperature (SST) and winds. We have been able for the first time to calculate the seasonal surface heat flux patterns which are consistent with the ocean's dynamics and thermodynamics and which agree with the observations.

The results show that the model, albeit simple, is capable of assimilating the sea surface temperature (SST) observations in deriving the surface heat flux. The oceanic model used is essentially the same as Seager et al. (1988). It adopts a constant-depth surface layer to simulate the features near the surface region. As is common in a reduced-gravity model, we assume that the surface pressure gradient varies with the thermocline depth alone. Fortunately by assuming this, the model physics are greatly simplified because the model dynamics and thermodynamics become decoupled. This permits the integration of the dynamic model and the variational parameter estimating to be performed separately.

The total number of the control parameters in this study is very large because the estimated flux field is a function of time and space. We perform the descent algorithm efficiently by applying the technique of scaling to improve the conditioning of the Hessian (the second derivative

matrix of the cost function). The scaling transforms the variables from units that typically reflect the physical nature of the problem to units that display certain desirable properties of the optimization. The basic rule of variable scaling is to make all the variables in the scaled problem to be order of unity so that each variable has a similar weight during the optimization. By scaling the variables, the derivatives of the cost function are also scaled implicitly. Experiments have shown that an initial well-scaled functional leads to a significant improvement in the performance of the descent algorithm.

In variational analysis, the solution of a problem is sought by minimizing the cost function. The use of the *a priori* information is investigated in the formulation of the cost function to obtain meaningful model parameters. Experimental evidence has verified that adding *a priori* information of the estimated parameters can increase the probability for the solution to be unique. Also the *a priori* information plays the role of bogus data. It serves not only to increase the number of observations but to improve the conditioning of the Hessian matrix. Hence the practical benefit of adding the *a priori* information is to precondition and to accelerate the convergence of the descent algorithm.

We learned from many test runs that the surface heat flux pattern can not be fully derived without the optimal adjustment of the model initial SST state. The importance of a correct initial SST condition in our study is to ensure a periodic seasonal cycle and therefore reduces the level of the data misfit.

The result illustrates that the model, albeit simple, is capable of assimilating the sea surface temperature (SST) observations in deriving the surface heat flux. The comparison with the existing heat flux atlases of Oberhuber (1988) and Fu et al. (1990) has shown that our adjoint procedure has successfully captured the seasonal signals of the surface heat flux distribution over the tropical Pacific ocean. However, our heat flux pattern gives a weaker strength in the variations all year round. The model is also inadequate to simulate the strong variations in the northwestern Pacific ocean over the Kuroshio region.

Examining the data misfits between the modeled SST and the observed SST, one finds that a larger departure exists mainly in the equatorial upwelling zone and the Kuroshio region. The modeled SST tends to be cooled more than the observed SST. We conjecture that this model-data misfit may be due to the model's own shortcomings. The model is formulated to study the equatorial ocean dynamics; it lacks the mid-latitude physics in resolving the features associated with the Kuroshio. The inclusion of the constant surface layer may not well represent the strength of the equatorial upwelling.

Nonetheless, the results from this research are very promising. It provides a way for extracting the surface heat flux information directly from the SST data. The optimal surface heat flux pattern estimated is ensured to be consistent with the model physics and the observations. It allows us to be able to explain the calculated model fields in terms of the model physics and therefore to discover the weakness of the model formulation by comparing with the data.

The methodology used here can be easily extended to determine the surface wind forcing field. It is possible to derive both the surface wind and heat flux forcing by simultaneously assimilating the available wind and SST dataset. As many applications have discovered, the adjoint method is so versatile and powerful that it can adjust any model parameter as long as there are sufficient observational data available.

Appendix A: Derivation of the Continuous Adjoint Equation

From section 6 the cost function is defined as:

$$\begin{aligned}
 J(T, Q, T_0) = & \frac{1}{2} \int_{\Sigma} (T - \hat{T})^2 d\sigma + \frac{1}{2} K'_Q \int_{\Sigma} (Q - \bar{Q})^2 d\sigma \\
 & + \frac{1}{2} K'_0 \int_{xy} (T_0 - \bar{T}_0)^2 dx dy
 \end{aligned} \tag{A1}$$

where the superscript T denotes the transpose, K'_0 and K'_Q are the computational weights.

The augmented Lagrangian is given by:

$$\begin{aligned}
 L(\lambda_T, T, Q, T_0) = & J(T, Q, T_0) + \\
 & \int_{\Sigma} \lambda_T \left\{ \frac{\partial T}{\partial t} + \delta_A \left(u \frac{\partial T}{\partial x} + v \frac{\partial T}{\partial y} \right) + \delta_A M(w_e) (T - T_d) - \delta_Q Q - \delta_{v_x} \frac{\partial^2 T}{\partial x^2} - \delta_{v_y} \frac{\partial^2 T}{\partial y^2} \right\} d\sigma
 \end{aligned} \tag{A2}$$

The condition that L is a stationary point requires the first variation of L vanish. We thereby obtain four Euler-Lagrange equations for λ_T , T , Q , and T_0 :

$$\frac{\partial L(\lambda_T, T, Q, T_0)}{\partial \lambda_T} = 0 \tag{A3}$$

$$\frac{\partial L(\lambda_T, T, Q, T_0)}{\partial T} = 0 \quad (\text{A4})$$

$$\frac{\partial L(\lambda_T, T, Q, T_0)}{\partial Q} = 0 \quad (\text{A5})$$

$$\frac{\partial L(\lambda_T, T, Q, T_0)}{\partial T_0} = 0 \quad (\text{A6})$$

The condition (A3) gives:

$$\frac{\partial T}{\partial t} + \delta_A \left(u \frac{\partial T}{\partial x} + v \frac{\partial T}{\partial y} \right) + \delta_A M(w_e) (T - T_d) - \delta_Q Q - \delta_{v_x} \frac{\partial^2 T}{\partial x^2} - \delta_{v_y} \frac{\partial^2 T}{\partial y^2} = 0 \quad (\text{A7})$$

which is identical to the original SST model equation (3.14), where the Heavyside function $M(w_e)$ is equal to its argument w_e when w_e is positive and equal to zero otherwise.

The condition (A4) obtains the equation for the Lagrange multiplier λ_T , namely, the adjoint equation. The practical procedure involves the partial integration of the model equation (A7) and is performed as follows:

$$\frac{\partial L}{\partial T} = \frac{\partial J}{\partial T} +$$

①

$$\frac{\partial}{\partial T} \int_{\Sigma} \lambda_T \left\{ \frac{\partial T}{\partial t} + \delta_A \left(u \frac{\partial T}{\partial x} + v \frac{\partial T}{\partial y} \right) + \delta_A M(w_e) (T - T_d) - \delta_Q Q - \delta_{v_x} \frac{\partial^2 T}{\partial x^2} - \delta_{v_y} \frac{\partial^2 T}{\partial y^2} \right\} d\sigma$$

②

③

④

⑤

⑥

⑦

⑧

There are eight terms contributing to the variation of L with respect to T . The first term gives:

$$\textcircled{1} = \int_{\Sigma} (T - \hat{T}) d\sigma \quad (\text{A8})$$

which is the square root of the data misfit. Performing the integration on the second term yields:

$$\begin{aligned} \textcircled{2} &= \frac{\partial}{\partial T} \int_{\Sigma} \left(\lambda_T \frac{\partial T}{\partial t} \right) d\sigma \\ &= \frac{\partial}{\partial T} \left\{ \int_{\Sigma} \frac{\partial}{\partial t} (\lambda_T T) d\sigma - \int_{\Sigma} \left(\frac{\partial \lambda_T}{\partial t} T \right) d\sigma \right\} \\ &= \frac{\partial}{\partial T} \left\{ \int_x \int_y [\lambda_T T]_{t=0}^{t=t_0} dx dy \right\} - \int_{\Sigma} \frac{\partial \lambda_T}{\partial t} d\sigma \\ &= - \int_{\Sigma} \frac{\partial \lambda_T}{\partial t} d\sigma \end{aligned} \quad (\text{A9})$$

where the periodic condition for both T and λ_T are used.

The boundary condition $u=0$ at the eastern and western end of the basin is applied in integrating the third term. One then obtains:

$$\begin{aligned} \textcircled{3} &= \frac{\partial}{\partial T} \int_{\Sigma} \delta_A \left(\lambda_T u \frac{\partial T}{\partial x} \right) d\sigma \\ &= \frac{\partial}{\partial T} \left\{ \int_{\Sigma} \delta_A \frac{\partial}{\partial x} (\lambda_T u T) d\sigma - \int_{\Sigma} \delta_A \left(\frac{\partial (\lambda_T u)}{\partial x} T \right) d\sigma \right\} \end{aligned} \quad (\text{A10})$$

$$= - \int_{\Sigma} \delta_A \frac{\partial(\lambda_T u)}{\partial x} d\sigma$$

Similarly, one finds

$$\begin{aligned} \textcircled{4} &= \frac{\partial}{\partial T} \int_{\Sigma} \delta_A \left(\lambda_T v \frac{\partial T}{\partial y} \right) d\sigma \\ &= \frac{\partial}{\partial T} \left\{ \int_{\Sigma} \delta_A \frac{\partial}{\partial y} (\lambda_T v T) d\sigma - \int_{\Sigma} \delta_A \left(\frac{\partial(\lambda_T v)}{\partial y} T \right) d\sigma \right\} \quad (\text{A11}) \\ &= - \int_{\Sigma} \delta_A \frac{\partial(\lambda_T v)}{\partial y} d\sigma \end{aligned}$$

where the condition $v=0$ at a solid northern and southern boundary has been used in neglecting the extra term.

The fifth and sixth terms give:

$$\textcircled{5} = \frac{\partial}{\partial T} \int_{\Sigma} \delta_A [\lambda_T M(w_e) (T - T_d)] d\sigma = \int_{\Sigma} \delta_A [\lambda_T M(w_e)] d\sigma \quad (\text{A12})$$

$$\textcircled{6} = 0 \quad (\text{A13})$$

The intergration of the friction term can be written as:

$$\textcircled{7} = - \frac{\partial}{\partial T} \int_{\Sigma} \delta_{vx} \left(\lambda_T \frac{\partial^2 T}{\partial x^2} \right) d\sigma$$

$$\begin{aligned}
&= -\frac{\partial}{\partial T} \left\{ \int_{\Sigma} \delta_{vx} \frac{\partial}{\partial x} \left(\lambda_T \frac{\partial T}{\partial x} \right) d\sigma - \int_{\Sigma} \delta_{vx} \left(\frac{\partial \lambda_T}{\partial x} \frac{\partial T}{\partial x} \right) d\sigma \right\} \quad (A14) \\
&= -\frac{\partial}{\partial T} \left\{ \int_{\Sigma} \delta_{vx} \frac{\partial}{\partial x} \left(\lambda_T \frac{\partial T}{\partial x} \right) d\sigma - \int_{\Sigma} \delta_{vx} \frac{\partial}{\partial x} \left(T \frac{\partial \lambda_T}{\partial x} \right) d\sigma + \int_{\Sigma} \delta_{vx} \left(T \frac{\partial^2 \lambda_T}{\partial x^2} \right) d\sigma \right\} \\
&= - \int_{\Sigma} \delta_{vx} \left(\frac{\partial^2 \lambda_T}{\partial x^2} \right) d\sigma
\end{aligned}$$

where it is known that there is no heat flux through the ocean sides, therefore, $\frac{\partial T}{\partial x} = 0$ and $\frac{\partial \lambda_T}{\partial x} = 0$ at the eastern and western end of the basin.

The last term can be intergrated in the same way:

$$\begin{aligned}
\textcircled{3} &= -\frac{\partial}{\partial T} \int_{\Sigma} \delta_{vy} \left(\lambda_T \frac{\partial^2 T}{\partial y^2} \right) d\sigma \\
&= -\frac{\partial}{\partial T} \left\{ \int_{\Sigma} \delta_{vy} \frac{\partial}{\partial y} \left(\lambda_T \frac{\partial T}{\partial y} \right) d\sigma - \int_{\Sigma} \delta_{vy} \left(\frac{\partial \lambda_T}{\partial y} \frac{\partial T}{\partial y} \right) d\sigma \right\} \quad (A15) \\
&= -\frac{\partial}{\partial T} \left\{ \int_{\Sigma} \delta_{vy} \frac{\partial}{\partial y} \left(\lambda_T \frac{\partial T}{\partial y} \right) d\sigma - \int_{\Sigma} \delta_{vy} \frac{\partial}{\partial y} \left(T \frac{\partial \lambda_T}{\partial y} \right) d\sigma + \int_{\Sigma} \delta_{vy} \left(T \frac{\partial^2 \lambda_T}{\partial y^2} \right) d\sigma \right\} \\
&= - \int_{\Sigma} \delta_{vy} \left(\frac{\partial^2 \lambda_T}{\partial y^2} \right) d\sigma
\end{aligned}$$

where the condition $\frac{\partial T}{\partial y} = 0$ and $\frac{\partial \lambda_T}{\partial y} = 0$ at a solid northern and southern boundary have been used.

Note that the derivation of the adjoint equation has been done for a solid northern and southern boundary. When the variational analysis is applied to a limited computational domain, the open boundary condition is adopted in the SST model. It can be shown, by deriving the adjoint equation in the finite difference form, that the open boundary condition for the adjoint is identical to the SST model.

Summing up (A8) to (A15), the condition that the first-order variation of L with respect to T vanishes gives the adjoint equation:

$$-\frac{\partial \lambda_T}{\partial t} - \delta_A \left\{ \frac{\partial(\lambda_T u)}{\partial x} + \frac{\partial(\lambda_T v)}{\partial y} \right\} + \delta_A \{ \lambda_T M(w_e) \} - \delta_{vx} \frac{\partial^2 \lambda_T}{\partial x^2} - \delta_{vy} \frac{\partial^2 \lambda_T}{\partial y^2} + (T - \hat{T}) = 0 \quad (\text{A16})$$

The condition (A5) gives the equation

$$K_Q' (Q - \tilde{Q}) - \delta_Q \lambda_T = 0 \quad (\text{A17})$$

whose left hand side is the gradient of the cost function with respect to the control field parameters Q , which is:

$$\nabla_Q J = K_Q' (Q - \tilde{Q}) - \delta_Q \lambda_T \quad (\text{A18})$$

Finally, we yield the equation from the condition (A6) which is:

$$K_T' (T_0 - \tilde{T}_0) -$$

$$\left\{ \frac{\partial \lambda_T}{\partial t} + \delta_A \left[\frac{\partial(\lambda_T u)}{\partial x} + \frac{\partial(\lambda_T v)}{\partial y} \right] - \delta_A \lambda_T M(w_e) + \delta_{vx} \frac{\partial^2 \lambda_T}{\partial x^2} + \delta_{vy} \frac{\partial^2 \lambda_T}{\partial y^2} \right\}_{t=0} = 0$$

$$(\text{A19})$$

The left hand side is the gradient of the cost function with respect to the initial SST field parameters, that is:

$$\nabla_{T_0} J = K'_0 (T_0 - \tilde{T}_0) - \left\{ \frac{\partial \lambda_T}{\partial t} + \delta_A \left[\frac{\partial(\lambda_T u)}{\partial x} + \frac{\partial(\lambda_T v)}{\partial y} \right] - \delta_A \lambda_T M(w_e) + \delta_{vx} \frac{\partial^2 \lambda_T}{\partial x^2} + \delta_{vy} \frac{\partial^2 \lambda_T}{\partial y^2} \right\}_{t=0}$$

(A20)

Appendix B: Verification of the Correctness of the Gradient Calculation

It is important to verify the correctness of the gradient calculation before carrying out the minimization of the cost function. One way to check if the correct gradient is found is described below. Let

$$J(T, u + \alpha h) = J(T, u) + \alpha h^T \nabla J_u(T, u) + O(\alpha^2) \quad (\text{B1})$$

be a Taylor expansion of the cost function. The term u represents the control parameters (the initial SST state and the heat flux field), α is a small scalar and h is a vector of unit length (such as $h = \nabla J / \|\nabla J\|^{-1}$). Rewriting (B1) one can define a function of α by

$$\phi(\alpha) = \frac{J(T, u + \alpha h) - J(T, u)}{\alpha h^T \nabla J_u(T, u)} = 1 + O(\alpha) \quad (\text{B2})$$

If the values of the cost function and the gradient are correctly calculated, the value of $\phi(\alpha)$ will linearly approach 1 with α decreasing through a wide range of magnitudes. If we find that the value of ϕ is linearly approaching a constant $C \neq 1$, it indicates that there are errors in the gradient calculation. The error may occur in the data management in the forward dynamical model (write out) and the adjoint model (read in), which results in the added forcing being wrong. If there is no linearity in

the variation of the value of ϕ with decreasing values of α , then the errors are probably due to an incorrect calculation of the cost function.

The variation of the value of the function $\phi(\alpha)$ with decreasing values of α is shown in Figure 17. It is clearly seen that, for values of α between 10^{-1} and 10^{-7} (which are not too close to the machine zero), a unit value of $\phi(\alpha)$ is obtained. The correctness of the gradient calculation is therefore verified. Table 2 gives values of the function $\phi(\alpha)$ as a function of α .

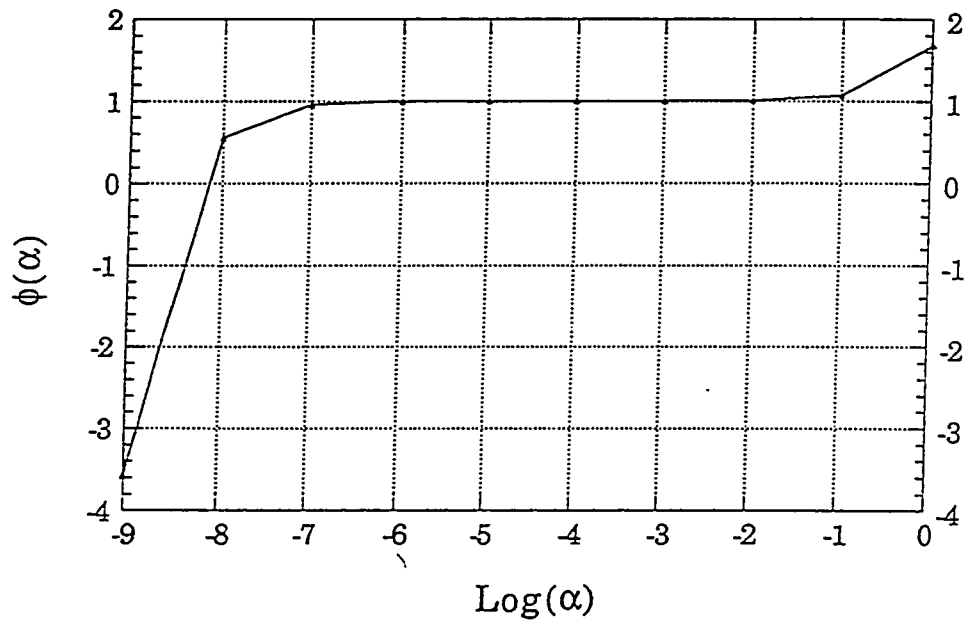


Figure 17. Verification of the gradient calculation

Table 2. Verification of the gradient of the cost function

α	$\phi(\alpha)$
10^1	1.6748334449
10^0	1.0675191363
10^{-1}	1.0067877039
10^{-2}	1.0007144947
10^{-3}	1.0000574353
10^{-4}	0.9998380197
10^{-5}	0.9972566599
10^{-6}	0.9507921824
10^{-7}	0.5506814043
10^{-8}	-3.5794943702
10^{-9}	-19.0676535243

Appendix C: Comparison with Residual Heat Flux

The SST equation used in our study can be viewed as a linear equation with non-constant coefficients:

$$\frac{\partial T}{\partial t} + \delta_A \left(u \frac{\partial T}{\partial x} + v \frac{\partial T}{\partial y} \right) + \delta_A M(w_e) (T - T_d) = \delta_Q Q + \delta_{v_x} \frac{\partial^2 T}{\partial x^2} + \delta_{v_y} \frac{\partial^2 T}{\partial y^2} \quad (C1)$$

The adjoint method searches for an optimal heat flux distribution by minimizing the cost function (A1) and adjusting the initial SST condition. When the optimal solution is obtained, the corresponding SST state gives the optimal representation of the observed SST field. From the data assimilation point of view, such a solution is dynamically balanced and observationally consistent.

One may argue by examining (C1) that the heat flux term can be viewed as the residual of the equation if all the other terms can be calculated. That is, one can use the observed SST values directly to compute each term of the equation (C1). The heat flux field is then obtained as the residual of the sum of all the other terms. Therefore, one has a much easier residual method to compute the heat flux pattern than the sophisticated data assimilation technique. If we do this, what is the difference between the residual heat flux and the optimal heat flux pattern, and what does this difference mean? Do we really need to

compute the heat flux with recourse to the fancy adjoint technique?

Figure 18a is the heat flux pattern in December from the residual calculation. Compared with the optimal heat flux pattern of Figure 18b, it can be seen that these two patterns have similar large scale features: the zero heat flux line is around 8°N across the whole basin; the ocean receives heat to the south of the zero line and releases heat to the north of the zero line; the maximum heat flux is centered in the eastern Pacific to the west of the coast of south America. However, the heating in the southern ocean in the residual calculation is stronger than in the optimal solution, especially the strength of the maximum center. The big difference between these two patterns is at the equator, where there are three eddy-like heating centers in the central Pacific existing only in the residual heat flux pattern.

The atlases of Oberhuber (1988) (Figure 12a) and Fu et al. (1990) (Figure 13a) show that there are no such intensive heating centers at the equator. Therefore, one may wonder what causes this false feature in the heat flux pattern by the residual calculation.

The observed data can always be divided into three parts: those that are consistent with the model dynamics, those that are inconsistent with the model dynamics, and those that are due to the observation error. In the case of our study, we can write the SST observation T_o as

$$T_o = T_m + T_e$$

where T_m denotes the part of the data consistent with the model, and T_e the part due to the model error and the observation error.

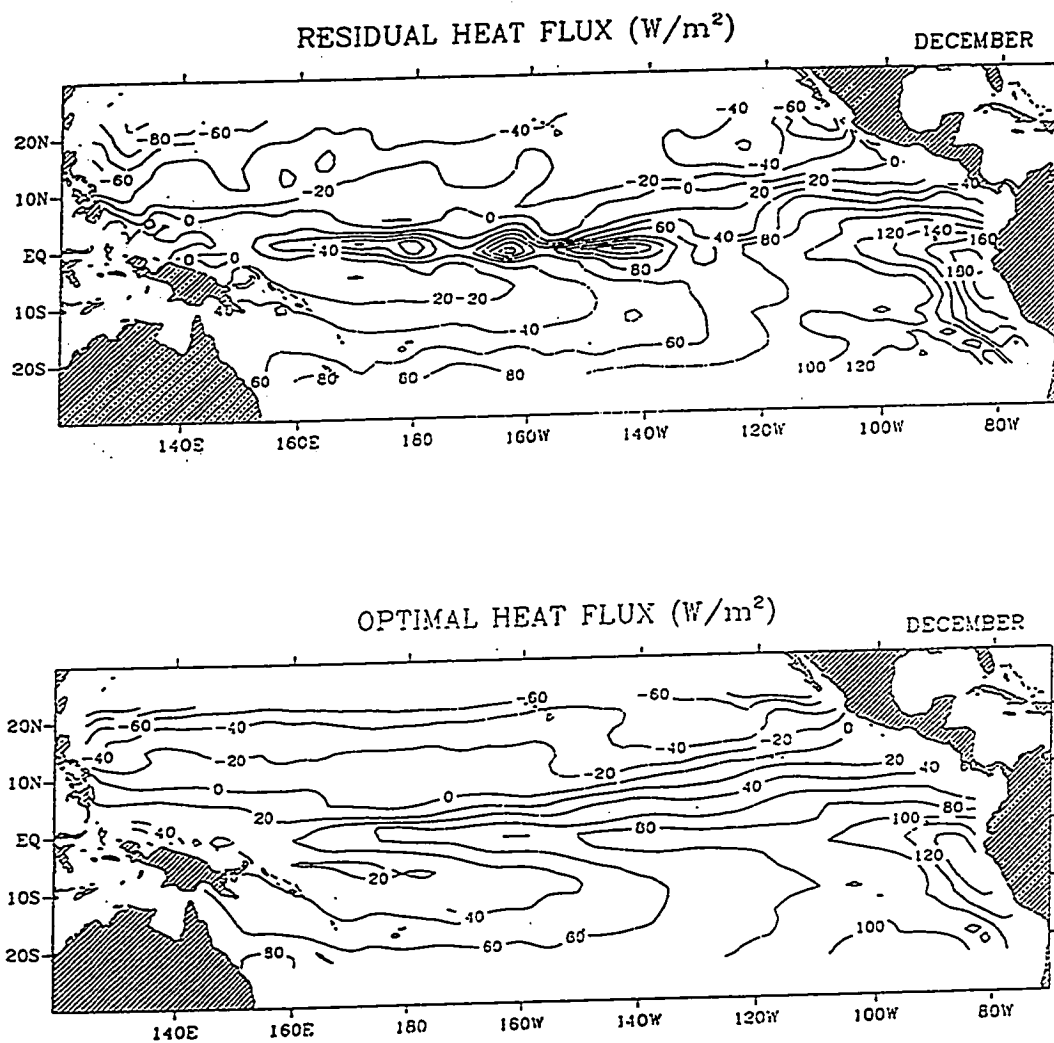


Figure 18. (a) Heat flux pattern from the residual calculation; (b) The optimal heat flux obtained from the adjoint procedure.

In the residual heat flux calculation, the value of T_o is used to compute the terms in equation (A1). The resulting heat flux, denoted as Q_o , can be expressed as

$$\frac{1}{\delta_Q} \left\{ \frac{\partial T_o}{\partial t} + \delta_A \left(u \frac{\partial T_o}{\partial x} + v \frac{\partial T_o}{\partial y} \right) + \delta_A M(w_e) (T_o - T_d) - \delta_{vx} \frac{\partial^2 T_o}{\partial x^2} - \delta_{vy} \frac{\partial^2 T_o}{\partial y^2} \right\} = Q_o \quad (B2)$$

While in the variational adjoint procedure, the heat flux pattern is determined optimally by minimizing the cost function (A1). The minimization procedure behaves like a filter and assimilates only the part of the SST data, T_m , which is compatible with the model dynamics. The evolution of the SST field is governed by the estimated heat flux and the optimally adjusted initial SST condition and satisfies the dynamical relation:

$$\frac{1}{\delta_Q} \left\{ \frac{\partial T_m}{\partial t} + \delta_A \left(u \frac{\partial T_m}{\partial x} + v \frac{\partial T_m}{\partial y} \right) + \delta_A M(w_e) (T_m - T_d) - \delta_{vx} \frac{\partial^2 T_m}{\partial x^2} - \delta_{vy} \frac{\partial^2 T_m}{\partial y^2} \right\} = Q_m \quad (C3)$$

where Q_m represents the dynamically consistent heat flux.

Subtracting (C3) from (C2) yields

$$Q_e = \frac{1}{\delta_Q} \left\{ \frac{\partial T_e}{\partial t} + \delta_A \left(u \frac{\partial T_e}{\partial x} + v \frac{\partial T_e}{\partial y} \right) + \delta_A M(w_e) T_e - \delta_{vx} \frac{\partial^2 T_e}{\partial x^2} - \delta_{vy} \frac{\partial^2 T_e}{\partial y^2} \right\} \quad (C4)$$

where $Q_e = Q_o - Q_m$. Therefore the difference between the residual heat flux and the optimal heat flux is represented by the quantity of Q_e , which is induced solely by T_e (the model and observation errors).

The question is now whether the three intensive heating centers at the equator in the residual heat flux pattern are attributable to the errors.

Let's do an experiment. Figure 19 is the data misfit between the observed SST and the modeled SST after the optimal heat flux pattern (shown in Figure 18b) is obtained. The heat flux corresponding to this misfit is not dynamically consistent with the model equation (C1) and is filtered out by the adjoint procedure. We add this data-misfit induced heat flux to the optimal solution of Figure 18b and display the resulting flux pattern in Figure 20. Compared with Figure 18a, these two patterns are remarkably similar. It is undoubtedly shown that it is the errors in the SST observations that create the extra heating centers at the equator in the residual heat flux calculation.

In general, the initial conditions, boundary conditions, and the forcing determine the trajectory of the partial differential equation (C1). It is shown in section 5.1.2 that the periodic seasonal cycle of the SST evolution can be obtained only if the optimal heat flux as well as the optimal initial condition are applied. It implies that the residual-calculated heat flux pattern cannot give the periodic solution of the equation (C1) due to the error. If such an error-contaminated heat flux is used as the forcing and a model-unbalanced observed SST state is chosen as the initial condition for the equation (C1), the model integration of (C1) will soon drive the SST field in an error-dominating state. This can be illustrated as follows.

Combining the continuity equation (3.5) with (C4) yields

$$\frac{\partial T_e}{\partial t} = -\delta_A \nabla(\underline{u} \cdot T_e) + \delta_Q Q_e - \delta_A M(w_e) T_e + \delta_A w_e T_e - \delta_{vx} \frac{\partial^2 T_e}{\partial x^2} - \delta_{vy} \frac{\partial^2 T_e}{\partial y^2} \quad (C5)$$

Equation (C5) is then integrated over the whole spatial domain. By assuming that all the boundaries are solid, one can obtain

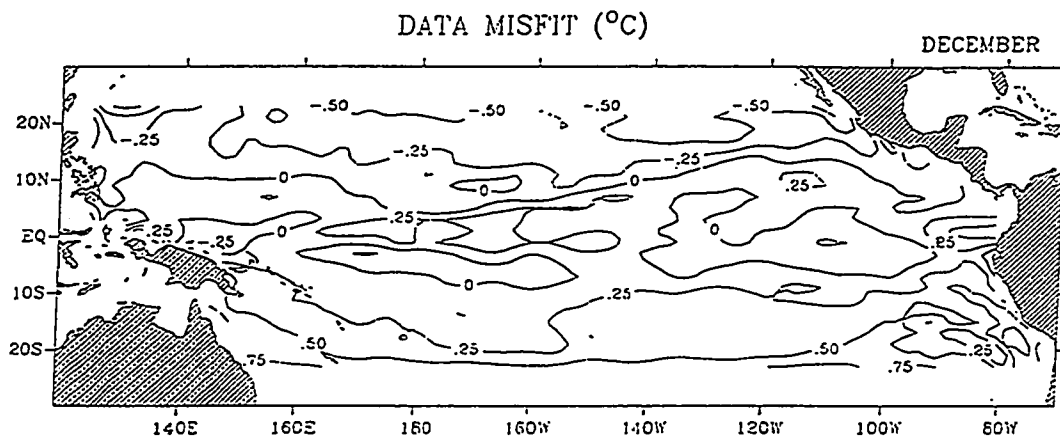


Figure 19. The data misfit between the observed SST and the modeled SST.

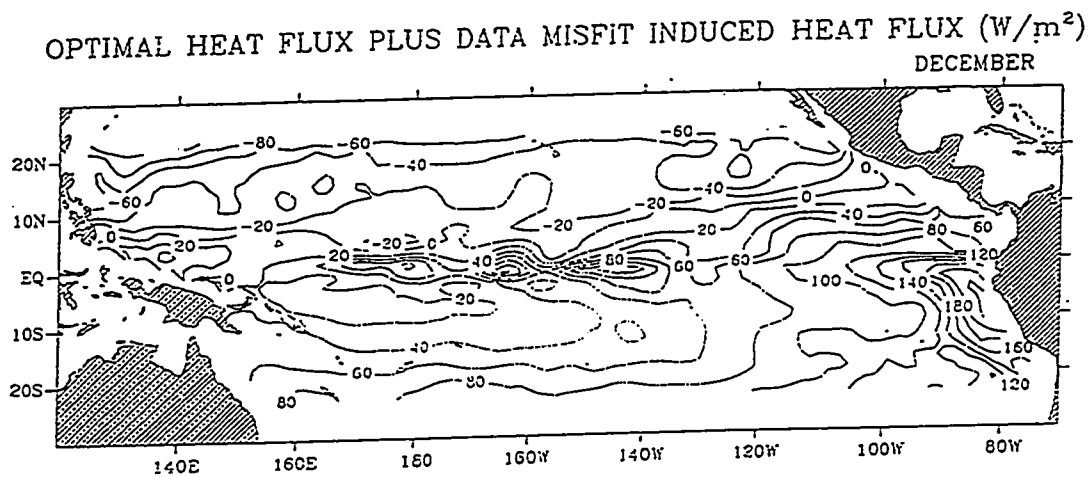


Figure 20. The heat flux pattern of the sum of the optimal heat flux and the data misfit induced heat flux. It is remarkably similar to Fig. 17a.

$$\frac{\partial \bar{T}_e}{\partial t} = \begin{cases} \delta_Q \bar{Q}_e & \text{for } w_e \geq 0 \\ \delta_Q \bar{Q}_e - \delta_A |w_e| T_e & \text{for } w_e < 0 \end{cases} \quad (\text{C6})$$

where the overbar ($\bar{\quad}$) denotes the spatial averaged values.

It can be seen from (C6) that the error is proportional to the value of the averaged heat flux in the upwelling area, and to the residual of the heat flux and downwelling in the downwelling area. Sizeable upwelling appears mainly in the equatorial region. It indicates that the equatorial region is the most error-sensitive region due to the error property of C6. We have seen in Figure 18 that the error is largest at the equator in the residual heat flux pattern. If this error grows linearly, the SST evolution will deviate far from the real state in a very short time.

We have illustrated here that the adjoint technique is a better method to determine the surface heat flux pattern. The adjoint determined heat flux pattern is consistent with both the model dynamics and the observations. Though it is a much more expensive procedure computationally than the simple residual calculation, the adjoint approach gives the correct way for extracting the model unknowns from the available observations.

Appendix D: Why can't the Cost Function be zero When Assimilating the Real Observed Data?

The cost function J in (A1) measures the lack-of-fit between the observation and the model counterpart plus the misfits between the estimated parameter fields and the chosen guess fields. The essence of the assimilation procedure is to make the cost function as small as possible. The cost has a smallest value of zero in the L_2 Euclidean norm. Therefore the global minimum of the cost function should be zero.

Analytically the cost function is zero when the solution of equations (A7), (A16), (A17) and (A19) is obtained. The question is: Can this be the case in real data assimilation? Numerous experiments have shown that the cost function cannot go to zero when assimilating *real* observations. Why can't the cost function be zero in real data assimilation? The answer to this problem will help in understanding why we can't recover the results from the residual calculation.

We first summarize the minimization procedure before proceeding with further discussion. At every iteration, the SST model (A7) is integrated forward in time; the adjoint model (A16), which is driven by the square-root of the misfits between the modeled SST and the observed SST, is integrated backward in time; the gradient information of (A18) and (A20) is then calculated and used in the minimization routine called

CONMIN to search of a new estimate for the control variables (the heat flux field and the initial SST state). CONMIN is a Beale-restarted, memoryless, variable metric, conjugate-gradient algorithm. It has been documented in Shanno (1978), Shanno and Phua (1980), Navon and Legler (1987), and Legler et al. (1989).

It has been verified that the zero value of the cost functional *can* be obtained when doing identical-twin data assimilation. In identical-twin experiments, the observations are taken to be model simulated data. By doing so, the "observations" are exactly consistent with the model dynamics and are error-free (no observation errors and no model errors). Heuristically, therefore, we conclude that the global minimum of the cost function can be obtained when the observations and the model dynamics are exactly compatible.

The only difference between the real data assimilation and the identical-twin experiment is that the real observations have errors (either due to observational error or due to the model inadequacy in representing the real world). Clearly, the problem of why the cost function can't be zero becomes the problem of which part of the minimization procedure is affected by the errors when using the real data.

The key point of this problem is in the minimization algorithm. The SST equation is forced by the surface heat flux, and the adjoint equation is forced by the square-root of the misfit between the modeled SST and the observed SST. The trajectories of the SST and the Lagrange multiplier will go the way what the applied forcing field would like them to go. In other words, these two equations can respond to any given forcing field.

Therefore the use of the real data will not affect the behavior of either the SST model or the adjoint model.

CONMIN is a conjugate-gradient (C-G) algorithm for use in large-scale unconstrained minimization problem. It searches a better approximation to the minimum of a cost function of N variables, u_1, u_2, \dots, u_N , with each iteration.

Within a given iteration an estimate is made of the best way to change each component of the vector u , so as to produce the maximum reduction of the cost function. In order to do this, the gradient of the cost function with respect to the variables needs to be calculated first. This gradient is then combined with information from the previous iterations to produce a search direction. The search direction is an estimate of the relative change in each component of the vector u to produce the maximum reduction in the cost function. The magnitude of the changes along the search direction is controlled by the step-size. The step-size in CONMIN is estimated optimally by using Davidon's cubic interpolation (Navon and Legler, 1987). The new vector u_{k+1} (where k denotes the iteration number) after an iteration is given by the previous vector u_k plus an optimal step size times the search direction. The iterative process is terminated when a chosen convergence criterion is satisfied.

CONMIN is the most efficient of the available C-G algorithms in tests conducted by Navon and Legler (1987). There are two main features in CONMIN which cause this routine to assimilate the large-scale model-consistent phenomena only.

The CONMIN algorithm uses a single step-size to control the magnitude of all the changes along the search direction at each iteration. More specifically, the step size used provides only a *general* information on how much the reduction should be made in the cost function in the *whole* variable domain; it does not put special weight on any particular search direction.

For identical-twin experiments, the observations are exactly consistent with the model physics. The information of misfits is distributed uniformly over the whole spatial domain. Therefore, the use of one step-size can provide a uniform change in all the search directions. The cost function is minimized in a way that the data misfits at all grid-points tend to go to zero simultaneously. The zero cost function can be obtained in this case.

For the real data assimilation, the data misfits are not uniformly distributed due to random errors. Since the estimation of the step-size is based on general information of the variable domain, the obtained step-size therefore reflects only the large-scale, model-consistent feature of the observational field.

The second feature is that the convergence criterion of the CONMIN algorithm is based on the information of the whole variable domain. If the norm of the gradient of the cost function is smaller than some prescribed convergence parameter ε , the convergence is then achieved. That is to say, the algorithm pays little attention to the localized large data misfits. As long as the misfits for the whole field are generally

small, the minimization process is completed. Hence the convergence criterion represents an averaged property of the whole field.

Examining the results from the residual calculation and from the minimization procedure (Figures 17(a-b)), one notices that the pattern of the residual heat flux is much noisier than that of the optimal calculated field. What are not recovered in the optimal calculation are those localized small phenomena, such as the three eye-like intensive heating center at the equator and the strength of the maximum center near the coast of South America. It is clearly shown in Figure 20 that these localized intensive heating are caused by the errors in the SST observations.

Therefore the CONMIN algorithm behaves as a "filter" when assimilating the real data. The properties possessed by the CONMIN algorithm determine that the minimization procedure selects the model-consistent part of the information only; and the algorithm converges when the total averaged misfit is small regardless of some localized large data misfits. Because of this reasoning, the cost function will never be zero as long as the model physics and the observations are not exactly compatible.

The CONMIN algorithm then converges to a local minimum instead of the global minimum which will give a zero cost functional. We have shown that the cost function can't be zero due to the errors in the real data. We also know that the CONMIN algorithm has only a *local* convergence property (None of the C-G algorithm have a global convergence property). The issue of the uniqueness of the local minimum is beyond the scope of this research.

Appendix E:

The Effect of Choice of the Guess Field \tilde{Q} on the Estimated Net Heat Flux Field

We have included *a priori* information about the estimated field parameters in the formulation of the cost function J in (A1), which takes the form:

$$\begin{aligned} J(T, Q, T_0) &= J_T + J_Q + J_{T_0} \\ &= \frac{1}{2} \int_{\Sigma} (T - \hat{T})^2 d\sigma + \frac{1}{2} K_Q' \int_{\Sigma} (Q - \tilde{Q})^2 d\sigma + \frac{1}{2} K_0' \int_{x,y} (T_0 - \tilde{T}_0)^2 dx dy \end{aligned} \tag{E1}$$

The usefulness of adding the term J_Q has been discussed extensively in section 3.3 and section 5.1,

By our definition, this added *a priori* information measures the closeness of the estimated parameters Q between two consecutive iterations of the minimization procedure. It implies that the solution of Q should be searched in the neighborhood of \tilde{Q} . Therefore the term \tilde{Q} is updated at every iteration. Mathematically, the form of this *a priori* information plays the role of a penalizing term in which \tilde{Q} corresponds to shifts of the origin. A similar procedure has been adopted by Carrera and Neuman (1986a and b) in estimating aquifer parameters in hydrology.

The *a priori* information is extra information which is not

contained in the model equation. It serves to reduce the range of possible solutions, or even cause the problem to be unique. But the question is: How certain is this information? Choosing the term \tilde{Q} to be the value of Q at the previous iteration is based on the character of the smoothness of the solution. Whether the obtained flux field is unique remains to be verified.

It would be helpful to answer the question if we can perform the parameter estimation procedure using different choices for the term \tilde{Q} . In this appendix, we present the results from two experiments. In the first experiment, we perform the minimization procedure for the first couple of iterations by setting \tilde{Q} to be the value of Q at the previous iteration (as done before). The value of \tilde{Q} after these first two iterations is then held and denoted by \tilde{Q}_2 . For the following iterations of the procedure, we calculate the differences between the newly estimated Q and the value of \tilde{Q}_2 . The reason for choosing the value of \tilde{Q}_2 is because, from our experience, the estimated flux field can be improved significantly from its first guess usually after two or three iterations.

The second experiment uses the Oberhuber's climatological net-heat-flux data as \tilde{Q} . Thus the differences between the estimated flux field and Oberhuber's flux field are minimized in addition to minimizing the misfits between the modeled SST and the observed SST.

Figures 21(a-d) and 22(a-d) show the estimated flux field from experiments 1 and 2. It is surprising to see that the estimated heat flux fields in these two maps are so remarkably resemble. Comparing with the flux pattern shown in Figures 12(a-d) (which uses updated values for \tilde{Q}), one also finds that all the estimated heat flux fields have similar spatial

structures in all four seasons though the intensity of the flux fields from experiments 1 and 2 are weaker. The optimal SST fields from these two experiments are given in Figures 23(a-d) and 24(a-d). They look very similar to each other. Compared with the observed SST field (Figures 6(a-d)), it is clear that experiments 1 and 2 have successfully captured the main features of the SST seasonal variations.

One may wonder why the estimated heat flux fields (Figures 12,21,22) all give a similar structure of the seasonal variations of the heat flux, regardless of choices of the value of \tilde{Q} . One may also ask why the heat flux fields from experiments 1 and 2 are weaker.

Examining the cost function J in (E1), one notices that there are three terms, i.e., J_T , J_Q and J_{T_0} in the formulation of J . The terms J_Q and J_{T_0} are added for the purpose of parameter estimation. It is the term J_T that contains the physical information from the SST equation which is the constraint in our minimization problem. Correspondingly, it is the square-root of J_T that drives the adjoint equation. Therefore, the major contribution to the minimization process is from the term J_T . This explains why the structures from all the experiments (Figures 12, 21, 22) look similar.

The weaker heat flux fields obtained from experiments 1 and 2 are as expected. The term J_Q functions as a penalty term. It penalizes the departure of the estimated flux field Q from the guess field \tilde{Q} . However, the optimally determined heat flux structure is very different from the structure of either Oberhuber's flux field or the flux field \tilde{Q}_2 . The minimization procedure therefore tends to give a weaker Q in order to

maintain less inconsistency between the simulated SST and the observed SST.

Figures 25(a-d) and 26(a-d) show the corresponding SST data misfit associated with experiments 1 and 2. It can be seen that the magnitude of the misfits is larger than that in Figures 16(a-d). The minimization process achieves the computational steady state within 4-8 iterations for both experiments (Figures 27(a-b)).

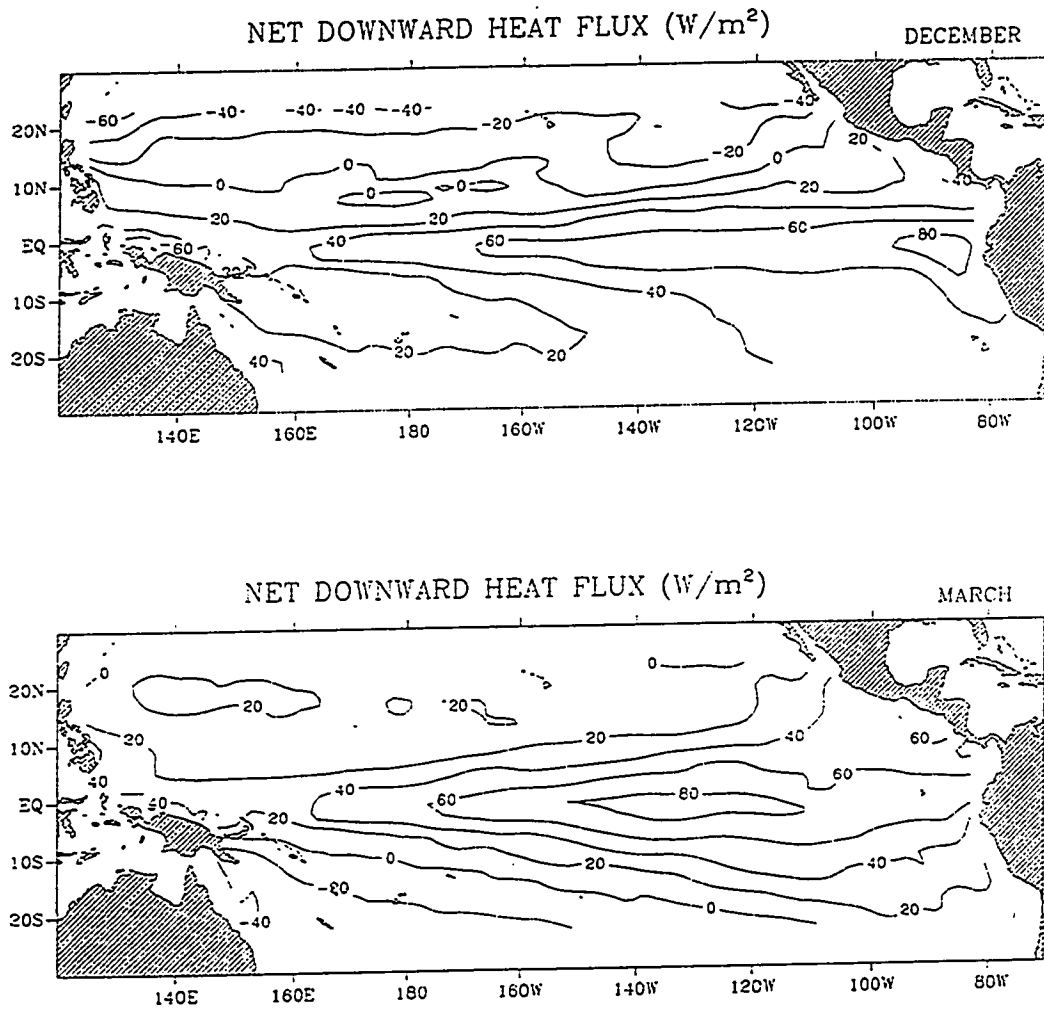


Figure 21. The pattern of the estimated net downward surface heat flux from experiment 1 in (a) December; (b) March; (c) June; and (d) September (the contour interval is 20 W/m^2).

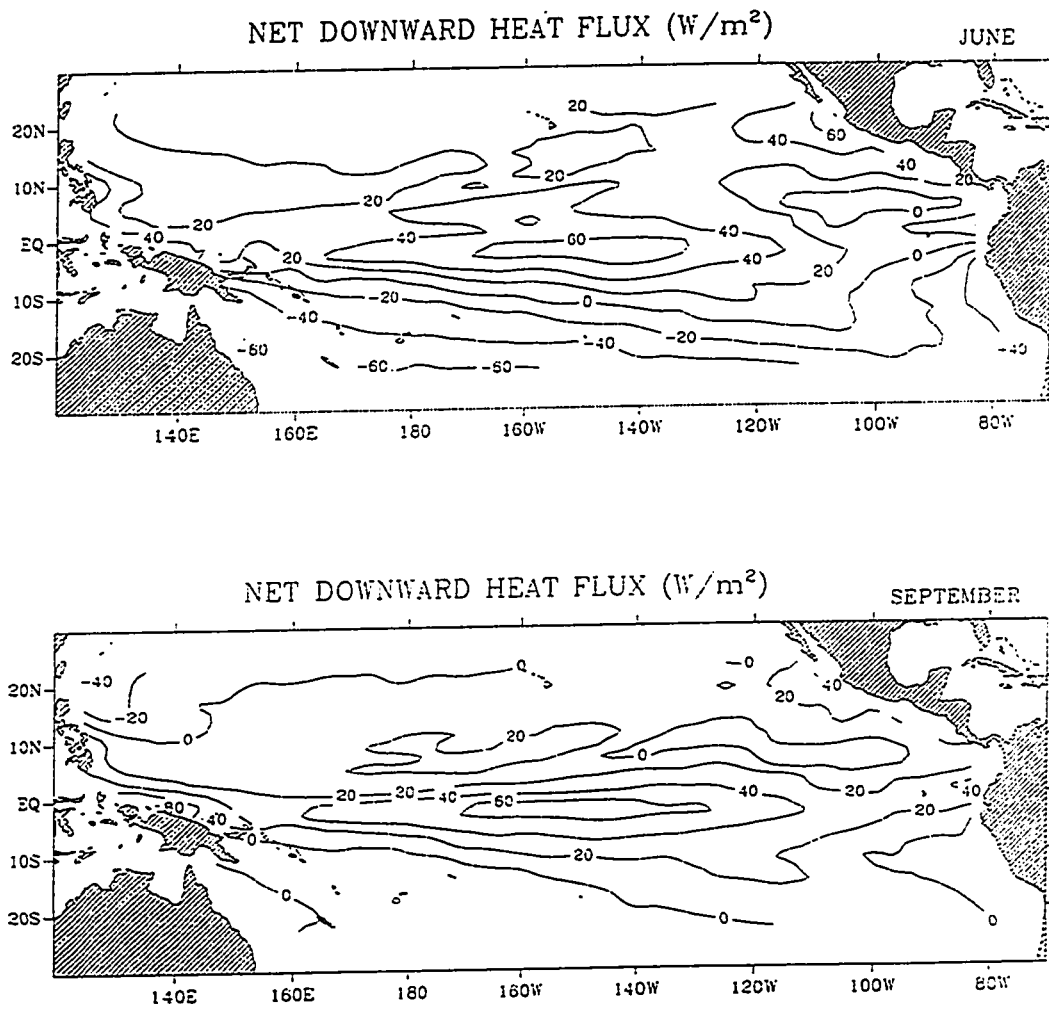


Figure 21 continued

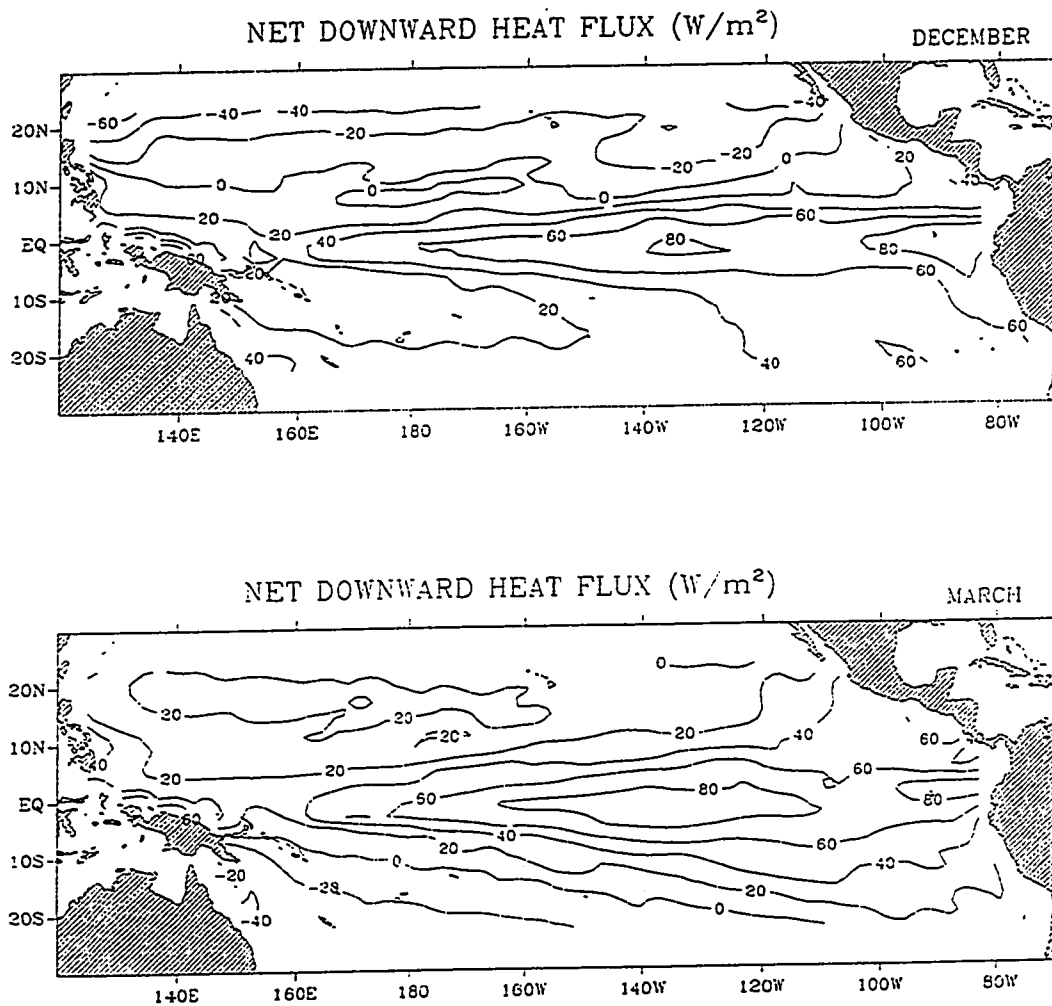


Figure 22. The pattern of the estimated net downward surface heat flux from experiment 2 in (a) December; (b) March; (c) June; and (d) September (the contour interval is 20 W/m^2).

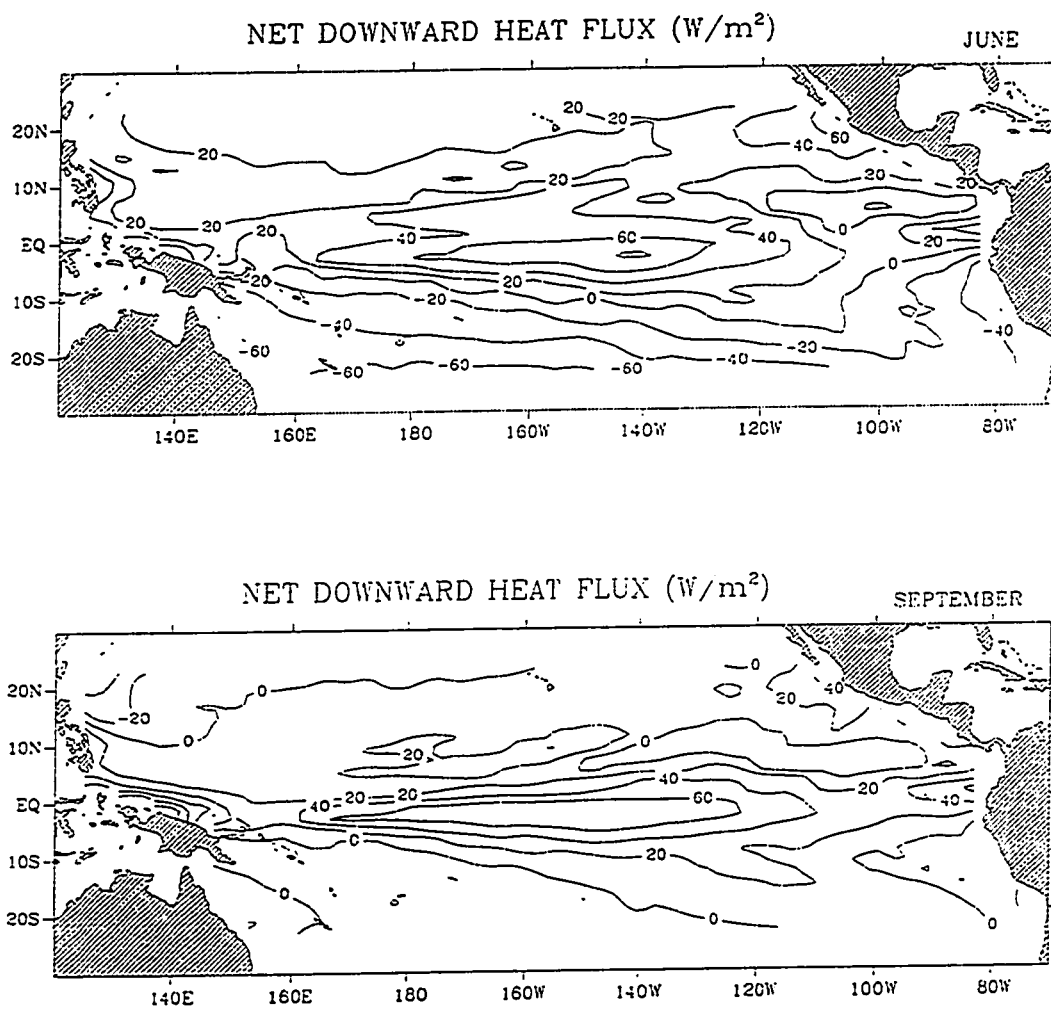


Figure 22 continued

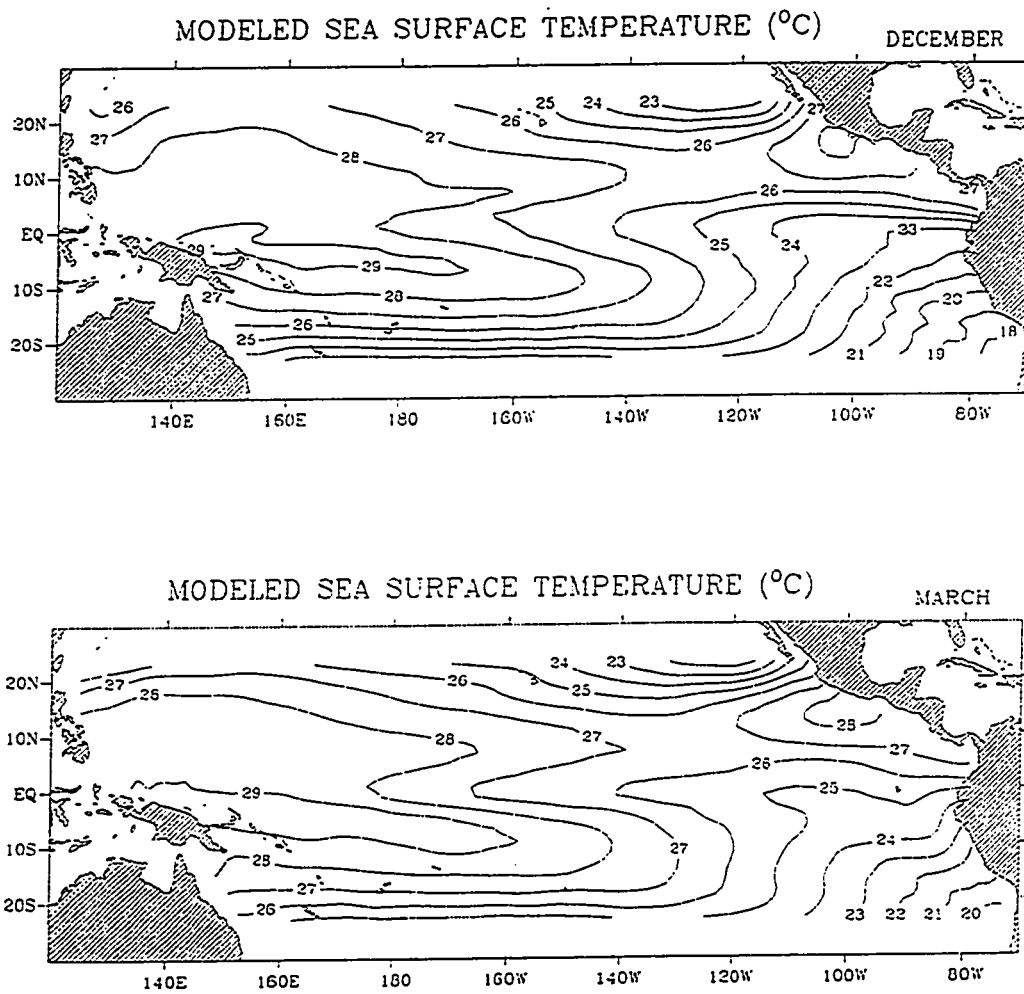


Figure 23. The pattern of the modeled sea surface temperature from experiment 1 in (a) December; (b) March; (c) June; and (d) September.

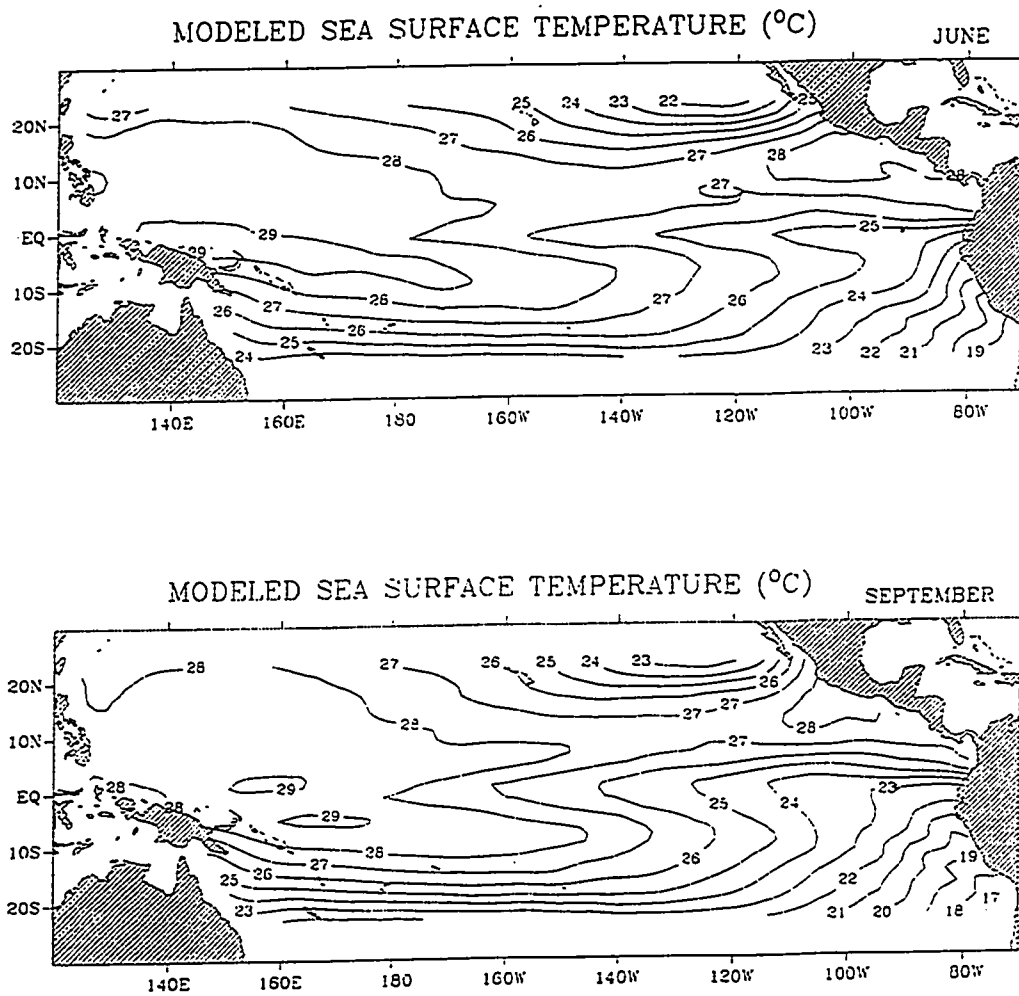


Figure 23 continued

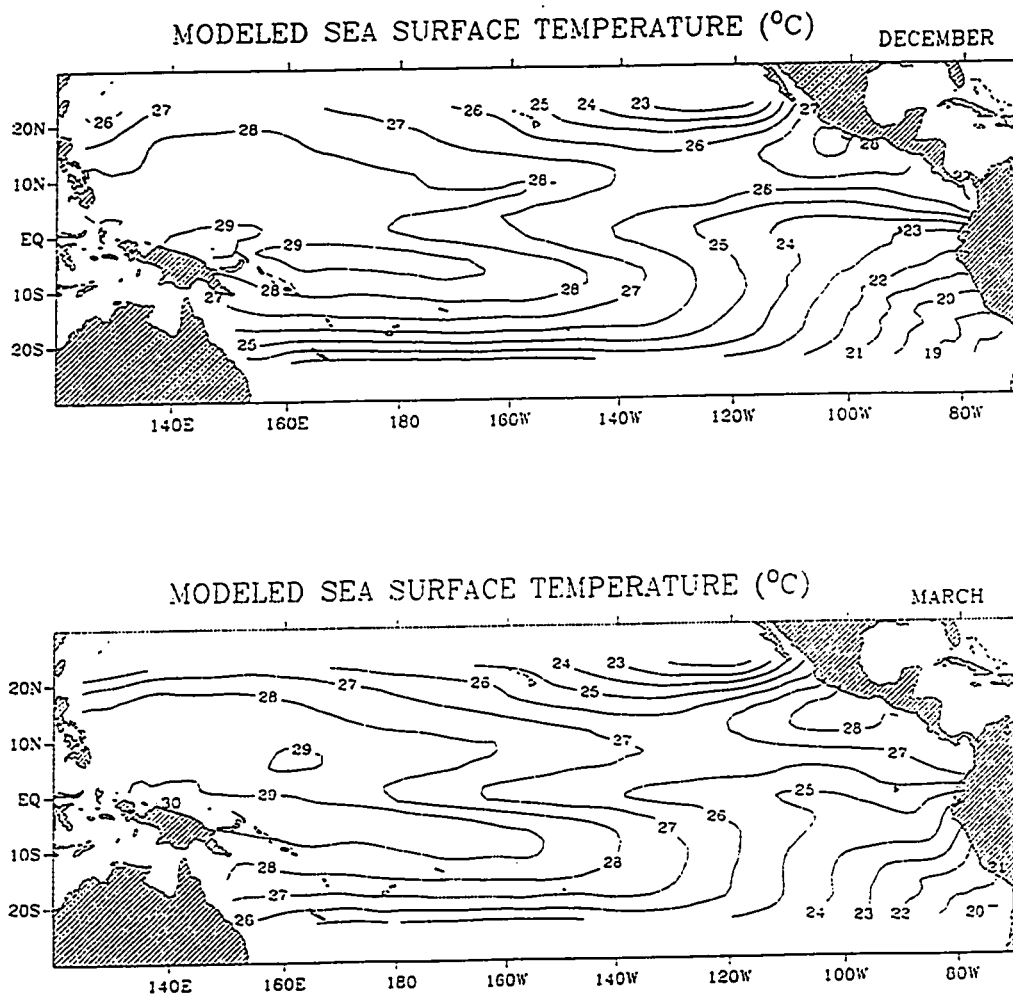


Figure 24. The pattern of the modeled sea surface temperature from experiment 2 in (a) December; (b) March; (c) June; and (d) September.

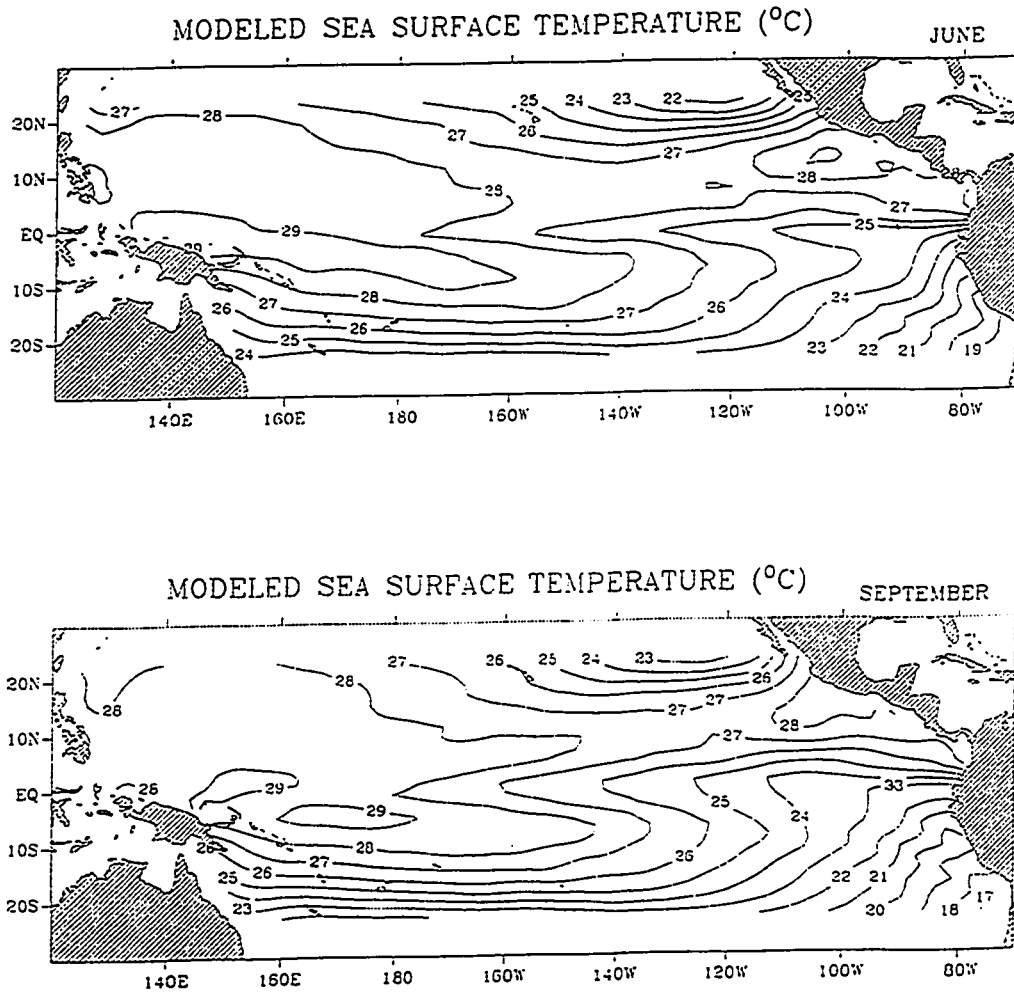


Figure 24 continued

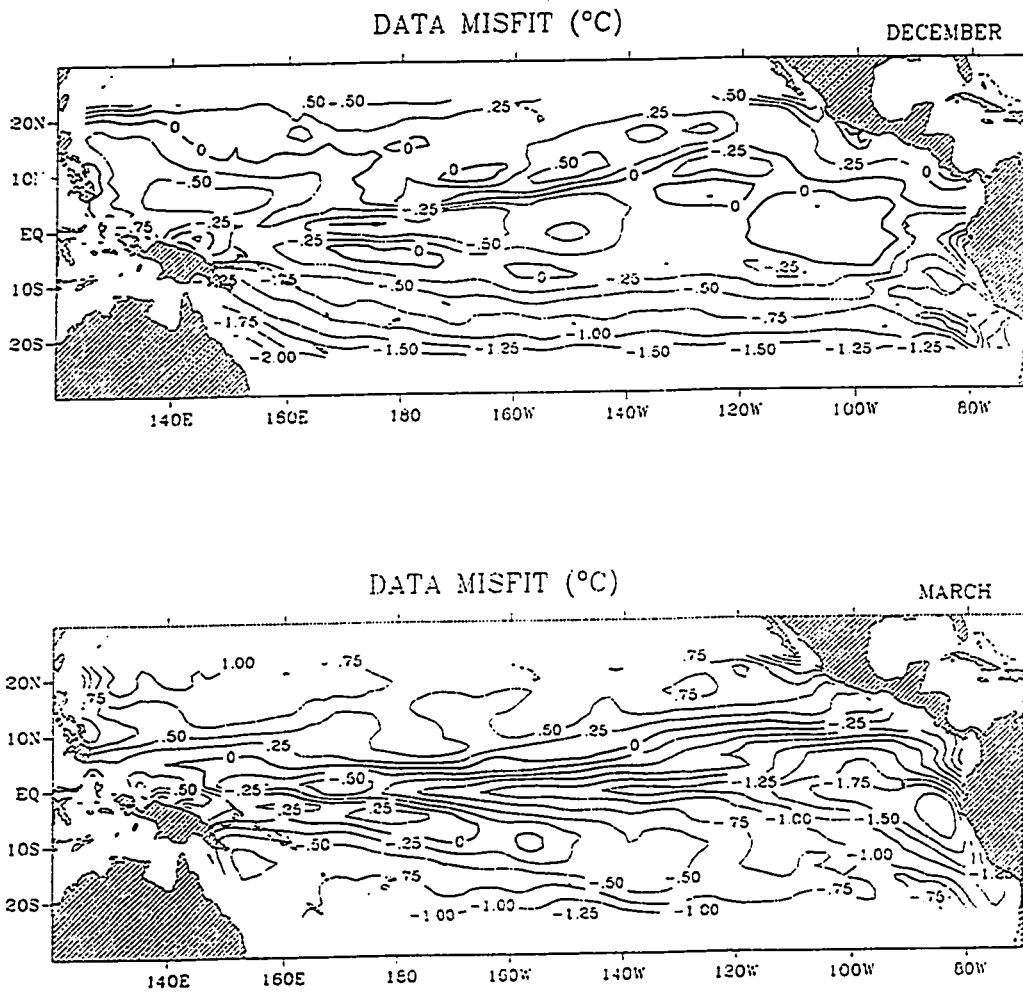


Figure 25. Data misfits between the modeled (experiment 1) and the observed SST in (a) December; (b) March; (c) June; and (d) September (the contour interval is 0.25°C).

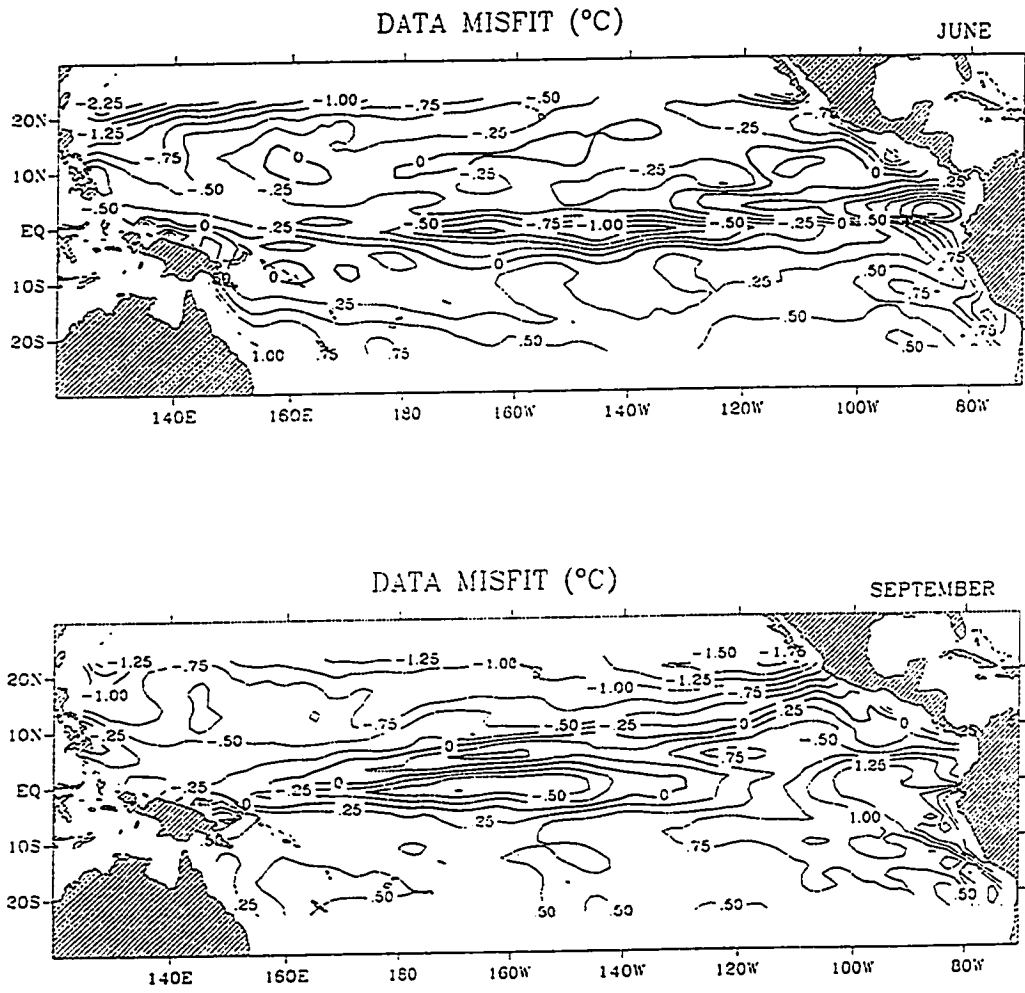


Figure 25 continued

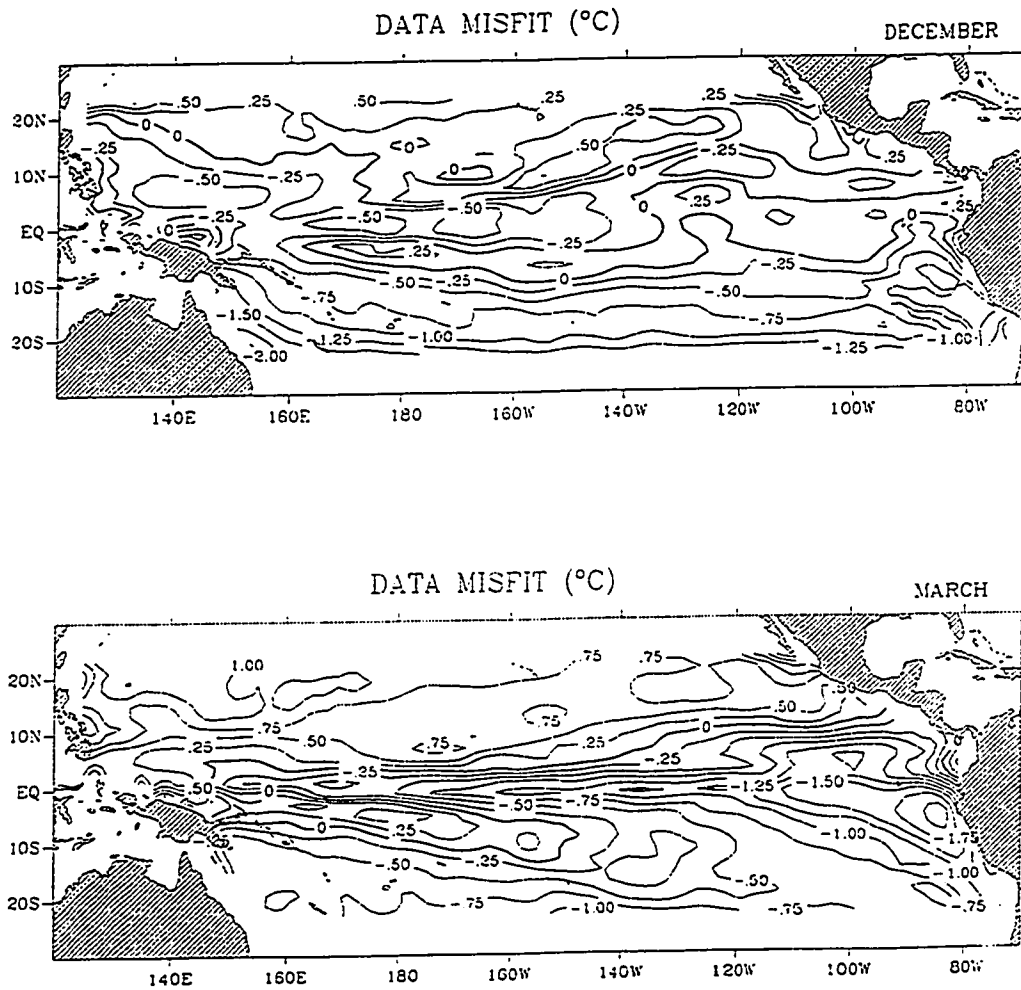


Figure 26. Data misfits between the modeled (experiment 2) and the observed SST in (a) December; (b) March; (c) June; and (d) September (the contour interval is 0.25°C).

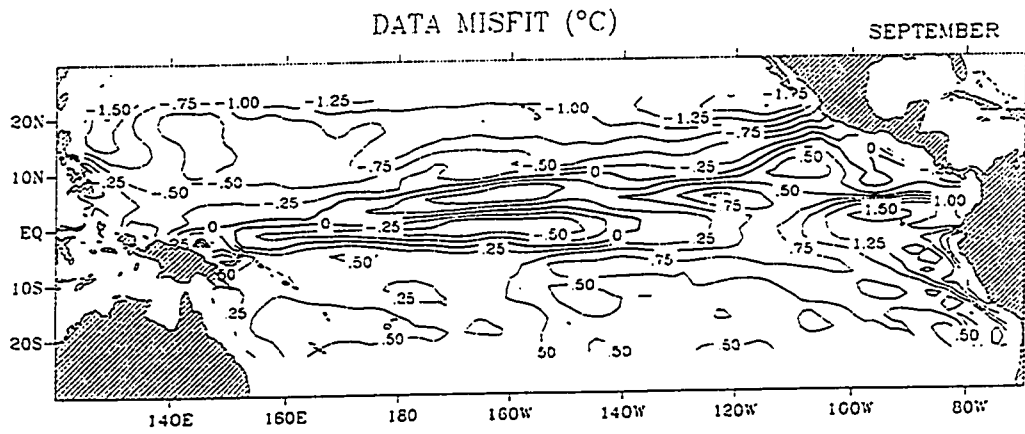
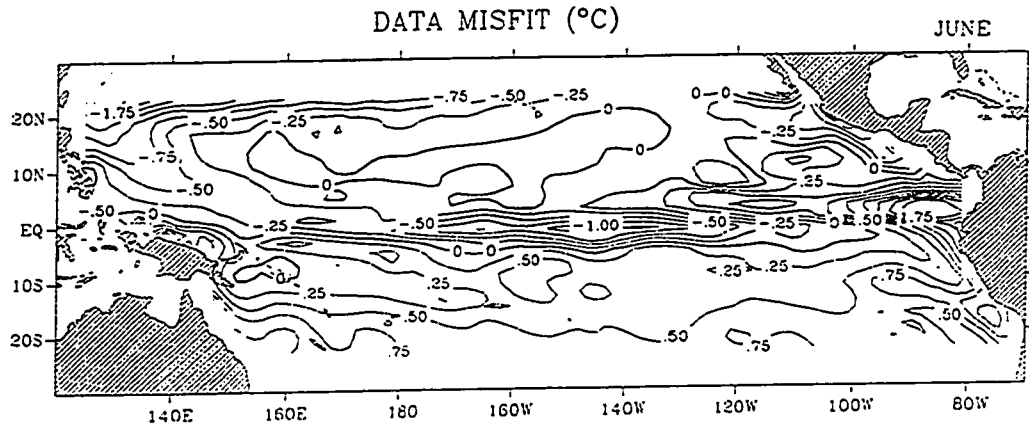


Figure 26 continued

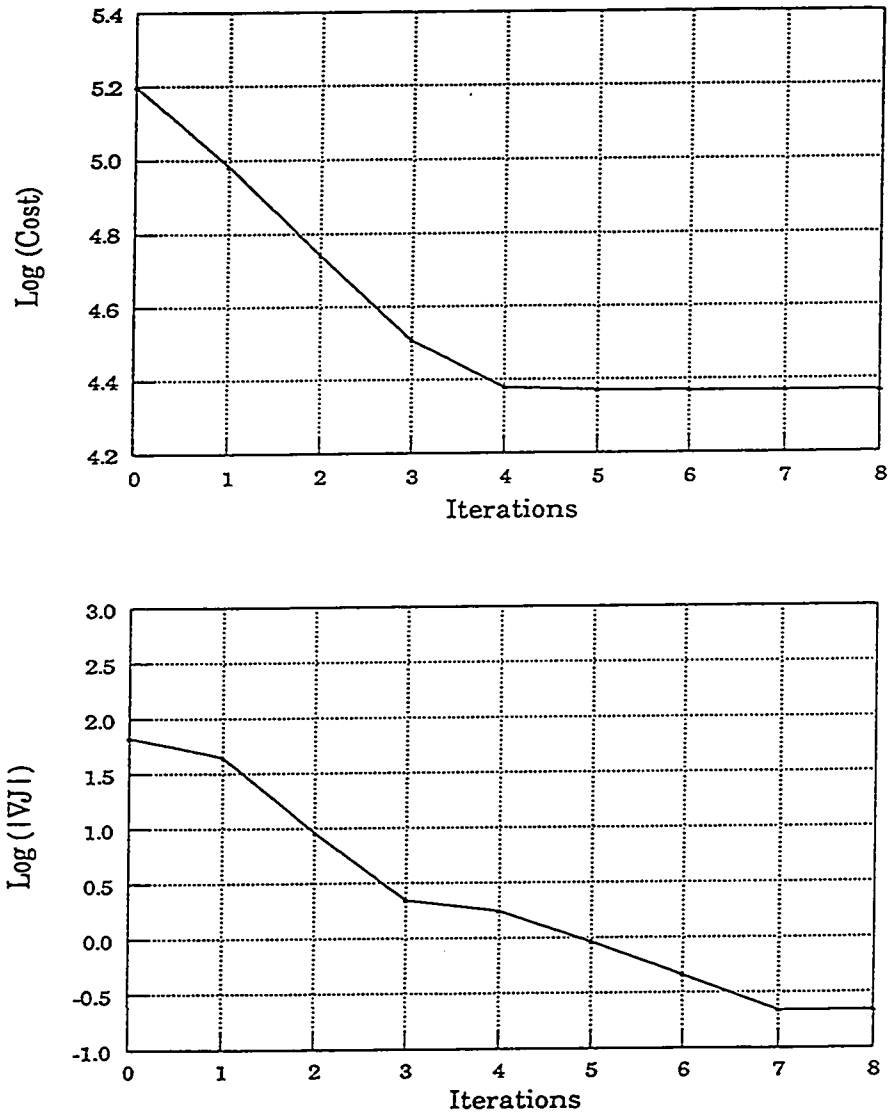


Figure 27. The evolution of the cost function and the norm of the gradient during the iterative process in (a) experiment 1; (b) experiment 2

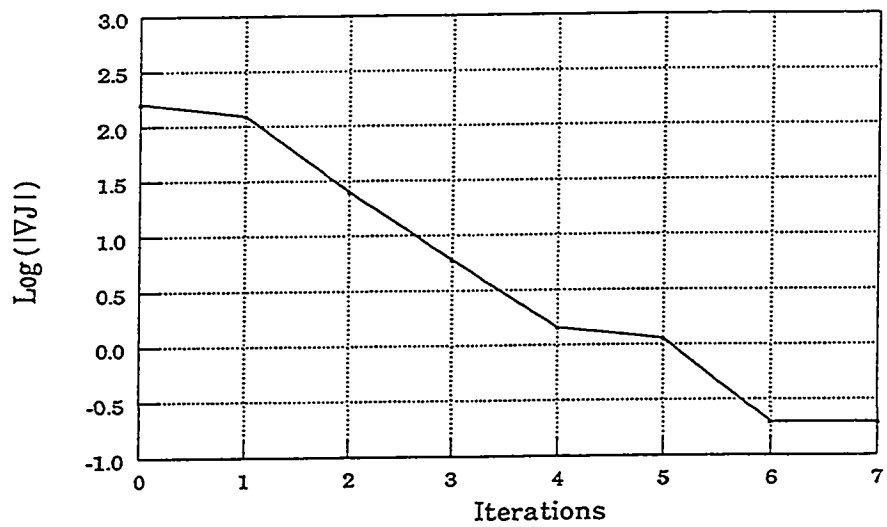
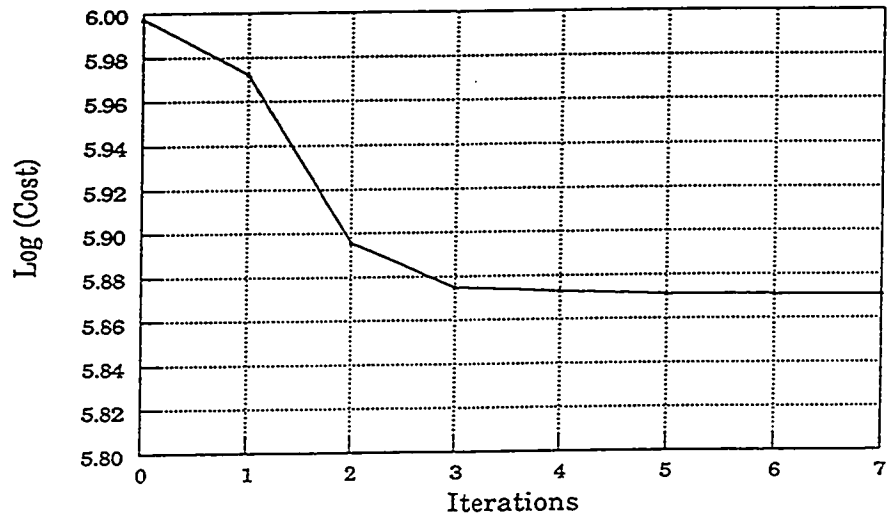


Figure 27 continued

8. References

- Anderson, D. L. T., 1991: Data assimilation in ocean models. *Strategies for Future Climate Research*, M. Latif, Ed., Max-Plank-Institut für Meteorologie, Hamburg, Germany, 193-225.
- Anthes, R. A., 1974: Data assimilation and initialization of hurricane prediction models. *J. Atmos. Sci.*, **31**, 701-719.
- Beale, E. M., 1972: A derivation of conjugate-gradients. *Numerical Methods for Non-linear Optimization*. F. A. Lootsma, Ed., Academic Press, 39-43.
- Bennett, A. F., and P. C. McIntosh, 1982: Open ocean modelling as an inverse problem: Tidal theory. *J. Phys. Oceanogr.*, **12**, 1004-1018.
- Bennett, A. F., and W. P. Budgell, 1987: Ocean data assimilation and the Kalman filter: Spatial regularity. *J. Phys. Oceanogr.*, **17**, 1583-1601.
- Bennett, A. F., 1990: Inverse methods for assessing ship-of-opportunity networks and estimating circulation and winds from tropical expendable bathythermograph data. *J. Geophys. Res.*, **95**, 16,111-16,148.
- Bennett, A. F., and R. N. Miller, 1991: Weighting initial conditions in variational assimilation schemes. *Mon. Wea. Rev.*, **119**, 1098-1102.
- Bergamasco, A., P. Malanotte-Rizzoli, W. C. Thacker, and R. B. Long, 1992: The seasonal steady circulation of the eastern Mediterranean determined with the adjoint method. Submitted to *Deep Sea Res.*, special issue for P.O.E.M.
- Bertsekas, D. P., 1982: *Constrained Optimization and Lagrange Multiplier Methods*. Academic Press, London, 395pp.
- Blanc, T. V., 1987: Accuracy of bulk-method-determined flux, stability, and sea surface roughness. *J. Geophys. Res.*, **92**, 3867-3876.
- Blumenthal, M.B. and M.A. Cane, 1989: Accounting for parameter

- uncertainties in model verification: An illustration with tropical sea surface temperature. *J. Phys. Oceanogr.*, **19**, 815-830.
- Bryson, A. E., Jr., and Y. C. Ho, 1975: *Applied Optimal Control*. Revised Printing. Hemisphere Publishing Corporation, New York, 481pp.
- Busalacchi, A. J. and J. J. O'Brien, 1980: The seasonal variability in a model of the tropical Pacific. *J. Phys. Oceanogr.*, **10**, 1929-1951.
- Cacuci, D.G., 1981: Sensitivity theory for nonlinear systems. I. Nonlinear functional analysis approach. *J. Math. Phys.*, **22**, 2794-2812.
- Camerlengo, A. L. and J. J. O'Brien, 1980: Open boundary conditions in rotating fluids. *J. Comp. Physics*, **35**, 12-35.
- Cane, M. A., 1979: The response of an equatorial ocean to simple wind stress patterns: I. Model formulation and analytical results. *J. Marine Res.*, **37**, 233-252.
- Carrera, J. and S. P. Neuman, 1986a: Estimation of aquifer parameters under transient and steady state conditions, 1: Maximum likelihood method incorporating prior information. *Water Resour. Res.*, **22(2)**, 199-210.
- Carrera, J. and S. P. Neuman, 1986b: Estimation of aquifer parameters under transient and steady state conditions, 2: Uniqueness, stability and solution algorithms. *Water Resour. Res.*, **22(2)**, 211-227.
- Cayan, D. R., 1990: Variability of latent and sensible heat fluxes over the oceans. Ph.D. Dissertation, University of California, San Diego, 199pp.
- Courtier, P., and O. Talagrand, 1987: Variational assimilation of meteorological observations with the adjoint vorticity equations. Part II. Numerical Results. *Quart. J. Roy. Meteor. Soc.*, **113**, 1329-1347.
- Daley, R., 1991: *Atmospheric Data Analysis*. Cambridge University Press, Cambridge, 457pp.
- Das, S. K., and R. W. Lardner, 1991: On the estimation of parameters of hydraulic models by assimilation of periodic tidal data. *J. Geophys. Res.*, **96**, 15,187-15,196.
- Das, S. K., and R. W. Lardner, 1991: Variational parameter estimation for a two-dimensional numerical tidal model. To appear in *Int. J. Numer. Methods Fluids*.

- Davies, H., and R. Turner, 1977: Updating prediction models by dynamic relaxation: An examination of the technique. *Quart. J. Roy. Meteor. Soc.*, **103**, 225-245.
- Dee, D., S. Cohn, A. Dalcher, and M. Ghil, 1985: An efficient algorithm for estimating noise covariances in distributed systems. *IEEE Trans. Automatic Control*, **30**(11), 1057-1065.
- Derber, J., 1987: Variational four-dimensional analysis using quasi-geostrophic constraints. *Mon. Wea. Rev.*, **115**, 998-1008.
- Derber, J., and A. Rosati, 1989: A global oceanic data assimilation system. *J. Phys. Oceanogr.*, **19**, 1333-1347.
- Esbensen, S. K., and Y. Kushnir, 1981: The heat budget of the global ocean: An atlas based on estimates from surface marine observations. Climate Research Institute, Oregon State University. Report No. 29, 133pp.
- Farrell, B. F., and A. M. Moore, 1992: An adjoint method for obtaining the most rapidly growing perturbation to oceanic flows. *J. Phys. Oceanogr.*, **22**, 338-349.
- Fiedler, P. C., 1992: Seasonal climatologies and variability of eastern tropical Pacific surface waters. NOAA Technical Report NMFS 109, 65pp.
- Fletcher, R., 1987: *Practical Methods of Optimization*. John Wiley & Sons, New York, 436pp.
- Fu, C., M. Zhang, J. Fletcher, B. Su, and X. Quan, 1990: *Atlas of Climate Physics of Tropical Pacific Ocean*. Science Press, Beijing, China, 190pp.
- Gaspar, P., and C. Wunsch, 1989: Estimates from altimeter data of barotropic Rossby waves in the northwestern Atlantic ocean. *J. Phys. Oceanogr.*, **19**, 1821-1844.
- Ghil, M., S. Cohn, J. Tavantzis, K. Bube, and E. Isaacson, 1981: Applications of estimation theory to numerical weather prediction. *Dynamic Meteorology: Data Assimilation Methods*, L. Bengtsson, M. Ghil, and E. Kallen, Ed., 139-224.
- Ghil, M., 1990: Sequential estimation in meteorology and oceanography: Theory and Numerics. *Proc. Intl. Symp. Assimilation of Observations in Meteorology and Oceanography*, Clermont-Ferrand, World Meteorological Organization, Geneva, 85-90.

- Ghil, M., and P. Malanotte-Rizzoli, 1991: Data assimilation in meteorology and oceanography. *Adv. Geophys.*, **33**, 141-266.
- Gill, P., W. Murray, and M. Wright, 1981: *Practical Optimization*. Academic press, London, 401pp.
- Haines, K., 1991: A direct method for assimilating sea surface height data into ocean models with adjustments to the deep circulation. *J. Phys. Oceanogr.*, **21**, 843-868.
- Hall, M. C. G. and D. G. Cacuci, 1983: Physical interpretation of the adjoint functions for sensitivity analysis of atmospheric models. *J. Atmos. Sciences*, **40**, 2537-2546.
- Hall, M. C. G., 1986: Application of adjoint sensitivity theory to an atmospheric general circulation model. *J. Atmos. Sciences*, **43**, 2644-2651.
- Halpern, D., R. A. Knox, D. S. Luther, and S. G. H. Philander, 1989: Estimates of equatorial upwelling between 140° and 110°W during 1984. *J. Geophys. Res.*, **94**, 8018-8020.
- Hastenrath, S., and P. Lamb, 1977: *Climatic Atlas of the Tropical Atlantic and Eastern Pacific Oceans*. Univ. of Wisconsin Press, 97pp.
- Harrison, D. E., W. S. Kessler, and B. S. Giese, 1989: Hindcasts of the 1982-83 El Niño: thermal and dynamic height variability along the ship of opportunity XBT tracks. *J. Phys. Oceanogr.*, **19**, 397-418.
- Harrison, D. E., 1991: Equatorial sea surface temperature sensitivity to net surface heat flux: Some ocean circulation model results. *J. Climate*, **4**, 539-549.
- Hestenes, M. R., 1980: Conjugate directions methods in optimization. *Applications of Mathematics*, **12**, Springer-Verlag, New York, 325pp.
- Hickey, B., 1975: The relationship between fluctuations in sea level, wind stress and sea surface temperature in the equatorial Pacific. *J. Phys. Oceanogr.*, **5**, 460-475.
- Hoke, J. E., and R. A. Anthes, 1976: The initialization of numerical models by a dynamic initialization technique. *Mon. Wea. Rev.*, **104**, 1551-1556.
- Holland, W. R., and P. Malanotte-Rizzoli, 1989: Assimilation of altimeter data into an ocean circulation model: space versus time resolution studies. *J. Phys. Oceanogr.*, **19**, 1507-1534.

- Horel, J. D., 1982: On the annual cycle of the tropical Pacific atmosphere and ocean. *Mon. Wea. Rev.*, **110**, 1863-1878.
- Jazwinski, A. H., 1970: *Stochastic Processes and Filtering Theory*. Academic Press, London, 376pp.
- Lanczos, C., 1968: *The Variational Principles of Mechanics*. 3rd ed. University of Toronto Press, Toronto, 375pp.
- Lardner, R. W., 1992: Optimal control of open boundary conditions for a numerical tidal model. To appear in *Computer Meth. Appl. Mech. & Engng.*
- Large, W. G., and S. Pond, 1982: Sensible and latent heat flux measurements over the ocean. *J. Phys. Oceanogr.*, **12**, 464-482.
- Le Dimet, F., and O. Talagrand, 1986: Variational algorithms for analysis and assimilation of meteorological observations: theoretical aspects. *Tellus*, **38A**, 97-110.
- Le Dimet, F., and I. M. Navon, 1988: Variational and optimization methods in meteorology: A review. FSU-SCRI-88-144, Florida State University, Tallahassee, Florida, 54pp.
- Leetmaa, A., J. P. McCreary, and D. W. Moore, 1981: Equatorial Currents: Observations and theory. *Evolution of Physical Oceanography*, B. A. Warren, and C. Wunsch, Ed., The MIT Press, Cambridge, MA, 164-183.
- Legler, D. M., I. M. Navon, and J. J. O'Brien, 1989: Objective analysis of pseudo-stress over the Indian ocean using a direct minimization approach. *Mon. Wea. Rev.*, **117**, 709-720.
- Legler, D. M., and I. M. Navon, 1991: VARIATM - A FORTRAN program for objective analysis of pseudostress wind fields using large-scale conjugate gradient minimization. *Computers & Geosciences*, **17**, 1-21.
- Lewis, J. M. and J. C. Derber, 1985: The use of adjoint equations to solve a variational adjustment problem with advective constraints. *Tellus*, **37A**, 309-322.
- Levitus, S., 1982: Climatological atlas of the world ocean. NOAA Professional Paper No. 13, 173pp.
- Lions, J. L., 1971: *Optimal Control of Systems Governed by Partial Differential Equations*. Springer-Verlag, Berlin, 369pp.

- Liu, D. C., and J. Nocedal, 1988: On the limited memory BFGS method for large scale optimization. Tech. Report NAM 03, Northwestern Univ., Evanston, IL, 26pp.
- Long, R. B., and W. C. Thacker, 1989a: Data assimilation into a numerical equatorial ocean model. I. The model and the assimilation algorithm. *Dyn. Atmos. Oceans*, **13**, 379-412.
- Long, R. B., and W. C. Thacker, 1989b: Data assimilation into a numerical equatorial ocean model. II. Assimilation experiments. *Dyn. Atmos. Oceans*, **13**, 413-439.
- Lorenc, A., 1986: Analysis methods for numerical weather prediction. *Quart. J. Roy. Meteor. Soc.*, **112**, 1177-1194.
- Luenberger, D.C., 1984: *Linear and Nonlinear Programming*. Addison-Wesley, 491pp.
- Malanotte-Rizzoli, P., R. E. Young and D. B. Haidvogel, 1989: Initialization and data assimilation experiments with a primitive equation model. *Dyn. Atmos. Oceans*, **13**, 349-378.
- Malanotte-Rizzoli, P., and R. E. Young, 1990: Can localized clusters of velocity data be useful for data assimilation? Submitted to *J. Phys. Oceanogr.*
- Marotzke, J., 1992: The role of integration time in determining a steady state through data assimilation. To appear in *J. Phys. Oceanogr.*
- McPhaden, M. J., 1983: Equatorial sea surface temperature variations on seasonal time scales. *Hydrodynamics of the Equatorial Ocean*, J. Nihoul, Ed., Elsevier Oceanography Series, Amsterdam, 1-15.
- Meehl, G. A., 1982: Characteristics of surface current flow inferred from a global current data set. *J. Phys. Oceanogr.*, **12**, 538-555.
- Menke, W., 1984: *Geophysical Data Analysis: Discrete Inverse Theory*. Academic Press, London, 260pp.
- Miller, R., 1986: Toward the application of the Kalman filter to regional open ocean modelling. *J. Phys. Oceanogr.*, **16**, 72-86.
- Miller, R., and M. Cane, 1989: A Kalman filter analysis of sea level height in the tropical Pacific. *J. Phys. Oceanogr.*, **19**, 773-790.
- Miller, R., and M. Ghil, 1990: Data assimilation in strongly nonlinear current system. *Proc. Intl. Symp. Assimilation of Observations in*

Meteorology and Oceanography, Clermont-Ferrand, World Meteorological Organization, Geneva, 93-98.

- Moore, A. M., 1991: Data assimilation in a quasi-geostrophic open-ocean model of the Gulf Stream region using the adjoint method. *J. Phys. Oceanogr.*, **21**, 398-427.
- Moore, D. W., and S. G. H. Philander, 1978: Modelling of the tropical oceanic circulation. *The Sea*, Vol. 6, Goldberg et al., eds., Wiley, New York, 319-361.
- Morse, P. and H. Feshbach, 1953: *Method of Theoretical Physics. Part I*. McGraw-Hill, New York.
- Navon, I. M., and R. de Villiers, 1983: Combined penalty-multiplier optimization methods to enforce integral invariants conservation. *Mon. Wea. Rev.*, **111**, 1228-1243.
- Navon, I. M., 1986: A review of variational and optimization methods in meteorology. *Variational Methods in Geosciences*, Y. Sasaki Ed., New York, 29-34.
- Navon, I. M. and D. Legler, 1987: Conjugate-gradient methods for large-scale minimization in meteorology. *Mon. Wea. Rev.*, **115**, 1479-1502.
- Navon, I. M., X. Zou, M. Berger, K. H. Phua, T. Schlick and F. X. Le Dimet, 1992: Numerical experience with Limited Memory Quasi-Newton and truncated Newton methods. *Optimization Techniques and Applications*, Vol. 1, K. H. Phua et al., eds., World Scientific Publishing Co., New York, 445-480.
- Navon, I. M., X. Zou, J. Derber, and J. Sela, 1992: Variational data assimilation with an adiabatic version of the NMC spectral model. *Mon. Wea. Rev.*, 1433-1446.
- Nazareth, L., 1979: A relationship between BFGS and conjugate-gradient algorithms and its implications for new algorithms. *SIAM J. Numer. Anal.*, **16**, 794-800.
- Oberhuber, J. M., 1988: An atlas based on the COADS data set: the budgets of heat, buoyancy and turbulent kinetic energy at the surface of the global ocean. Max-Planck-Institut für Meteorologie, Hamburg, Germany, 100pp.
- O'Brien, J. J., 1986: The diffusive problem. *Advanced Physical Oceanographic Numerical Modelling*, J. J. O'Brien, Ed., D. Reidel Publishing Company, Dordrecht, 127-144.

- Olbers, D., and M. Wenzel, 1988: Determining diffusivities from hydrographic data by inverse methods with applications to the circumpolar current. *Oceanic Circulation Model: Combining Data and Dynamics*. D. L. T. Anderson and J. Willebrand, Ed., D. Reidel Publishing Company, Dordrecht, 95-139.
- Parrish, D., and S. Cohn, 1985: A Kalman filter for a two dimensional shallow-water model: Formulation and preliminary experiments. National Meteorological Center, Office Note 304.
- Panchang, V. G., and J. J. O'Brien, 1989: On the determination of hydraulic model parameters using the adjoint state formulation. *Modeling Marine Systems*, A. M. Davies, Ed., CRC Press, Boca Raton, 6-18.
- Philander, S. G. H., and A. D. Siegel, 1985: Simulation of El Niño of 1982-1983. *Proc. 16th Int. Liege Colloq. on Ocean Hydrodynamics*, J. Nihoul, Ed., Elsevier Oceanography Series, Amsterdam, 517-541.
- Philander, S. G. H., and W. J. Hurlin, 1988: The heat budget of the tropical Pacific ocean in a simulation of the 1982-83 El Niño. *J. Phys. Oceanogr.*, **18**, 926-931.
- Robinson, A. R., and L. J. Walstad, 1987: The Harvard open ocean model: calibration and application to dynamical process, forecasting and data assimilation studies. *Applied Numerical Mathematics*, **3**, 89-131
- Sasaki, Y., 1970: Some formations in numerical variational analysis. *Mon. Wea. Rev.*, **98**, 875-883.
- Schopf, P. S., and M. A. Cane, 1983: On equatorial dynamics, mixed layer physics and sea surface temperature. *J. Phys. Oceanogr.*, **13**, 917-935
- Schröter, J., and C. Wunsch, 1986: Solution of nonlinear finite difference ocean models by optimization methods with sensitivity and observational strategy analysis. *J. Phys. Oceanogr.*, **16**, 1855-1874.
- Schröter, J., 1989: Driving of non-linear time-dependent ocean models by observation of transient tracers - a problem of constrained optimization. *Oceanic Circulation Model: Combining Data and Dynamics*. D. L. T. Anderson and J. Willebrand, Ed., D. Reidel Publishing Company, Dordrecht, 257-286.
- Seager, R., S.E. Zebiak and M.A. Cane, 1988: A model of the tropical Pacific sea surface temperature climatology. *J. Geophys. Res.*, **93**, 1265-1280.

- Shanno, D. F., 1978: On the convergence of a new conjugate-gradient method. *SIAM J. Numer. Anal.*, **15**, 1247-1257.
- Shanno, D. F., and K. H. Phua, 1980: Remark on algorithm 500 - a variable method subroutine for unconstrained nonlinear minimization. *ACM Tran. Math. Softw.*, **6**, 618-622.
- Shea, D. J., K. E. Trenberth, and R. W. Reynolds, 1990: A global monthly sea surface temperature climatology. NCAR Technique Note, NCAR/TN-345+STR, 167pp.
- Sheinbaum, J. and D.L.T. Anderson, 1990a: Variational assimilation of XBT data. Part I. *J. Phys. Oceanogr.*, **20**, 672-688.
- Sheinbaum, J. and D.L.T. Anderson, 1990b: Variational assimilation of XBT data. Part II. Sensitivity studies and use of smoothing constraints. *J. Phys. Oceanogr.*, **20**, 689-704.
- Smedstad, O.M. and J.J. O'Brien, 1991: Variational data assimilation and parameter estimation in an equatorial Pacific Ocean model. *Progress in Oceanography*. **26**, 179-241.
- Stricherz, J. N., J. J. O'Brien, and D. M. Legler, 1992: *Atlas of Florida State University Tropical Pacific Winds for TOGA 1966-1985*. A Mesoscale Air-Sea Interaction Group Technical Report.
- Talagrand, O. and P. Courtier, 1987: Variational assimilation of meteorological observations with the adjoint vorticity equation. Part I: Theory. *Quart. J. Roy. Meteor. Soc.*, **113**, 1311-1328.
- Tarantola, A., 1987: *Inverse Problem Theory: Methods for Data Fitting and Model Parameter Estimation*. Elsevier, Amsterdam, 613pp.
- Thacker, W.C, 1987: Three lectures on fitting numerical models to observations. *External Rep. GKSS 87/E/65*, 64pp., GKSS Forschungszentrum Geesthacht, Geesthacht, Federal Republic of Germany.
- Thacker, W.C, 1988: Fitting models to data by enforcing spatial and temporal smoothness. *J. Geophys. Res.*, **93**, 10,655-10,665.
- Thacker, W.C, 1989: The role of the Hessian matrix in fitting models to measurements. *J. Geophys. Res.*, **94**, 6177-6196.
- Thacker, W.C. and R.B. Long, 1988: Fitting dynamics to data. *J. Geophys. Res.*, **93**, 1227-1240.

- Tziperman, E., and A. Hecht, 1988: Circulation in the eastern Levantine basin determined by inverse methods. *J. Phys. Oceanogr.*, **18**, 506-518.
- Tziperman, E., and W. C. Thacker, 1989: An optimal control/adjoint equations approach to studying the oceanic general circulation. *J. Phys. Oceanogr.*, **19**, 1471-1485.
- Tziperman, E., and P. Malanotte-Rizzoli, 1991: The climatological seasonal circulation of the Mediterranean Sea. *J. Marine Res.*, **49**, 411-434.
- Tziperman, E., and W. C. Thacker, and K. Bryan, 1992: Computing the steady oceanic circulation using an optimization approach. *Dyn. Atmos. Oceans*, **16**, 379-403.
- Verron, J., and W. R. Holland, 1989: Impacts de donnees d'altimetrie satellitaire sur les simulations numeriques aux latitudes moyennes. *Ann. Geophys.*, **7**, 31-46.
- Wang, Z., I. M. Navon, F. X. Le Dimet, and X. Zou, 1992: The second order adjoint analysis: Theory and applications. To appear in *Meteor. Atmos. Phys.*
- Weare, B. C., P. T. Strub, and M. D. Samuel, 1981: Annual mean surface heat fluxes in the tropical Pacific ocean. *J. Phys. Oceanogr.*, **11**, 705-717.
- Webb, D. J., and A. Moore, 1986: Assimilation of altimeter data into ocean models. *J. Phys. Oceanogr.*, **16**, 1901-1913.
- Woodruff, S. D., R. J. Slutz, R. L. Jenne, and P. M. Steuver, 1987: A comprehensive ocean-atmosphere data set. *Bull. Amer. Meteor. Soc.*, **68**, 1239-1250.
- Wunsch, C., 1978: The North Atlantic general circulation west of 50°W determined by inverse methods. *Rev. Geophys. Space Phys.*, **16**, 583-620.
- Wunsch, C., 1987: Using transient tracers: The regularization problem. *Tellus*, **39B**, 477-492.
- Wunsch, C., 1988: Transient tracers as a problem in control theory. *J. Geophys. Res.*, **93**, 8099-9110.

- Wunsch, C., 1989: Tracer inverse problems. *Oceanic Circulation Model: Combining Data and Dynamics*. D. L. T. Anderson and J. Willebrand, Ed., D. Reidel Publishing Company, Dordrecht, 1-78.
- Wyrtki, K., 1981: An estimate of equatorial upwelling in the Pacific. *J. Phys. Oceanogr.*, **11**, 1205-1214.
- Yu, L., and J.J. O'Brien, 1991: Variational estimation of the wind stress drag coefficient and the oceanic eddy viscosity profile. *J. Phys. Oceanogr.*, **21**, 709-719.
- Yu, L., and J.J. O'Brien, 1992: On the initial condition in parameter estimation. *J. Phys. Oceanogr.*, **22**, 1361-1364.
- Zebiak, S. E., 1985: Tropical atmosphere-ocean interaction and the El Niño/Southern Oscillation phenomenon. Ph. D. dissertation, M.I.T., 261pp.
- Zebiak, S. E., and M.A. Cane, 1987: A model El Niño - Southern oscillation. *Mon. Wea. Rev.*, **115**, 2262-2278.
- Zou, X., I. M. Navon, and F. X. LeDimet, 1992: An optimal nudging data assimilation scheme using parameter estimation. *Quart. J. Roy. Meteor. Soc.*, **118**, 1163-1186.
- Zou, X., I. M. Navon, and F. X. LeDimet, 1992: In complete observations and control of gravity waves in variational data assimilation. To appear in *Tellus*.
- Zou, X., I. M. Navon, and J. Sela, 1992: Control of gravity oscillations in variational data assimilation. To appear in *Mon. Wea. Rev.*

9. Biography Sketch

Lisan Yu received her B.S. in Meteorology in July 1985 from Shandong College of Oceanography, Qingdao, People's Republic of China. She was a graduate student in meteorology before she came to the United States to study with Dr. J.J O'Brien in the Fall of 1987. She obtained her M.S. in Physical Oceanography in March 1990 from the Florida State University.

During the course of her studies at FSU, she has been selected as a graduate student fellow of the Supercomputer Computations Research Institute. She has also received several scholarships to attend the workshops including the summer workshop on "Physics of Equatorial Oceans" at the University of Rhode Island in June 1991; the NATO-Advanced Study Institute on "Modelling Oceanic Climate Interactions" at the Centre of Physics in Les Houches, France, in February 1992; and the workshop on "Adjoint Applications in Dynamic Meteorology" in Asilomar, CA, in August 1992. She has presented papers at scientific meetings and has published four papers all in major oceanographic journals.

She is going to do her postdoctoral research with Dr. P. Malanotte-Rizzoli at the Massachusetts Institute of Technology.

Publications:

- L. Yu, and J.J. O'Brien, 1991: Variational estimation of the wind stress drag coefficient and the oceanic eddy viscosity profile. *J. Phys. Oceanogr.*, **21**, 709-719.
- L. Yu, J.J. O'Brien, and J. Yang, 1991: On the remote forcing to the circulations in the Bay of Bengal. *J. Geophys. Res.*, **96**, 20,449-20,454.
- J. Yang, and L. Yu, 1992: Propagation of equatorially trapped waves on a sloping thermocline. *J. Phys. Oceanogr.*, **22**, 573-582.
- L. Yu, and J.J. O'Brien, 1992: On the initial condition in parameter estimation. *J. Phys. Oceanogr.*, **22**, 1361-1364.